Response to the Reviewers

We are submitting a response to the reviews as recommended by the editor. We thank the reviewers for the helpful comments which enabled us to improve the manuscript.

Reviewer 1

Lutsch et al. presented multiannual FTIR measurements of several gases (CO, HCN, and C2H6) at ten NDACC sites located both at high and middle latitudes and reported the analysis of the long-term variability of the corresponding column abundances. The analysis focused on wildfire pollution events and included identification and source attribution of such events using a tagged CO simulation with the GEOS-Chem global model. The analysis confirms that GEOS-Chem with GFAS emissions is capable of adequately simulating the impact of biomass burning on CO column abundances in the Arctic. The presented data of multi-year FTIR measurements can be of interest to the scientific community. However, the manuscript has major flaws explained in my comments below. If the major issues are sufficiently addressed, the manuscript will likely require an additional review focusing on minor issues.

Comment 1.1 — I find that the manuscript lacks sufficiently novel findings. The main results of the analysis, at least as they are formulated in the abstract and conclusions, are descriptive and rather trivial. In particular, the fact that biomass burning plumes from fires in North America and Northern Asia can be transported into the Arctic, leading to strong enhancements in ambient concentrations of CO and other species, has been known long ago. Furthermore, the manuscript makes the impression that virtually all the established experimental facts (or their close analogs) discussed by the authors have been reported in the scientific literature previously. The authors should have tried to emphasize any new findings and to formulate a clear scientific message (or messages).

Reply: The authors have revised the manuscript to emphasize the focus of our findings and the novelty of our results. We quantify the impact of more than 60 wildfire events, globally, on 6 Arctic sites and 4 mid-latitude sites using FTIR measurements of multiple trace gas species. Previous studies have only considered individual wildfire events and at fewer sites. In addition to replicating published emissions ratios, we provide, for the first time, a comprehensive set of emission ratios across multiple wildfire events and trace gas species. The reported emission ratios agree with published values, demonstrating the ability of FTIR to capture wildfire plumes, as well as providing much needed longer-term estimates of emissions ratios and their variability. Furthermore, we identify and characterize the contribution of biomass burning to CO measurements specifically at each FTIR site.

Comment 1.2 — The manuscript would benefit if they could look deeper into the origin and nature of some episodes by addressing, for example, the following questions: How far the plumes were transported before they reached the FTIR sites? What is the typical age of the major plumes at the high-latitude sites? Are there any specific meteorological conditions that favor long-range transport of the biomass burning plumes into the Arctic? Are the emission factors specified in GFAS for HCN and C2H6 consistent with the measurements?

Reply: The authors thank the reviewer for their suggestions. We have revised the manuscript to include travel time calculations for each of the identified events and the typical age of the major plumes. The travel time calculations also enabled the calculation of the emission ratios from the calculated enhancement ratios from FTIR measurements. The emission ratios were compared to previous literature values.

Comment 1.3 — 2. The manuscript is poorly structured, unnecessarily long, and, consequently, is difficult to read. My suggestions in this respect are that the presentation of the results (in particular, in Section 3.1) has to be structurally separated from their discussion/interpretation. The analysis methods described in Sections 3.2 - 3.5 just before the corresponding results should be introduced and explained in Section 2 ("Methods"). The discussion of volume mixing ratio profiles and averaging kernels, which does not result in any significant findings, should be shortened, while the corresponding figures (Figs. 5-8) provided as Supplement. The content of Section 3.5, where GEOS-Chem tagged CO simulation is validated against the FTIR CO measurements, should be provided before the GEOS-Chem simulation is first used in the analysis (that is, before Section 3.3).

Reply: The authors have shortened and restructured the manuscript to improve its clarity. The presentation of the results has been explicitly separated from the discussion. The methods of Sections 3.2-3.5 were moved to Section 2. Section 3.5, the GEOS-Chem versus FTIR comparisons were moved as suggested. We have moved parts of the discussion related to the retrieved FTIR profiles and averaging kernels to appendix materials.

Comment 1.4 — The methods used in the analysis are questionable and need to be better justified or otherwise revised. Specifically, the enhancements of CO due to wildfire pollution events are identified with respect to the fit to FTIR data according to Eq. 3. However, this fit describes not only the "ambient concentration" of CO as apparently assumed by authors but also takes into account the contribution of biomass burning to the observed CO columns. Accordingly, the real wildfire pollution events are likely much stronger and longer than those identified in the manuscript, as, in fact, confirmed by Fig. 12. Further, while estimating the enhancement ratios for HCN and C2H6 with respect to CO, the authors do not take into account "the background" concentrations of these species. However, the simulation results shown in Fig. 12 indicate that the background concentrations can constitute more than half of the CO columns during the selected events. Therefore, the enhancement ratios reported in Table 5 can be quite different from the actual enhancement ratios in biomass burning emissions, and the corresponding discussion on page 14 is mostly irrelevant. Finally, I doubt that the lengthy source attribution procedure described in Section 3.3 is really necessary, especially taking into account the uncertainty of the simulation data. Would not the source attribution estimates be more reliable if they were obtained simply by averaging the model data over the whole event identified using the FTIR measurements?

Reply: The authors agree that Equation 3 does not only account for the ambient concentrations of each species, but also includes a contribution from the biomass burning sources. However, the contribution of the biomass burning sources to the fitted function is representative of an increase in the seasonal background of CO due to the accumulation of CO from biomass burning sources during the wildfire season as opposed to anomalous enhancements. These anomalous enhancements captured in the CO times series (as the result of a smoke plume passing over the site) are assumed to result in increased CO columns well above the seasonal background driven by biomass burning emissions. A statement on this was added to L234-237 of the revised manuscript.

The contribution of wildfire pollution may indeed be longer and stronger than that detected in the FTIR measurements, which may be limited as result of non-clear sky conditions and therefore may not capture the full duration of a wildfire plume. Furthermore, the long fire-affected periods observed in Figures 12-16 (Figures 7-10 of the revised manuscript) do not in reality correspond to the plumes observed in the FTIR measurements. The relative contribution of the the biomass burning sources have a cumulative influence, with increasing contribution to the CO column during the fire season. The detected events in the FTIR measurements are representative of an individual isolated event within the large domain of the tagged CO source regions.

The enhancement ratio does not take into consideration the background concentrations as doing so can introduce errors as a result of mixing of air masses during transport as well as the the uncertainty in calculating the background or ambient concentrations themselves. The enhancement ratio is defined as the slope or rate of change of the species of interest with respect to CO. Since, the enhancement ratio is calculated as the slope of the correlated fire-affected measurements, assuming a constant background over the fire-affected period and correcting for the background will not have an influence on the calculated slope. This assumption has been used extensively in past studies examining the enhancement ratios derived from FTIR measurements (e.g. Paton-Walsh et al., 2010, Vigouroux et al., 2012, Viatte et al., 2013, Viatte et al., 2015, Lutsch et al., 2016, Lutsch et al., 2019) and this has been noted in the revised manuscript on lines 260-264.

The source attribution discussion of Section 3.3 has been revised based on the reviewer's suggestion and added to the revised manuscript on L285-287.

Comment 1.5 — Abstract. It is not quite clear what the authors mean by saying about "ambient concentrations" in view of my previous comment. Furthermore, the manuscript discusses the column abundances, not the concentrations.

Reply: The authors have revised this statement to refer to the "seasonal background" used in this work and to also more accurately describe the method in response to the previous comment.

Comment 1.6 — P. 2, lines 15-28. Several major research directions (the Arctic climate, black carbon, boreal wildfires, and emissions wildfires) are discussed in just one paragraph. I suggest splitting this paragraph into smaller but logically linked paragraphs.

Reply: The authors have made this revision in the revised manuscript.

Comment 1.7 — Page 2, lines 34-37. I see a contradiction here: if reactive species are short-lived, then why long-range transport is a reason to measure their concentrations?

Reply: Short-lived reactive species that are measured using FTIR (e.g. C2H2, CH3OH, H2CO, HCOOH and NH3) may have lifetimes that range from days to weeks which may be long enough to undergo long-range transport to the Arctic (Viatte et al., 2015, Lutsch et al., 2016, Lutsch et al., 2019). Additionally, these species may have secondary sources within a smoke plume, while the injection of a smoke plume into the free troposphere may further extend their lifetime. Measuring these species by a network of FTIR instruments can provide insight into the potential for them to undergo long-range transport. A statement on this was added to L36-40 of the revised manuscript.

Comment 1.8 — Page 7, the last paragraph. It is not quite clear how the time series were obtained. Are the data shown in Figs. 2-4 are averages over all the measurements available for a given week over the period of sixteen years? Or, are they weekly-means averaged over the sixteen years? There is a similar question regarding the calculation of sigma.

Reply: The time series are the averages (and standard deviations) of all the measurements over the sixteen year period available for the given week of the year. The figure captions have been revised to clarify this.

Comment 1.9 — Page 8, lines 210-215 and 223-226. I suggest the authors should make a distinction between the facts evident in Fig. 2 and the assumptions which are not directly supported by the measurements discussed in Sect. 3.1.1. Section 3.1.2. How the a priori profiles were determined? Why the a priori profile standard deviation is shown only for the Thule site. What does the deviation of the retrieved profile from the a priori one signifies in the context of this study?

Reply: The authors have revised these statements (L333-334 and L347-348, respectively) where the contribution of wildfire contribution to CO is shown and discussed.

The a priori profiles are determined from a 40 year average (1980-2020) of the Whole Atmosphere Community Climate Model (WACCM). A statement on this was added to L370-374. A standard deviation was only shown for Thule as a monthly a priori profile was used, while all other sites used a single a priori profile.

Deviations of the retrieved profiles from the a priori are the result of the measurement and these profiles correspond to the column abundances presented here as stated on L375-L376.

Comment 1.10 — Page 12, line 354. The correlation coefficient value of 0.5 normally indicates a very weak correlation. How would the results of the analysis change if the threshold value of the correlation coefficient were chosen to be larger or smaller than 0.5?

Reply: We have revised the methods to use a higher cut-off value of r=0.6 to improve the reliability of the estimated emission ratios. In many cases, a strong correlation (r>0.8) was observed. It was found that a r∼0.6 generally corresponded to a fire-affected period based on a qualitative assessment of the GEOS-Chem time series. Decreasing the threshold of r below 0.5 for both HCN and C2H6 enhancement ratios resulted in a number false detections when no wildfire enhancement was observed in the GEOS-Chem time series. Increasing the threshold above 0.6 resulted in a number of missed detections, where all species were enhanced but may not be particularly well correlated.

Comment 1.11 — Page 12, lines 364-365. Why are the authors sure that AOD simultaneously enhanced with CO AERONET measurements provides evidence for wildfire emissions. Cannot these enhancements be due to strong anthropogenic pollution?

Reply: The authors agree that enhanced AOD and CO may also be indicative of anthropogenic pollution events; however, the AERONET data was used in conjunction with the GEOS-Chem time series to determine if the AOD was of wildfire origin. A statement on this was added on L237-246 of the revised manuscript.

Comment 1.12 — Page 15, line 443, and Fig.11. Can the authors explain why the oxidation of CH4 tends to have a maximum in winter when OH concentration in the northern hemisphere is minimal?

Reply: CO produced by CH4 oxidation follows the same seasonal cycle of CO. It is produced at lower-latitudes and is transported pole-ward where it accumulates during the winter months due to the lack of OH.

Reviewer 2

This paper presents source areas of measured CO and other gases, using the tag tracer experiments of GEOS-Chem. The CO emitted from the boreal wildfires are contributed to the episodic CO increase over the Arctic sites, mainly coming from North America and Asia. The topic of this study is interesting and the results of FTIR data is valuable, while there are no scientific new results in this manuscript (episodic increases due to wildfires are well known). In addition, this paper only shows the list of results and there is no sufficient discussion. Thus, I recommended major revision before publication.

Comment 2.1 — There are many figures which are not necessary needs. In addition, some figures can be summarized. For example, Figs. 11-13 are summarized to the percentage contributions to each site.

Reply: In response to the previous reviewers comments, the number of figures was reduced by moving the non-essential figures to the appendix. The authors believe the information of Figures 11-13 are best represented as figures rather than tables and therefore have left them as figures.

Comment 2.2 — The authors will improve the papers to include the descriptions of scientific new results and discussion related to these results.

Reply: This comment has been addressed in response to a similar comment made by Reviewer # 1.

Comment 2.3 — l.l. 470-475 The injection level and the transport pathway of CO are probably simulated in GEOS-Chem and the details will be analyzed.

Reply: The authors believe that this is outside the scope of this paper. The focus of the paper is on the use and the interpretation of the FTIR measurements presented. However, injection heights are simulated in GEOS-Chem as stated on L187-190.

Comment 2.4 — Typos. l. 545: 0.89 -> 0.86 maximum of 0.84 is only for Rikubetsu in Fig. 16

Reply: The authors have corrected this typo in the revised manuscript.

List of Revisions

Below is a list of the major changes made in the revised manuscript. All changes are shown in the marked version of the revised manuscript.

- Abstract was revised.
- Introduction was revised.
- Method Section 2.4 - Description of the FLEXPART model was added.
- Section 2.5 - Methods were revised.
- Section 3 - Results were explicitly separated from discussion.
- Section 3.1.2 - VMR profiles and averaging kernels combined into single subsection.
- Section 3.1.2 - Figures and non-essential text moved to the appendix.
- Section 3.2 - GEOS-Chem comparison to FTIR measurements moved before model results are presented, as suggested by reviewer 1.
- Section 3.2 - Non-essential plots were removed and values summarized in Table 3.
- Section 3.3 - Revised to reflect new results.
- Section 4 - Discussion separated from results.
- Section 4.1 - Emission ratio discussion was added.
- Section 5 - Conclusions revised to reflect new results.

Detection and Attribution of Wildfire Pollution in the Arctic and Northern Mid-latitudes using a Network of FTIR Spectrometers and GEOS-Chem

Erik Lutsch[1], Kimberly Strong[1], Dylan B.A. Jones[1], Thomas Blumenstock[2], Stephanie Conway[1], Jenny A. Fisher[3], James W. Hannigan[4], Frank Hase[2], Yasuko Kasai[5], Emmanuel Mahieu[6], Maria Makarova[7], Isamu Morino[8], Tomoo Nagahama[9], Justus Notholt[10], Ivan Ortega[4], Mathias Palm[10], Anatoly V. Poberovskii[7], Ralf Sussmann[11], and Thorsten Warneke[10]

[1]Department of Physics, University of Toronto, Toronto, ON, Canada
[2]Karlsruhe Institute of Technology, IMK-ASF, Karlsruhe, Germany
[3]Centre for Atmospheric Chemistry, University of Wollongong, Wollongong, NSW, Australia
[4]National Center for Atmospheric Research, Boulder, CO, USA
[5]National Institute for Information and Communications Technology (NICT), Tokyo, Japan
[6]Institute of Astrophysics and Geophysics, University of Liège, Liège, Belgium
[7]St. Petersburg State University, St. Petersburg , Russia
[8]National Institute for Environmental Studies (NIES), Tsukuba, Japan
[9]Institute for Space-Earth Environmental Research (ISEE), Nagoya University, Nagoya, Japan
[10]Institute of Environmental Physics, University of Bremen, Bremen, Germany
[11]Karlsruhe Institute of Technology, IMK-IFU, Garmisch-Partenkirchen, Germany

Correspondence: elutsch@physics.utoronto.ca

Abstract. We present a multi-year time series of column abundances of carbon monoxide (CO), hydrogen cyanide (HCN), and ethane (C_2H_6) measured using ~~Fourier transform~~ Fourier-transform infrared (FTIR) spectrometers at ten sites affiliated with the Network for Detection of Atmospheric Composition Change (NDACC). Six are high-latitude sites: Eureka, Ny-Ålesund, Thule, Kiruna, Poker Flat, and St. Petersburg, and four are mid-latitude sites: Zugspitze, Jungfraujoch, Toronto, and Rikubetsu. For each site, the inter-annual trends and seasonal variabilities of the CO time series are accounted for, allowing ~~ambient concentrations~~ background column amounts to be determined. Enhancements above ~~ambient levels~~ the seasonal background were used to identify possible wildfire pollution events. Since the abundance of each trace gas emitted in a wildfire event is specific to the type of vegetation burned and the burning phase, correlations of CO to the long-lived wildfire tracers HCN and C_2H_6 allow for further confirmation of the detection of wildfire pollution~~, while complementary measurements of aerosol optical depth from nearby AERONET sites confirm the presence of wildfire smoke~~. A GEOS-Chem tagged CO simulation with Global Fire Assimilation System (~~GFAS~~GFASv1.2) biomass burning emissions was used to determine the source attribution of CO concentrations at each site from 2003-2018. ~~The influence of the various wildfire sources is found to differ between sites while North American~~ For each detected wildfire pollution event, FLEXPART back-trajectory simulations were performed to determine the transport times of the smoke plume. Accounting for the loss of each species during travel, the enhancement ratios of HCN and C_2H_6 with respect to CO were converted to emission ratios. We report mean emission ratios with respect to CO for HCN and C_2H_6 of 0.0047 and ~~Asian boreal wildfires fires were found to be the greatest contributors to episodic CO~~

~~enhancements in the summertime at all sites~~0.0092, respectively, with a standard deviation of 0.0014 and 0.0046, respectively, determined from 23 boreal North American wildfire events. Similarly, we report mean emission ratios for HCN and C_2H_6 of 0.0049 and 0.0100, respectively, with a standard deviation of 0.0025 and 0.0042, respectively, determined from 39 boreal Asian wildfire events. The agreement of our emission ratios with literature values illustrates the capability of ground-based FTIR measurements to quantify biomass burning emissions. We provide a comprehensive dataset that quantifies HCN and C_2H_6 emission ratios from 62 wildfire pollution events. Our dataset provides novel emission ratio estimates, which are sparsely available in the published literature, particularly for boreal Asian sources.

1 Introduction

The Arctic is a major receptor for pollution from mid-latitude regions (Stohl et al., 2006; Law and Stohl, 2007; Shindell et al., 2008). Boreal wildfires are well known to have considerable impacts on the Arctic atmosphere and climate (Amiro et al., 2009; Warneke et al., 2009). ~~Black carbon, also known as soot, is a strong contributor to global warming (Bond and Sun, 2005 and references therein). Black carbon in the Arctic has been studied extensively and it has been found that a substantial fraction of Arctic black carbon is transported from boreal wildfires (Stohl et al., 2006; Sharma et al., 2004, 2006; Wang et al., 2011; Sharma et al., 201~~ ~~. Black carbon is well known to contribute to episodes of poor air quality and warm the atmosphere by absorbing radiation and covering snow- and ice-covered surfaces, indirectly exerting snow-albedo effects (McConnell et al., 2007; Ramanathan and Carmichael, 20~~ ~~. Boreal wildfires may also influence the carbon cycle (Conard and Ivanova, 1997; Schimel and Baker, 2002; Mack et al., 2011; Santín et al~~ ~~. In boreal wildfire events, considerable quantities of carbon monoxide (CO), carbon dioxide (CO_2) and methane () are emitted (van der Werf et al., 2017). Boreal wildfire emissions of CO, CO_2 and are dependent on burning phase, with greater emissions of CO_2 and from flaming combustion, with CO emissions dominated by smoldering and residual phase combustion (Andreae and Merlet, 2001 and the references therein). Emissions of CO, , nitrogen oxides (NO_X) and volatile organic compounds (VOCs) from wildfires may then be oxidized to form CO_2 and ozone (O_3) (Levine, 2003)~~In the Northern hemisphere, boreal wildfires are a dominant source of particulate and trace gas emissions, brought on by persistent warm and dry conditions resulting in increased fire risk and ignition from lightning. Both periods of greater fire risk and lighting activity are expected to occur with increasing frequency at Northern high-latitudes as a result of anthropogenic-induced climate change (Krause et al., 2014; Verave . The magnitude and intensity of boreal wildfire activity are also projected to increase with future climate change (Amiro et al., 2009; Wester .

~~Wildfires also~~ Boreal wildfires contribute to the emission of a large number of reactive trace gas species, including ~~VOCs~~volatile organic compounds (VOCs), which promote the production of tropospheric ozone (O_3) and the formation of aerosols (Jaffe et al., 1999, 2004; Parrington et al., 2013; Wentworth et al., 2018) and therefore negatively impact air quality. Emissions of these species remain highly uncertain as a result of the dependence of emissions on fuel types (Andreae and Merlet, 2001; Akagi et al., 2011; Andreae, 2019); emissions from a particular event are strongly influenced by local meteorology, which has a direct influence on the burning phase and the emission of each species (Yokelson et al., 1996, 1999, 2003; Goode et al., 1999, 2000). Additionally, these reactive species are short-lived~~and are not easily measured downwind of the fire source. Wildfire~~

~~plumes may be subject to~~ , but may have lifetimes that range from days to weeks, which may be long enough for them to undergo long-range transport ~~, and therefore~~ to the Arctic. Furthermore, these species may have secondary sources within a smoke plume, while the injection of a smoke plume into the free troposphere may further extend their lifetime. Therefore it is necessary to measure the concentrations of these reactive trace gas species downwind in order to predict their influence on a global scale.

~~In the Northern hemisphere, boreal wildfires are a dominant source of biomass burning, brought on by persistent warm and dry conditions resulting in increased fire risk and ignition from lightning. Both periods of greater fire risk and lighting activity are expected to occur with increasing frequency at Northern high-latitudes as a result of anthropogenic-induced climate change (Krause et al., 2014; Veraverbeke et al., 2017). The magnitude and intensity of boreal wildfire activity are also projected to increase with future climate change (Amiro et al., 2009; Westerling et al., 2006; Flannigan et al., 2009; Wotton et al., 2010; Boulanger et a~~

~~.~~

Quantifying the influence of biomass burning on the Arctic atmosphere requires long-term, dedicated measurements of the transported emissions in the Arctic. The Arctic is a difficult region to study as a result of the lack of dedicated measurement stations. Ground-based solar-absorption Fourier-transform infrared (FTIR) spectrometers have proven to be a useful tool for quantifying trace species abundances. The Network for the Detection of Atmospheric Composition Change (NDACC; www.ndacc.org; De Mazière et al., 2018) provides a global network of FTIR instruments that routinely measure the biomass burning tracers CO, hydrogen cyanide (HCN) and ethane (C_2H_6), in addition to a multitude of other trace gas species. The FTIR instruments of NDACC have previously been utilized to study biomass burning emissions. Zhao et al. (1997, 2000, 2002) identified Asian and Siberian biomass burning sources as major contribution to the measured concentrations of CO, HCN and C_2H_6 from ground-based FTIR measurements in Rikubetsu (43°N, 143°E), Japan. Paton-Walsh et al. (2004, 2005, 2010) used solar-absorption FTIR measurements in Australia (Darwin (34°S, 150°E) and Wollongong (34°S, 150°E)) to quantify emissions of various trace gas species from Australian wildfires. Vigouroux et al. (2012) examined the influence of biomass burning in Southern Africa and Madagascar on FTIR measurements of HCN, C_2H_6, acetylene (C_2H_2), methanol (CH_3OH) and formic acid (HCOOH) at Reunion Island (21°S, 55°E) located in the Indian Ocean.

More recently, FTIR measurements in the Arctic have proven to be particularly useful, providing observational coverage of trace gas species where measurements from other platforms are scarce or non-existent. Viatte et al. (2013) identified enhancements of CO, HCN and C_2H_6 in FTIR measurements at Eureka (80°N, 86°W), Canada that were attributed to the 2010 Russian wildfires. A subsequent study by Viatte et al. (2014) demonstrated the utility of FTIR in measuring the biomass burning species acetylene (C_2H_2~~,~~), methonal (CH_3OH~~, HCOOH~~), formic acid (HCOOH) and formaldehyde (H_2CO) at Eureka. Analogous retrievals of these species were also performed for measurements from a second high-Arctic site at Thule (77°N, 69°W), Greenland and emission ratios and emissions factors were derived for these species from FTIR measurements at both Thule and Eureka by Viatte et al. (2015). Measurements of ammonia (NH_3) by solar-absorption FTIR spectroscopy was first demonstrated by Paton-Walsh et al. (2004) and later by Dammers et al. (2015). Lutsch et al. (2016) provided the first measurements of NH_3 in the ~~high-Arctic~~ high Arctic and determined emission ratios and ~~emissions~~ emission factors for the 2014 Northwest Territories wildfires of Canada. The contribution of 2017 Canadian wildfires to NH_3 in the Arctic was examined using FTIR measurements at Eureka and Thule by Lutsch et al. (2019). The results of these studies highlight the ability of FTIR spectroscopy to measure a number of trace gas species, many of which are difficult to assess using satellite-based or other platforms. Furthermore, the ability of ground-based FTIR instruments to measure a variety of trace gas species over a long-term time period is particularly useful in order investigate composition of transported wildfire plumes.

~~However, each of these~~ These previous studies have illustrated the ability of FTIR measurements to quantify biomass burning emissions by determining the emission ratios and emission factors of various trace gas species. Accurate emission ratios and emission factors are required to simulate biomass burning in chemical transport models; however, previously reported values are highly variable (Andreae and Merlet, 2001; Akagi et al., 2011; Andreae, 2019 and the references therein) as a result of the natural variability of emissions as well as possible discrepancies in sampling methods.

Each of these previous mentioned FTIR studies have only considered individual events or events that occurred in a short time series. Measurements using FTIR have been routinely made since the mid-1980s (Zander et al., 2008) and the number of measurement sites have increased since the inception of the Network for Detection of Stratospheric Change (NDSC; Kurylo, 1991) in 1991, which has been formally known as NDACC since 2005 (De Mazière et al., 2018). Several global FTIR sites have been measuring the biomass burning tracers CO, HCN and C_2H_6 over the last two decades. Yurganov (2004) identified enhanced CO columns in 1998 detected using FTIR measurements at several Northern mid- to high-latitude NDACC FTIR sites from 1996-2002. The 1998 CO anomaly was attributed to Siberian wildfires. A similar study by Yurganov et al. (2005) examined the 2002 and 2003 CO anomalies from Siberian wildfires using satellite-based, in situ and FTIR measurements in the Northern hemisphere. Currently, no study has explicitly examined the long-term and inter-annual variability of biomass burning species using FTIR measurements. A recent study by Petetin et al. (2018) investigated the impact of biomass burning on CO concentrations measured by the In-service Aircraft for a Global Observing System (IAGOS), which focused on airport clusters in Europe, North America, Asia, India and Southern Africa over the period 2002-2017. To our knowledge, no ~~study of this kind has been performed for~~ previous study has assessed the contribution of biomass burning to CO measurements in the Arctic and high-latitude regions.

In this paper, the influence of wildfires on atmospheric composition from 2003-2018 is examined using FTIR measurements of multiple trace gas species from three high-Arctic NDACC sites: Eureka, Canada; Ny-Ålesund, Norway and Thule, Greenland. Three Arctic sites are also included: Kiruna, Sweden; Poker Flat, Alaska and St. Petersburg , Russia. Additional measurements are obtained at four mid-latitude sites: Zugspitze, Germany; Jungfraujoch, Switzerland; Toronto, Canada and Rikubetsu, Japan. Potential wildfire pollution events are first identified in the CO time series at each site through the detection of anomalous enhancements of CO. For the CO enhancements detected at each site, enhancement ratios of HCN and C_2H_6 with respect to CO are calculated. Since CO, HCN and C_2H_6 are co-emitted from biomass burning sources, a ~~strong~~ linear correlation for the enhancement ratios of HCN and C_2H_6 indicate wildfire pollution events. The detection of wildfire pollution at each site was further confirmed using total aerosol optical depth (AOD) measurements from adjacent AERONET (Aerosol Robotic Network) sites. A GEOS-Chem tagged CO simulation from 2003-2018 was performed to identify the source attribution for the detected events at each FTIR site in addition to quantifying the contribution to CO from various biomass burning source regions.

This paper quantifies the impact of more than 60 detected wildfire events, on six Arctic sites and four mid-latitude sites using FTIR measurements of multiple trace gas species. In addition to replicating published emissions ratios, we provide, for the first time, a comprehensive set of emission ratios for HCN and C_2H_6 across multiple wildfire events. The reported emission ratios comport with published values, demonstrating the ability of FTIR to capture wildfire plumes, as well as provide much needed longer-term estimates of emissions ratios and their variability. Furthermore, we identify and characterize the contribution of biomass burning to CO measurements specifically at each FTIR site.

The structure of this paper is summarized as follows. ~~Section 2~~ Sections 2.1-2.4 provides an overview of each ~~site and presents the retrieved products for CO, HCN and . Descriptions of the AERONET data and~~ FTIR site, the GEOS-Chem tagged CO simulation~~used in this study are also discussed in this section~~, AERONET data, and FLEXPART model used in the this study. Section 2.5 describes the methods used to detect wildfire pollution events in the FTIR time series. A comparison of the GEOS-Chem model to FTIR measurements is provided in Section 3.2. The retrieved FTIR products for CO, HCN and C_2H_6 are presented ~~and discussed~~ in Section 3.1 ~~. The method for the detection of biomass burning pollution events is described in Section 2.5.1 and source attribution using the GEOS-Chem tagged CO simulation is shown in Section ??. The contribution of the GEOS-Chem CO tracers to FTIR measurements are presented and discussed~~and the detected wildfire pollution events at each FTIR site are presented in Section 3.3. In Section 4.1, the calculated emission ratios are discussed, while in Section 4.2~~and a comparison of the GEOS-Chem CO time series to FTIR measurements at all sites is shown in Section 3.2~~, a description of the wildfire contribution to CO measurements at each site is provided. The conclusions and summary of this study are highlighted in Section 5.

2 Methods

2.1 FTIR Sites and Retrievals

The NDACC FTIR sites included in this study were selected to provide coverage of high- and mid-latitude regions and are listed in Table 1. Due to the broad spectral range measured at high resolution, typically from 700-4400 cm^{-1} at 0.0035 cm^{-1} resolution, a multitude of trace gas species may be retrieved from solar-absorption FTIR measurements. Measurements of CO, HCN, and C_2H_6, all of which are standard products of the NDACC ~~IRWG~~ Infrared Working Group (IRWG) are the focus of this study. Retrievals of each species were performed by processing of solar-absorption spectra using the SFIT4 (https://wiki.ucar.edu/display/sfit4/) or PROFITT9 (Hase et al., 2004, for Kiruna and Zugspitze) retrieval algorithm which use the optimal estimation method (Rodgers, 2000) to obtain volume mixing ratio (VMR) profiles and integrated column abundances by iteratively adjusting VMR profiles to minimize the difference between the measured and calculated spectra (Pougatchev et al., 1995; Rinsland et al., 1998). Further details of the instrumentation and retrievals for each FTIR site are given in the references listed in Table 1.

2.1.1 High-Arctic Sites

The highest-latitude FTIR site of NDACC is Eureka, located on Ellesmere Island in the Canadian Archipelago. It has been shown in previous studies that Eureka is regularly influenced by the transport of boreal wildfire emissions from North America and Asia (Viatte et al., 2013, 2014, 2015; Lutsch et al., 2016, 2019). Located approximately 500 km from Eureka is the site Thule on the Northwest coast of Greenland, which provides complementary measurements to Eureka as wildfire pollution events detected at Eureka are generally also observed in measurements at Thule (Viatte et al., 2015; Lutsch et al., 2019). Ny-Ålesund in Spitsbergen, Norway is the second highest-latitude FTIR site of NDACC. Ny-Ålesund is isolated from the direct influence of anthropogenic and wildfire emissions, but is affected by the long-range transport of pollution originating from Northern hemisphere mid-latitudes. For the purposes of this study, Eureka, Ny-Ålesund and Thule will be referred to as the “clean" high-Arctic (>75°N) sites because they are free of local pollution sources.

2.1.2 Arctic Sites

The Arctic sites are defined as those located between 60°N and 75°N, and include Poker Flat, Alaska; Kiruna, Sweden; and St. Petersburg, Russia. Poker Flat is strongly influenced by the transport of anthropogenic pollution from Siberia and Asia (Kasai et al., 2005b). Asian anthropogenic emissions have been found to be a predominant source of pollution in Alaska, with a greater influence in years with strong El Niño conditions (Fisher et al., 2010). Siberian wildfires are a substantial source of summertime pollution in Alaska (Jaffe et al., 2004; Warneke et al., 2009) in addition to local wildfires within the boreal forests of Alaska. It should be noted that for this reason, and the dependence of FTIR measurements on clear-sky conditions, smoke plumes within Alaska may prevent measurements by FTIR. As a result, summertime measurements at Poker Flat can be sparse.

Kiruna is mainly influenced by anthropogenic emissions from mid-latitude Europe; however, aerosol smoke layers from injection of Canadian wildfire emissions into the lower stratosphere have been identified in the past at Kiruna (Fromm et al., 2000). Similarly, the urban site of St. Petersburg would be most sensitive to local sources within Europe. Both Kiruna and St. Petersburg may sample the long-range transport of boreal Asian plumes that could circle the Northern Hemisphere (Damoah et al., 2004), although such plumes would be well aged and diluted. Through injection of wildfire emissions into the upper troposphere and lower stratosphere, North American boreal wildfire plumes may be efficiently transported to Europe (Khaykin et al., 2018; Hu et al., 2019). Although the effects of the long-range transport of wildfire emissions on air quality are likely to be minimal, they can have an influence on tropospheric composition of long-lived species.

2.1.3 Alpine Sites

Both Zugspitze and Jungfraujoch are considered clean Alpine sites, isolated from local pollution sources and therefore provide measurements that are representative of background concentrations of central Europe (Franco et al., 2015). For the purpose of this study, as the result of the close proximity between the two sites (∼200 km), Zugspitze and Jungfraujoch are considered to be complementary to one another. Differences in measured column amounts between the two sites as a result of long-range transport are likely due to their altitude differences, 2964 m a.s.l. and 3580 m a.s.l. for Zugspitze and Jungfraujoch, respectively.

It has been previously shown that Zugspitze is weakly influenced by nearby pollution sources, while Jungfraujoch is considered a remote site, mainly influenced by long-range transport (Henne et al., 2010). However, as a result of the high altitudes of these sites, the measured composition is largely driven by long-range transport in the mid to upper troposphere.

2.1.4 Mid-latitude Sites

Toronto, an urban site, is most sensitive to local pollution sources in southeast Canada and the United States (Whaley et al., 2015) and periodically subject to wildfire pollution episodes as demonstrated by ~~Griffin et al. (2013); Whaley et al. (2015)~~ Griffin et al. (2013) and Whaley et al. (2015). Rikubetsu, located in Hokkaido, Japan, is free of considerable local anthropogenic pollution sources, with contributions of CO mainly due to transported Asian anthropogenic emissions (Zhao et al., 2000). In the summertime, Rikubetsu is influenced by the transport of biomass burning pollution from within Asia (Li et al., 2000), while the region of Hokkaido is often affected by pollution episodes from Siberian wildfires of boreal Asia (Jeong et al., 2008; Tanimoto et al., 2000; Yasunari et al., 2018).

2.2 GEOS-Chem

To interpret the influence of anthropogenic, chemical, and biomass burning sources on CO columns at each FTIR site, the GEOS-Chem chemical transport model is used (http://geos-chem.org/; Bey et al., 2001b) in a tagged simulation of CO at a horizontal resolution of 2°×2.5° with 47 vertical hybrid levels. GEOS-Chem version 12.1.1 (The International GEOS-Chem User Community, 2018) was used and driven by global meteorological inputs from the MERRA-2 (Modern-Era Retrospective Analysis for Research and Applications, Version 2; Gelaro et al., 2017) from the NASA Global Modeling and Assimilation Office (GMAO). MERRA-2 is produced with the GMAO/GEOS-5 (Goddard Earth Observing System) Data Assimilation System Version 5.12.4. The GEOS-Chem simulation was initialized with a 1-year spin-up from 1 January 2002 to 1 January 2003. Chemical and transport operator time-steps of 1 hr and 10 min, respectively, were used.

Biomass burning emissions are from GFASv1.2 (Global Fire Assimilation System, Kaiser et al., 2012; Giuseppe et al., 2018) which assimilates Moderate Resolution Imaging Spectroradiomter (MODIS) burned area and fire radiative power (FRP) products to estimate emissions for open fires. GFASv1.2 emissions have a 0.1°×0.1° horizontal resolution with ~~3-hourly~~ daily temporal resolution. GFAS was chosen for the availability of emissions over the analysis period from 2003-2018. Global anthropogenic emissions are provided from the EDGARv4.3.1 (Emission Database for Global Atmospheric Research, Crippa et al., 2016) emissions inventory, overwritten by regional emission inventories in the Northern hemisphere as described in Fisher et al. (2010). Biogenic emissions of precursor VOCs are from the Model of Emissions of Gases and Aerosols from Nature (MEGANv2.1; Guenther et al., 2012) and biofuel emissions are taken from Yevich and Logan (2003).

The main loss mechanism for CO is from photochemical oxidation by the hydroxyl radical (OH). The OH fields are prescribed in the tagged CO simulation and were obtained from the TransCom experiment (Patra et al., 2011) which implements semi-empirically calculated tropospheric OH concentrations from Spivakovsky et al. (2000) to reduce the high bias of OH from the GEOS-Chem full-chemistry simulation (Shindell et al., 2006). Surface emissions in GEOS-Chem are released within the boundary layer, and boundary layer mixing is implemented using the non-local mixing scheme of Holtslag and Boville

(1993). Biomass emissions are released by uniformly distributing emissions from the surface to the mean altitude of maximum injection based on the injection height information as described in Rémy et al. (2017) which includes an injection height parameterization by Sofiev et al. (2012) and a plume rise model by Freitas et al. (2007).

GEOS-Chem version 12.1.1 tagged CO simulation includes the improved secondary CO production scheme of Fisher et al. (2017), which assumes production rates of CO from $\mathrm{CH_4}$ and NMVOC oxidation from a GEOS-Chem full-chemistry simulation therefore reducing the mismatch between the CO-only simulation and the full-chemistry simulation. The anthropogenic source regions are shown in Figure 1, while biomass burning source regions are implemented following the standard GFED (Giglio et al., 2013) regions and are also shown in Figure 1.

2.3 AERONET

The Aerosol Robotic Network (AERONET; https://aeronet.gsfc.nasa.gov; Holben et al., 1998) is a federation of ground-based remote sensing aerosol networks established by NASA and PHOTONS (PHOtométrie pour le Traitement Opérationnel de Normalisation Satellitaire; Univ. of Lille 1, CNES, and CNRS-INSU). AERONET consists of a network of CIMEL sun photometers which provides globally distributed observations of spectral aerosol optical depth (AOD). At each AERONET site, observations are recorded every 15 minutes and are cloud screened. Inversion of aerosols products and cloud screening for the AERONET Version 3 database are described in (Giles et al., 2019). AERONET sites selected for this study were based on the availability of data during the operational period of the FTIR instruments and proximity to the FTIR site. The selected AERONET sites nearest to the NDACC FTIR sites are listed in Table 1.

2.4 FLEXPART

The FLEXPART (FLEXible PARTicle, Stohl et al., 2005) Lagrangian transport model version 10.02 is used to diagnose the potential emission sensitivity (PES) of FTIR measurements in order to estimate the travel times of identified wildfire plumes at each FTIR site. The model is driven by meteorological data from the National Centers for Environmental Prediction (NCEP) Climate Forecast System (CFSv2) 6-hourly product (Saha et al., 2011) at 0.5°×0.5° horizontal resolution. In this study, an ensemble of 24,000 particles are released from the location of each FTIR site for each day of fire-affected measurements. The particles are released from the surface to an altitude of 12.71 km at each FTIR site, which corresponds to the FTIR tropospheric column. The FLEXPART model is run backwards in time for a total of 14 days, simulating the transport of the released particles. The FLEXPART output is the surface residence time of the released particles in each 0.5°×0.5° model output grid box. The residence time is related to the PES and is indicative of the sensitivity of the released particles to source emissions.

2.5 Detection and Attribution of Wildfire Pollution Events

2.5.1 Enhancement Detection in FTIR CO Time Series

As will be shown in Section 3.1.1, a seasonal cycle of CO is observed, with the amplitude varying by site location. Over a long time series, CO may be subject to inter-annual trends as a result of changing emissions of CO and its precursors. Additionally, non-clear sky conditions and instrument downtime result in periodic gaps in measurements and non-uniform time intervals between measurements. As a result of these factors it can be difficult to determine baseline or ambient column amounts of CO and therefore to detect enhancements of CO in the FTIR time series. To mitigate these influences, we account for the seasonal cycle and inter-annual variability of the CO time series measured at each FTIR site following Thoning et al. (1989):

$$C(t) = a_0 + a_1 t + a_2 t^2 + \sum_{n=1}^{4} b_n \cos(2\pi n t) + c_n \sin(2\pi n t), \tag{1}$$

where C is the CO column amount as a function of time t. The coefficients a_n account for the inter-annual trends of CO, while the fourth-order Fourier series with coefficients b_n and c_n captures the seasonal cycle of CO. The choice of order for both the polynomial and Fourier components of the fits were limited to third and fourth order, respectively, following past studies (Thoning et al., 1989; Zellweger et al., 2009).

Enhancements in CO are identified following Zellweger et al. (2009). First, the fitted function is subtracted from the data to yield the residual. Assuming a normal distribution of baseline values around the fitted function, the negative residual is mirrored into the positive direction. Enhanced CO measurements are defined as those greater than a specified threshold of the mirrored residual above the fitted function. The threshold is defined as a multiple of the standard deviation σ of the mirrored negative residual. The threshold is 1σ for all sites, with the exception of Rikubetsu and Poker Flat where a 2σ standard deviation was used as a result of the greater variability CO due to nearby Asian anthroponenic and biomass burning sources respectively. It should be noted that the contribution of the biomass burning sources to the fitted function of Equation 1 is representative of an increase in the seasonal background of CO due to the accumulation of CO from biomass burning sources during the wildfire season. Enhanced CO measurements detected by the method described above would therefore correspond to anomalous enhancements which exceed the seasonal background.

For each event, all fire-affected measurements are found based on a qualitative assessment of the CO time series in conjunction with GEOS-Chem CO and AERONET AOD time series. Periods of fire-affected measurements are determined for periods in which an increase in the GEOS-Chem total biomass burning contribution to CO is observed. The total biomass burning contribution of is defined as the sum of all biomass burning tracers in Table 2. The AERONET AOD provides additional evidence for the presence wildfire smoke when enhanced AOD is observed simultaneously with enhanced FTIR CO and GEOS-Chem biomass burning CO. It should be noted that enhanced AOD may also be the result of anthropogenic pollution; however, enhanced AOD is likely of wildfire origin when simultaneously enhanced with GEOS-Chem biomass burning CO. Furthermore, aerosol scavenging from a smoke plume may result in the absence of enhanced AOD (Franklin et al., 2014). For these reasons, AOD is only used as a supplementary means of identifying wildfire pollution.

2.5.2 Trace Gas Correlations

To isolate potential wildfire pollution events, we exploit the fact that trace gas emissions from wildfires are specific to burning phase and vegetation type (Ward and Hardy, 1991; Yokelson et al., 1999; Andreae and Merlet, 2001; Yokelson et al., 2009; Akagi et al., 20 and therefore it would be expected that emissions of CO, HCN and C_2H_6 originating from a wildfire source would be correlated within a plume. Emissions at the fire source are characterized by the emission ratio (ER; Andreae and Merlet, 2001; Akagi et al., 2011) relative to CO, which quantifies the amount of a trace gas species emitted relative to the amount of CO emitted. Since FTIR observations of this kind are measuring the emissions downwind of the source, the enhancement ratio (EnhR; Lefer et al., 1994) is considered:

$$\mathrm{EnhR_X} = \frac{\mathrm{d[X]}}{\mathrm{d[CO]}} \tag{2}$$

where [X] is the column amount of the trace gas of interest, and [CO] is the column of CO. The enhancement ratio is related to the emission ratio with the influence of plume aging by chemical loss, deposition and dilution of the plume during transport. Lifetimes of CO, HCN and C_2H_6 are generally longer than plume transport times which range from several days to approximately two weeks (Damoah et al., 2004) and therefore these species do not undergo considerable chemical loss. Furthermore, we do not take into account the background concentrations, which can cause uncertainty in interpreting the enhancement ratio as the ambient conditions are likely to vary along the plume trajectory (Yokelson et al., 2013). This assumption has been employed extensively in past studies of wildfire emissions using FTIR (Paton-Walsh et al., 2010; Vigouroux et al., 201 as taking into account a constant background of each species does not influence the slope of the trace gas correlations.

To calculate the enhancement ratios from the FTIR measurements, the detected CO enhancements for each event were paired with the nearest HCN and C_2H_6 measurement taken within 1 hr at all sites with the exception of St. Petersburg and Toronto where a 2 hr window was used. The time interval was chosen to maximize the number of pairs since CO, HCN and C_2H_6 are measured using different spectral filters and hence the measurements do not occur simultaneously. For events with paired measurements of HCN or C_2H_6 with CO that are fewer than 6, the event is omitted. Setting a minimum number of pairs mitigates the potential of false detections as a result of spurious measurements.

The unified least-squares fitting procedure of York et al. (2004) which accounts for errors in both the ordinal and abscissa coordinates was used to determine a linear regression for the paired fire-affected measurements. The errors correspond to the reported retrieval uncertainties of the respective species. The slope of the linear regression is the enhancement ratio for the respective species defined in Equation 2. To identify enhancements due to wildfire pollution events, we require that the correlation coefficient (r) be greater than or equal to 0.6 for both the enhancement ratios of HCN and C_2H_6, unless otherwise stated.

HCN is retrieved from NDACC Filter 2 measurements, which is generally covered at least once per measurement sequence of all filters. Similarly, C_2H_6 is retrieved through filter NDACC filter 3. All filters have a different response to the input solar beam intensity and therefore, the measurement noise may vary between subsequent measurements of different filters. For this reason, adequate signal may not be obtained through all filters in the case of partially cloudy or non-clear sky conditions. It was found that for all sites, with the exception of Jungfraujoch, there are a greater number of CO measurements than HCN or C_2H_6. Because of this non-uniform distribution of measurements, the number of detected wildfire events is limited by the number of paired measurements for HCN or C_2H_6 with CO. For this reason, for Ny-Ålesund, Poker Flat and Rikubetsu, the enhancement ratio correlation criteria were omitted, resulting in a lower confidence for the detected wildfire pollution events.

Lastly, source attribution of the detected wildfires events was performed using the GEOS-Chem tagged CO simulation. For each event, the mean contribution of each of the biomass burning CO tracers over the period of the event was determined. The source region was then attributed to the CO tracer for which the mean contribution was a maximum.

2.6 Estimation of Plume Travel Times

For each of the detected wildfire pollution events at each FTIR site, the travel times of the plume from the source region to the FTIR site was determined as follows. For each day of fire-affected measurements, the FLEXPART model was initialized releasing an ensemble of 24,000 air-tracer particles over a 24 hr period. Particles were released from the surface of the FTIR site to a maximum altitude of 12.71 km, corresponding to the FTIR tropospheric columns used in this study. The FLEXPART model was run backwards in time for 14 days to yield the surface residence time of the released particles at a temporal resolution of 3 hrs and horizontal resolution of $0.5°\times0.5°$ with global coverage. The daily GFAS global CO emissions were regridded from $0.1°\times0.1°$ to $0.5°\times0.5°$ to match the horizontal resolution of the FLEXPART output.

For each day of the FLEXPART output, the daily total residence time in each model grid box was determined. The product of GFAS CO emissions (molec s^{-1}) and the residence time (s) of the FLEXPART air-tracer particles is indicative of the sensitivity of the released particles to wildfire CO emissions. The travel time for each FLEXPART simulation is then estimated by the number of days backwards in time for which the sensitivity is a maximum for the identified wildfire source region of the respective event. A mean travel time for each plume is determined by the mean of all travel times for each day of fire-affected measurements in the identified event; the standard deviation is an estimation of the uncertainty.

2.7 Emission Ratios

The enhancement ratios (Section 2.5.2), which were used to isolate wildfire pollution events, and the travel times (Section 2.6) were used to calculate the emission ratio (ER) of the respective trace gas species. The emission ratio represents the wildfire source emissions, assuming the plume was unaged (Lefer et al., 1994). To calculate the emission ratio, we assume the first-order loss of each species following Viatte et al. (2013, 2015) and Lutsch et al. (2016). The emission ratio may then be related to the enhancement ratio as:

$$\mathrm{ER}_X = \mathrm{EnhR}_X \cdot \frac{\exp\left(\frac{t}{\tau_X}\right)}{\exp\left(\frac{t}{\tau_{CO}}\right)}. \tag{3}$$

where X is the trace gas of interest, t is the plume travel time and τ if the lifetime of the species. We assume lifetimes of 30, 75 and 45 days for CO, HCN and C_2H_6, respectively, following Viatte et al. (2013, 2015); Lutsch et al. (2016). For each identified wildfire event the emission ratio of HCN and C_2H_6 is calculated using Equation 3 and mean travel time for the event. The uncertainty of the calculated emission ratios include the enhancement ratio uncertainty, determined from the standard error of the linear regression, and the travel time uncertainty. The uncertainty of the lifetime of each species was not included as the lifetime can be variable during plume transport and therefore cannot be quantified.

3 Results~~& Discussion~~

3.1 Retrieved FTIR Products

3.1.1 Time Series

The weekly-mean time series of CO, HCN and C_2H_6 tropospheric partial columns for each site are shown in Figures 2, 3 and 4 respectively. The tropospheric partial columns are the integrated column amounts from the surface to an altitude of 12.71 km at each site. In this study, all presented column amounts correspond to this partial column for CO, HCN and C_2H_6. The weekly mean is taken over all years of measurements for the respective species at each site, while the shaded region indicates a 1σ deviation from the mean. For all sites, the seasonal cycle of CO shows a maximum in winter and early spring (February-March), with decreasing total columns through the spring. The main sources of CO are the combustion of fossil fuels and biomass burning, while oxidation of VOCs and CH_4 are also a considerable source (Holloway et al., 2000). The main sink of CO is due to reaction with OH, leading to a lifetime of approximately 1-2 months (Bey et al., 2001a). In winter and spring months, decreased sunlit hours limits OH production by photolysis of ozone, therefore minimizing the loss of CO. The seasonal cycle of OH largely drives the seasonal variations of CO. Transport of CO from mid-latitude to high-latitude regions also contributes to the seasonal cycle as the isentropic transport is greater in the winter and spring months (Klonecki, 2003; Stohl et al., 2006). Furthermore, the stronger seasonal cycle of OH production also contributes to the greater seasonal amplitudes at high latitudes as observed in Figure 2.

Enhanced tropospheric columns of CO are observed in the summertime, mainly in July-September at all sites as illustrated in Figure 2 as a result of the hemispheric influence of boreal wildfires (Honrath, 2004). These enhancements are most pronounced at the clean high-Arctic sites of Eureka and Thule, which are strongly influenced by boreal fires in North America and Asia ~~. Similar enhancements are also observed at the other Arctic sites of Ny-Ålesund and Kiruna, but are not as pronounced, which is partly due to the longer transport times to these sites~~as will be shown in Section 4.2. Ny-Ålesund also exhibits an increase in CO beginning in August as a result of the accumulation of CO from Northern Hemisphere biomass burning sources. Poker Flat, located in the boreal forests of Alaska is greatly influenced by boreal wildfire emissions in these regions; however, in many instances these events result in smokey conditions that prevent FTIR measurements. As a result detection of enhancements at Poker Flat are likely to be underestimated due to the strong influence of wildfire smoke.

A slight increase in CO concentrations is observed at Zugspitze and Jungfraujoch as a result of the long-range transport of boreal wildfire emissions. Emissions from these events are often lofted into the free troposphere where long-range transport is ~~favoured~~ favored (Jaffe et al., 2004; Val Martin et al., 2006). However, the transport of emissions over continental scales results in the dilution of the smoke plume and therefore, the enhancements observed at Zugspitze and Jungfraujoch are not as pronounced as for the other sites.

St. Petersburg and Toronto are urban sites that are strongly influenced by local anthropogenic sources, but enhanced columns of CO are observed in July and August as a result of the boreal wildfire influence as will be shown in Section 4.2. Rikubetsu is strongly affected by anthropogenic CO sources from Asia, resulting in the large variability of CO (Zhao et al., 1997, 2002). The greatest enhancements at Rikubetsu are observed in July and August, due to boreal Asian wildfires in Siberia as will discussed in Section 4.2.

HCN has a long atmospheric lifetime ranging from days to months, while its dominant source is due to biomass burning emissions (Li et al., 2000, 2003, 2009). Plant and fungal emissions represent a minor source of HCN, while dry deposition to the ocean and oxidation by OH are the main sinks (Cicerone and Zellner, 1983). As a result, HCN will accumulate in the Northern hemisphere in the summer months due to the influence of wildfire and biogenic emissions. The seasonal cycle of HCN peaks in the summer months with low total columns in the winter and fall as illustrated in Figure 3. A sharp maximum is observed in August at the high-Arctic sites (Eureka, Thule and Ny-Ålesund) due to activation of its biogenic sources and the onset of wildfire emissions. A similar increase in the HCN total columns is observed at the high-latitude sites (Kiruna, Poker Flat and St. Petersburg), although not as pronounced. For Toronto, enhanced total columns are also observed in August due to wildfires, consistent with the CO time series. Rikubetsu shows the greatest concentrations of HCN in the spring in May, with a secondary peak in August. The springtime enhancements of HCN are due to the earlier onset of East and Southeast Asian biomass burning, which occurs annually from March to May (Streets et al., 2003).

The seasonal cycle of C_2H_6 is similar to that of CO, as shown in Figure 4. The primary sources of C_2H_6 include natural gas production, biofuel use and biomass burning (Rudolph, 1995; Logan et al., 1981; Xiao et al., 2008). The main loss of C_2H_6 is due to reaction with OH, resulting in an average lifetime of approximately three months (Xiao et al., 2008). The summertime wildfire influence of C_2H_6 is less pronounced than for CO and HCN. Enhancements of C_2H_6 are particularly evident at Eureka and Thule, due to the generally clean background of these sites, while wildfire enhancements of C_2H_6 are not evident at the other sites due to the influence of local sources in addition to dilution of the plume during long-range transport. Therefore, C_2H_6 enhancements due to wildfire pollution are not generally apparent over background concentrations. Additionally, the emissions of C_2H_6 are an order of magnitude lower than those of HCN for boreal forest, temperate forests and peatland burning sources (Andreae and Merlet, 2001; Akagi et al., 2011; Andreae, 2019).

3.1.2 ~~Volume Mixing Ratio~~ Retrieved VMR Profiles and Total Column Averaging Kernels

The VMR profiles of CO, HCN and C_2H_6 for all sites are shown in the appendix Figures A1, A2 and A3. A priori profiles for CO, HCN and C_2H_6 are from a 40-year (1980-2020) mean from the Whole Atmosphere Community Climate Model (WACCMv4; Eyring et al., 2007; Marsh et al., 2013) which has been chosen the NDACC IRWG for use by all sites. For all sites, a single a priori profile is used for each species, with the exception of Thule where monthly-mean a priori profiles derived from the 40-yr WACCMv4 simulation are used. In all cases, the profiles of each species are similar between sites and tend not to show drastic differences. It should be noted, that these profiles do not represent the true atmospheric profile of the species due to limited vertical resolution of the measurement, which is inherent in remote sensing measurements of this kind. The retrieved profiles generally follow a similar shape to the a priori profile, where deviations from the a priori are a result of the measurement. ~~The information content of the retrieval will be discussed in the following section.~~ In general, the profiles of all species exhibit greatest variability in the troposphere due to the abundance of these species in this region~~as these species are considered to be primarily tropospheric. The the~~. The tropospheric column of CO, HCN and C_2H_6 comprise, on average, greater than approximately 90% of the total column for CO, 95% for HCN, and 98% for C_2H_6.

~~The VMR profiles of CO (Figure A1) exhibit the greatest values in the lower free troposphere (surface-6 km) at all sites, with values ranging from approximately 120-170 ppbv, with greater concentrations at the polluted sites of Toronto, St. Petersburg and Rikubestu. These sites also illustrate a peak CO concentration at the surface layer due to the influence of local or nearby emissions. For Rikubetsu, a slight increase in concentration from the surface (~170 ppbv) to 1 km (~175 ppbv) with concentrations decreasing with altitude as a result of the transport of CO in the free troposphere from nearby Asian sources is observed. Decreasing concentrations and reduced variability of the retrieved profiles with altitude is observed at all sites as transported CO is generally well mixed. Poker Flat shows greatest variability of the CO profiles due to the transport of Asian pollution in the spring and wildfires in Eurasia and Alaska in the summer (Kasai et al., 2005b).~~

~~The VMR profiles of HCN (Figure A2) are variable amongst sites, with surface-layer concentrations ranging from ~190-310 pptv. For most sites, a peak in the concentration is observed between 6-10 km, with decreasing concentrations above. The HCN vertical profiles generally show increasing concentrations from the surface to the mid-troposphere and decreasing concentrations above. The urban sites, St. Petersburg and Toronto show decreasing concentrations from the surface due to the influence of local anthropogenic sources, mainly automobile use (Baum et al., 2007; Moussa et al., 2016). Accumulation of HCN in the upper troposphere is the result of its long lifetime and limited dry deposition to the ocean (Singh, 2003). This is most evident at Ny-Ålesund, which is isolated from local sources and illustrates an upper-troposphere peak between 7-9 km, with a concentration of approximately 330 pptv.~~

~~The VMR profiles of (Figure A3) follow a similar vertical structure to that of CO as a result of their common sources. For the urban sites, St. Petersburg and Toronto, the concentration is greatest at the surface layer, approximately 2 ppbv and 2.4 ppbv respectively, as a result of local sources. Rikubetsu shows a peak near 1.7 km of 1.6 ppbv, due to the transport of emissions in the free troposphere from nearby Asian sources. For Arctic sites, Eureka, Ny-Ålesund, Kiruna and Poker Flat, profiles show a broad peak in the free troposphere, generally between 1-7 km, which is indicative of the long-range transport of pollution.~~

3.1.3 ~~Averaging Kernels~~

~~The averaging kernel characterizes the vertical information content of the retrievals as described in Rodgers (2000). We consider the total column averaging kernel ($\mathbf{a}$), rather than the averaging kernel matrix ($\mathbf{A}$). We define the total column averaging kernel vector:~~

$$\mathbf{a} = \mathbf{C}^T\mathbf{A},$$

~~where $\mathbf{C}$ is the total column operator in units of molecules cm^{-2} and T denotes the transpose. The VMR averaging kernel matrix $\mathbf{A}$ is in VMR/VMR units. The total column averaging kernel may be normalized:~~

$$\hat{a}_i = a_i / C_i,$$

~~where i is the index of the ith level of the FTIR vertical retrieval grid. The normalized total column averaging kernel ($\hat{\mathbf{a}}$) is unitless and represents the sensitivity to a change in partial column for the vertical level i. The normalized total column averaging kernel may then be applied to the partial column profile to obtain the smoothed column, as will be discussed further in Section 3.2. For this purpose~~For the purposes of this study, normalized total column averaging kernel values near unity throughout the troposphere are desired, which would minimize biases due to differences in the vertical sensitivities when computing the ratios of columns of different species ~~, as will be done in the following section.~~

in calculating the enhancement ratio described in Section 2.5.1. The mean normalized total column averaging kernels, referred to as simply the total column averaging kernel hereinafter, for CO, HCN and C_2H_6 are ~~shown in~~ described in the Appendix A and shown in appendix Figure A4. For all sites, the total column averaging kernels of CO show a value near 1 throughout the troposphere, with a slight decrease to values below unity above 5 km. For HCN, the total column averaging kernels increase from the surface, with maximum values in the upper troposphere. The total column averaging kernels of C_2H_6 show similar structure to HCN, with maximum values in the mid to upper troposphere. For all sites, it can be concluded that CO retrievals exhibit minimal sensitivity bias in the troposphere. For HCN and C_2H_6, the total column averaging kernel is greatest in the upper troposphere.

~~For all species and sites, the total column averaging kernels are not highly variable in time. The variability of the total column averaging kernel is mainly due the changes in the vertical distribution of the species. In particular,~~

3.2 GEOS-Chem to FTIR CO Comparison

In order to use the GEOS-Chem tagged CO simulation to interpret the FTIR, it is necessary to evaluate the performance of the model with respect to FTIR measurements. To do so, GEOS-Chem CO partial column profiles are smoothed by the normalized FTIR CO total column averaging kernel ~~values generally increase with greater concentration of the species. There is some dependence on the solar zenith angle (SZA) of the measurement which varies seasonally, as the SZA is related to the sampled slant path through the atmosphere. At high SZAs, the longer slant path results in greater degrees of freedom for signal (DOFS), and hence greater averaging kernel values. The a priori covariance matrix, which is site and species dependent, also influences the~~ following Rodgers and Connor (2003):

$$\hat{x}_m = x_a + \mathbf{a}^T(\mathbf{x}_m - \mathbf{x}_a), \tag{4}$$

where $\hat{x}_m$ is the smoothed model total column, x_a is the FTIR a priori total column, $\mathbf{x}_m$ is the model partial column profile, $\mathbf{a}$ is the FTIR total column averaging kernel~~.~~

3.3 ~~Detection of Wildfire Pollution Events~~

~~As was illustrated in Section 3.1.1 and Figure 2, a seasonal cycle of CO is observed, with the amplitude varying by site location. Over a long time series, CO may be subject to inter-annual trends~~ , and $\mathbf{x}_a$ is the FTIR a priori partial column profile. Although the smoothing has a minor influence on the smoothed partial column ($\sim$1%) it is performed here to mitigate any biases as a result of ~~changing emissions of CO and its precursors. Additionally, non-clear sky conditions and instrument downtime result in periodic gaps in measurements and non-uniform time intervals between measurements. As a result of these factors it can be difficult to determine baseline or ambient concentrations of CO and therefore to detect enhancements of CO in the FTIR time series. To mitigate these influences, we account for the seasonal cycle and inter-annual variability of the CO time series measured at each FTIR site following Thoning et al. (1989):~~

~~$C(t) = a_0 + a_1 t + a_2 t^2 + \sum_{n=1}^{4} b_n \cos(2\pi n t) + c_n \sin(2\pi n t),$~~

the a priori profile. The GEOS-Chem CO profiles, FTIR CO profiles and total column averaging kernels are daily averaged and the daily averaged GEOS-Chem profiles are subsequently smoothed. Correlations of the smoothed GEOS-Chem and FTIR CO tropospheric partial columns are shown in Table 3.

~~where C is the column CO concentration as a function of time t. The coefficients a_n account for~~ For all sites, moderate to strong linear correlations are observed with correlation coefficients (r) ranging from a minimum of 0.66 for Toronto to a maximum of 0.86 at Ny-Ålesund, Thule and Kiruna. The slope of the linear regression is indicative of the ~~inter-annual trends of CO, while the fourth-order Fourier series with coefficients b_n and c_n captures the seasonal cycle of CO. The choice of order for both the polynomial and Fourier components of the fits were limited to third and fourth order following past studies (Thoning et al., 1989; Zellweger et al., 2009).~~

~~Enhancements in CO are identified following Zellweger et al. (2009). First, the fitted function is subtracted from the data to yield the residual. Assuming a normal distribution of baseline values around the fitted function, the negative residual is mirrored into the positive direction. Enhanced CO measurementsare defined as those greater than~~ GEOS-Chem bias relative to the FTIR measurements, with a slope greater than 1.0 representing a high-bias and a slope less than 1.0 representative of a ~~specified threshold of the mirrored residual above the fitted function. The threshold is defined as a multiple of the standard deviation σ of the mirrored negative residual as listed in Table **??**. The threshold is 1σ for~~ low-bias. For all sites, ~~with the exception of Rikubetsu where a 2σ standard deviation was used as a result of the greater variability CO due to nearby Asian sources. The selected values are listed in Table **??**.~~

~~The detected CO enhancements at each site are then binned by date to define individual events. The time window selected for binning is listed in Table **??** for each site and based on the measurement density at the respective site. Enhanced CO measurements separated in time by this duration are binned as separate events, while consecutive measurements within this time window are defined as a single event. Binning events minimizes the influence of varying plume composition, and also separates CO enhancements that may not be of wildfire origin. This is particularly important for the calculation of the enhancement ratio which will be described below. Longer separation times are selected for sites that are likely to be continually influenced by~~

~~wildfire emissions. These values are summarized in Table ??. At this stage, no attribution of the detected CO enhancements to any source has been performed and these enhanced periods simply indicate possible pollution events.~~

~~To isolate potential wildfire pollution events, we exploit the fact that trace gas emissions from wildfires are specific to burning phase and vegetation type (Ward and Hardy, 1991; Yokelson et al., 1999; Andreae and Merlet, 2001; Yokelson et al., 2009; Akagi et al., 20~~ ~~and therefore it would be expected that emissions of CO, HCN and originating from a wildfire source would be correlated within a plume. Emissions at the fire source are characterized by the emission ratio (ER; Andreae and Merlet, 2001; Akagi et al., 2011) relative to CO, which quantifies the amount of a trace gas species emitted relative to the amount of CO emitted. Since FTIR observations of this kind are measuring the emissions downwind of the source, the enhancement ratio (EnhR; Lefer et al., 1994) is considered:~~

$$\mathrm{EnhR}_{\mathrm{X}} = \mathrm{slope}\left(\frac{[\mathrm{X}]}{[\mathrm{CO}]}\right)_{\Delta t=1\mathrm{hr}}$$

~~where Xis the column of the trace gas of interest, and CO is the column of CO. The enhancement ratio is related to the emission ratio with the influence of plume aging by chemical loss, deposition and dilution of the plume during transport. Lifetimes of CO, HCN and are generally longer than plume transport times which range from several days to approximately two weeks (Damoah et al., 2004) and therefore these species do not undergo chemical considerable chemical loss. Furthermore, we do not take into account the background concentrations which can cause uncertainty in interpreting the enhancement ratio as the ambient conditions are likely to vary along the plume trajectory (Yokelson et al., 2013).~~

~~To calculate the enhancement ratios from the FTIR measurements, the detected CO enhancements for each event were paired with the nearest HCN and measurement taken within 1 hr. A 1-hr time interval was chosen to maximize the number of pairs since CO, HCN and are measured using different spectral filters and hence the measurements do not occur simultaneously. For events with paired measurements of HCN or with CO that are fewer than 5, the event is omitted. Setting a minimum number of pairs mitigates the potential of false detections as a result of spurious measurements.~~

~~The unified least-squares fitting procedure of York et al. (2004) which accounts for errors in both the ordinal and abscissa coordinates was used to determine a linear regression for the paired fire-affected measurements. The slope of the linear regression is the enhancement ratio for the respective species defined in Equation 2. To identify enhancements due to wildfire pollution events, we require that the correlation coefficient (r)be greater than or equal to 0.5 for both the enhancement ratios HCN and , unless otherwise stated, as summarized in Table ??.~~ GEOS-Chem has a low bias as seen in Table 3. The slopes range from a minimum of 0.49 at Jungfraujoch to a maximum of 0.84 at Rikubetsu.

~~HCN is retrieved from NDACC Filter 2 measurements, which is generally covered at least once per measurement sequence of all filters. Similarly, is retrieved through filter NDACC filter 3. All filters have a different response to the input solar beam intensity and therefore, the measurement noise may vary between subsequent measurements of different filters. For this reason, adequate signal may not be obtained through all filters in the case of partially cloudy or non-clear sky conditions. It was found that for all sites, with the exception of Jungfraujoch, there are a greater number of~~ The underestimation of GEOS-Chem CO is common amongst global CTMs as a result of errors in emissions, transport, and biases in the OH concentrations

(Shindell et al., 2006). It is likely that the consistent underestimation of GEOS-Chem CO at all sites is partly due to a high bias of OH (Muller et al., 2018). Seasonal variability of the GEOS-Chem bias is observed as shown Table 3. The consistent underestimation of GEOS-Chem at Zugspitze and Jungfraujoch may be the result of excessive stratosphere-to-troposphere exchange (Fischer et al., 2000; Hoor et al., 2002; Pan et al., 2004) contributed by the coarse model resolution, resulting in a low bias of CO ~~measurements than HCN or . Because of this non-uniform distribution of measurements, the number of detected wildfire events is limited by the number of paired measurements for HCN or with CO. For this reason, for Ny-Ålesund, Poker Flat and Rikubetsu , the enhancement ratio correlation criteria (shown in Table ??) were omitted, resulting in a lower confidence for the detected wildfire pollution events. However, for detected events at these sites,~~ in the upper troposphere. A similar underestimation of GEOS-Chem CO in a full-chemistry simulation in comparison to Jungfraujoch FTIR measurements was observed by Té et al. (2016). The high altitude of Zugspitze and Jungfraujoch makes these sites more susceptible to this bias in comparison to the ~~adjacent AERONET sites provide additional evidence for the detection of wildfire emissions if the measured AOD is simultaneously enhanced with CO as shown in Figure ??. Furthermore, the GEOS-Chem tagged CO simulation provides further confidence in~~ lower altitude sites (Ordóñez et al., 2007). The underestimation at Toronto, and the ~~detected wildfire pollution events as discussed in the following section.~~ lower correlation (0.66) than all other sites is possibly the result of the temporal and spatial variability of CO being not well captured due to the coarse model resolution (2°×2.5°).

3.3 ~~Source Attribution~~

~~A GEOS-Chem tagged CO simulation was performed as described in Section 2.2 for the time period of 2003-2018, giving 6-hourly instantaneous VMR profiles of the tracers listed in Table 2. The~~ Seasonal variability of the GEOS-Chem ~~simulation provides a means of evaluating the source attribution for the detected wildfire pollution events in the FTIR time series. Source attribution is performed as follows. First,~~ minus FTIR relative difference is also observed as shown in Table 3. The representation of the seasonal variability of transport at mid-latitudes and errors in the seasonality are likely to be contributing factors to the variability of the GEOS-Chem ~~CO VMR profiles in the grid box containing the respective FTIR site were converted to partial column profiles and linearly interpolated and regridded onto the FTIR vertical retrieval grid.This was necessary in order to account for the differences in the surface levels of the model and the FTIR sites (Barret et al., 2003) . For each of the detected events, the period of fire-affected measurements is considered. For this fire-affected window, we define the first-order rate of change of the CO partial column contribution for each of the~~ minus FTIR CO difference. However, biomass burning emissions are also seasonally dependent and underestimation of GEOS-Chem CO may be partially reflective of an underestimation of GFAS emissions. Particularly evident is the greater underestimation of GEOS-Chem ~~tagged biomass burning CO tracers:~~

$$\frac{\mathrm{d}[\mathrm{CO}]_\mathrm{X}}{\mathrm{d}t} = \frac{[\mathrm{CO}]_\mathrm{X}(t_i) - [\mathrm{CO}]_\mathrm{X}(t_{i-1})}{t_i - t_{i-1}},$$

~~where $[\mathrm{CO}]_\mathrm{X}$ is the column (in molec cm^{-2}) of the CO tracer X and t_i is the time of~~ at Rikubetsu in the summer months, during the boreal wildfire season. Eureka and Thule exhibit a greater underestimation of GEOS-Chem ~~timestep. Within a~~

~~wildfire pollution event, it is expected that a rapid increase of the CO contribution would be observed, resulting in a positive value $d[\mathrm{CO}]_\mathrm{X}/dt$. Similarly, as the plume passes or dissipates, a negative value of $d[\mathrm{CO}]_\mathrm{X}/dt$ would be observed. Considering this, the so-called impulse is then defined:~~

$$I_\mathrm{X} = \int\limits_{t_0}^{t_f} \left| \frac{\mathrm{d}[\mathrm{CO}]_\mathrm{X}}{\mathrm{d}t'} \right| \mathrm{d}t'$$

~~where t_0 and t_f correspond to the start time and end times of the detected event. The absolute value is used since we do not discriminate against positive of negative rates of change. Since the model output timesteps are discrete and constant, using the definition of Equation **??**, Equation **??** may be approximated as:~~

$$I_\mathrm{X} = \sum_{i=1}^{N} \left| [\mathrm{CO}]_\mathrm{X}(t_i) - [\mathrm{CO}]_\mathrm{X}(t_{i-1}) \right|$$

~~where N is the number of~~ in July and August when the boreal wildfire influence is greatest as will be shown in Section 8. A similar decrease in the GEOS-Chem ~~output timesteps for the detected FTIR event from t_0 and t_f. The result of Equation **??** can be easily interpreted. For a wildfire event, the concentration would rapidly increase as the plume approaches the FTIR site and rapidly decreasing CO concentrations as the plume passes. In contrast, anthropogenic, chemical or biogenic sources of CO are less likely to contribute to episodic enhancements, as these sources tend to vary on seasonal timescales and are more likely to contribute to background concentrations of CO rather than anomalous enhancements. However, the transport of anthropogenic emissions in the winter and spring may result in episodic pollution events. Detection of anthropogenic pollution events was mitigated by the use of the correlation criteria for the enhancement ratios of HCN and C_2H_6 as mentioned previously. For Ny-Ålesund, Poker Flat and Rikubetsu where no correlation criteria was used, winter and spring anthropogenic events were identified and removed based on a qualitative assessment of the~~ minus FTIR relative difference is also observed at Kiruna, Poker Flat, St. Petersburg and Toronto. These differences could be indicative of the unresolved plume transport in the model as a result of its coarse vertical resolution (Rastigejev et al., 2010; Eastham and Jacob, 2017). Additionally, the summertime low CO bias in GEOS-Chem ~~and AERONET AOD time series.~~ may also be contributed by an underestimation of the secondary production of CO from biogenic emissions of NMVOCs.

~~The value of I_X would be greatest for the GEOS-Chem tagged CO tracer contributing to the episodic enhancement detected by the FTIR instrument, and for the reasons stated above, is likely to be of wildfire origin. The source of the detected FTIR enhancement therefore corresponds to~~

3.3 Detected Wildfire Pollution Events

Wildfire events in the the FTIR time series at each site were identified using the method described in Section 2.5. Enhancements of CO were first identified following Section 2.5.1 and correlated with coincident measurements of HCN and C_2H_6 to calculate their enhancement ratios with respect to CO as described in Section 2.5.2. For the period of fire-affected measurements for each identified event, source attribution was determined using the GEOS-Chem tagged CO ~~tracer for which I_X from Equation ?? is a maximum~~simulation. The source attribution for the detected wildfire pollution events in the FTIR time series is illustrated in Figure 5.

~~The mean enhancement~~ The mean travel times determined using the FLEXPART back-trajectory simulations and the calculated emission ratios of HCN and ~~C_2H_6 are summarized~~ C_2H_6 are tabulated in Table 4~~for the detected~~.

The detected episodic wildfire pollution events ~~from BONA and BOAS~~ at all sites ~~. Similar enhancement ratios of HCN and C_2H_6 are observed at Eureka and Thule for both BONA and BOAS. This similarity is expected due to the close proximity of these sites. For Kiruna, slightly lower mean enhancement ratios of HCN were observed of 0.005 for both BONA and BOAS . The enhancement ratio of C_2H_6 at Kiruna is greater than Eureka and Thule, which likely represents the longer travel times of the plume resulting in the dilution of the plume with the background, which can be interpreted as follows. Assuming lifetimes~~ were attributed to either BONA or BOAS sources. Missed detections of wildfire events in the the FTIR time series are largely the result of the gaps in measurements, which may either be due to non-clear-sky conditions or instrument downtime. For Poker Flat, the presence of nearby wildfire sources result in large gaps in measurement as a result of the wildfire smoke. Coincident measurements of CO, HCN and ~~C_2H_6 of 30, 75 and 45 days following Viatte et al. (2013, 2015) and Lutsch et al. (2016), the enhancement ratio (EnhR) is given with respect to the emission ratio (ER):~~

$$\mathrm{EnhR}_X = \mathrm{ER}_X \cdot \frac{\exp\left(-\frac{t}{\tau_X}\right)}{\exp\left(-\frac{t}{\tau_{CO}}\right)}.$$

~~It is easily seen from Equation 3 that the enhancement ratios of HCN and C_2H_6 would increase with longer plume travel times t. For example, assuming a 7 day travel time, the enhancement ratios of HCN and C_2H_6 would be a factor of 1.15 and 1.08 greater than their respective emission ratio. For a 14 day travel time, the enhancement ratios of HCN and C_2H_6 would increase by a factor of 1.32 and 1.16, respectively, from their respective emission ratios~~C_2H_6 are generally not limiting factors for the detection of wildfire events. Under normal conditions, measurements are made by cycling through a series of spectral filters and all filters are usually sampled equally. The NDACC IRWG recommends the use of seven broadband spectral filters. They are used at all sites, with the exception of St. Petersburg and Jungfraujoch, where non-standard filters are used. Measurements of CO can be made through two of the seven spectral filters, while HCN and C_2H_6 are made through a single spectral filter. When a sufficient number of CO enhancements were detected, the coincident criteria of six paired measurements of HCN or C_2H_6 for the calculation of the enhancement ratio was achieved. However, ~~this is neglecting the influence of plume dilution. With longer travel times,~~ the ~~plume is likely to mix with the background resulting in the~~ exception being Ny-Ålesund, Poker Flat and Rikubetsu, where the the lower measurement density of these sites prevented the calculation of enhancement ratios. For all sites where the enhancement ratios of HCN and C_2H_6 were used as part of the detection, there may be missed events due to assigning a minimum correlation coefficient of 0.6 to the calculations. There may be cases where CO, HCN and C_2H_6 are simultaneously enhanced due to wildfire emissions; however, there may be poor correlation as a result of mixing of the plume with ambient air, or mixing of plumes of separate sources. However, setting a minimum correlation coefficient for the enhancement ~~ratios tending to background values. Therefore, the enhancement ratio of C_2H_6 would likely be greater than the enhancement ratio of HCN as a result of the greater mean columns of C_2H_6 in comparison to HCN observed at all sites, as illustrated in Figures 3 and 4.~~ would ensure that only coherent plumes are detected, therefore providing more reliable estimates of the emission ratios.

~~With the exception of Toronto, which is likely influenced by local HCN sources~~The reported mean travel times are found to vary by site and source region as shown in Table 4. A minimum mean plume travel time of 3 days was found for Poker Flat from BONA sources due to nearby Alaskan wildfire sources. The travel times are typically longer at all sites, ~~the greatest HCN enhancement ratios are observed at Eureka and Thule, with greater values for the BOAS events, 0.008 and 0.009 for Eureka and Thule, respectively. It is possible that this could reflect the greater HCN emissions of BOAS due to the substantial fraction of peat burning from these events (Yurganov et al., 2011; R'Honi et al., 2013). Lower enhancement ratios of HCN are observed at all other sites(except Toronto) for both~~ 10 days or greater for BOAS sources. Comparable travels times between BONA and BOAS sources are observed for Ny-Ålesund, Kiruna, Zugspitze and Jungfraujoch. For Eureka, Thule and Toronto, mean travel times of 8, 9 and 7 days are found for BONA and are shorter than BOAS, due to the proximity of these sites to BONA sources. ~~The lower enhancement ratios of HCN likely reflect the longer travel times to these sites and the dilution of the plume as described above.~~

~~Episodic wildfire pollution events at all sites are attributed to either BONA or BOAS sources, with two detected events from SEAS at Jungfraujoch.~~ Temporal correlation of events amongst all sites is observed, with events occurring near in time at different sites is attributed to the same source. Particularly evident are the 2012 Siberian wildfires (Kozlov et al., 2014; Teakles et al., 2017) observed at several sites and attributed to BOAS. Similarly, the 2017 Canadian wildfires (Khaykin et al., 2018; Peterson et al., 2018; Kirchmeier-Young et al., 2019; Lutsch et al., 2019) are also observed at a number of sites. Although, the majority of detected events from 2003-2018 are attributed to BOAS (63), from 2013-2018 there is an observed increase in the number of events attributed to BONA, with ~~24 BONA and 14~~ 18 BONA and 17 BOAS events detected during this period amongst all sites. Prior to 2013, ~~17 BONA and 37~~ 14 BONA and 46 BOAS events were detected. The recent increase in BONA events could be indicative of changes in large-scale climatic patterns (Macias Fauria and Johnson, 2008) resulting in an increase in lighting-induced wildfires (Macias Fauria and Johnson, 2006; Veraverbeke et al., 2017). However, this apparent increase in BONA events does not take into account the possibility of missed detections due to instrument downtime or cloudy sky conditions. ~~Contributions~~ The calculated emission ratios will be discussed in the following section and the contributions of the biomass burning source regions to CO tropospheric columns at each site will be ~~discussed in the following section~~presented in Section 4.2.

4 Discussion

4.1 Emission Ratios

The calculated emission ratios of HCN and C_2H_6 are compared to the literature values in Table 4. For BONA, our mean emission ratios of HCN range from 0.0026 (Zugspitze) to 0.0052 (Thule), whereas our mean emission ratios of C_2H_6 range from 0.0081 (Thule) to 0.0136 (Kiruna). Our values derived from FTIR-based methods are well within the range of literature values derived from ground-, satellite- and aircraft-based methods. Furthermore, across all sites, our mean emission ratios of C_2H_6 are greater than the mean emission ratios of HCN. Similarly, previous studies have reported greater C_2H_6 relative to HCN emission ratios, with the exception of the values reported by Hornbrook et al. (2011) and Simpson et al. (2011).

For BOAS, our mean emission ratios of HCN range from 0.0021 (Zugzpitze) to 0.0072 (Thule), whereas our mean emission ratios of C_2H_6 range from 0.0071 (St. Petersburg) to 0.0105 (Eureka). There are a limited number of literature values for BOAS, particularly those derived from aircraft-based studies. Notwithstanding, our FTIR-derived HCN and C_2H_6 emission ratios are within the range of available published values (Table 4) across all sites, with the exception of C_2H_6 in Toronto. The higher C_2H_6 emission ratio estimate for Toronto, relative to other sites, may be explained by nearby anthropogenic sources of C_2H_6, which may contaminate the plume and yield higher emission ratio estimates (Franco et al., 2016; Tzompa-Sosa et al., 2017). As was observed for BONA, the mean C_2H_6 emission ratios are greater than the mean HCN emission ratios for BOAS across all sites. This comparison of C_2H_6 to HCN emission ratios is in agreement with published findings, with the exception of Hornbrook et al. (2011).

Our FTIR-derived HCN emission ratios are greater than published estimates based on Atmospheric Chemistry Experiment Fourier Transform Spectrometer (ACE-FTS) measurements, as reported by Tereszchuk et al. (2011); Rinsland et al. (2007); Tereszchuk et a
for BONA and Tereszchuk et al. (2013) for BOAS. Solar occultation measurements of the ACE-FTS have a lower altitude range, of approximately 6 km. Consequently, a plume detected by ACE-FTS may correspond to flaming combustion and injection of emissions into the upper troposphere. Flaming, relative to smoldering combustion is associated with lower HCN emissions (Urbanski, 2013). Indeed, literature values of HCN ratios derived from ground-based FTIR measurement were higher than those derived from ACE-FTS solar occultation measurements (Griffin et al., 2013; Viatte et al., 2015; Lutsch et al., 2016)
.

Aircraft instruments tend to measure the composition of fresh plumes with minimal plume aging. Therefore, the variability of the emission ratios reported for aircraft-based studies is likely to be reflective of the variability of emissions due to multiple factors that influence the emissions within a wildfire event, such as the type of vegetation that is burned (Akagi et al., 2011; Andreae and Me
, the burning phase (Yokelson et al., 1996, 1999, 2003; Goode et al., 1999, 2000; Urbanski, 2013) and pyrolsis temperature (Sekimoto et al
of the burn. These factors, however, are likely to vary regionally and may also vary with time in a particular event.

Taken together, our FTIR-derived mean emission ratios of HCN and C_2H_6 for BONA and BOAS sources are congruent with published literature values, supporting the validity of the use of FTIR-based methods to quantify the transport of emissions from BONA and BOAS sources. We report HCN and C_2H_6 emission ratios across multiple sites in the Arctic and mid-latitude regions. Moreover, the FTIR-derived emission ratios presented here provide novel estimates for regions wherein published values are not available, particularly for BOAS sources, adding to the sparsely populated dataset, and providing greater insight into the variability of emissions.

Precise knowledge of the emission ratios of various trace and particulate species is required for more accurate modeling of biomass burning emissions in chemical transport models. The emission ratio, may be converted to an equivalent emission factor with the use of the emission factor of the reference species, usually CO. The emission factor of CO is determined from reported literature values (i.e., Andreae and Merlet 2001; Akagi et al. 2011; Andreae 2019) which are derived from laboratory or field measurements, relating the mass of CO emitted per unit mass of dry matter burned for various vegetation types. Given the dependence of the emission factor of the species of interest on the emission factor of CO, it is advantageous to consider the emission ratios. Biomass burning emission inventories are dependent on a single emission factor for each species per vegetation type or biome. These values are obtained from literature values such as reported by Akagi et al. (2011, ?); Andreae and Merlet (2001); Andr . These literature values are the reported means of emission ratios or emission factors obtained from laboratory studies or field observations from ground-based, aircraft or satellite measurement platforms. Measurements of emission ratios by these methods may only sample a single or small number of events. Aircraft measurements are often made on a campaign basis, targeting biomass burning plumes near the source or along a flight transect. As a result measurements made by aircraft-based measurements may only sample the plume over a short period of time and may not capture the natural variability of emissions.

Satellite observations are particularly useful as they provide global coverage; however, emission ratios derived from satellite observations are limited by the instrument's capability to measure multiple trace gas species simultaneously. To our knowledge, the only satellite-based measurements of HCN and C_2H_6 emission ratios for boreal vegetation types are reported by Rinsland et al. (2007) and Tereszchuk et al. (2011, 2013) using ACE-FTS. Although ACE-FTS has global coverage, observations of biomass burning plumes is dependent on the temporal and spatial sampling of the instrument intersecting the biomass burning plume. As result, measurements within of a biomass burning plume, may only occur in a small number of instances.

Ground-based measurements, particularly by FTIR have sampled boreal wildfire plumes on several occasions (i.e., Viatte et al. 2013, 201 and Lutsch et al. 2016) providing emission ratios of both HCN and C_2H_6. Each of these studies, have only considered a single or select number of events. Measurements of emissions ratios using FTIR are dependent on the smoke plume passing over the FTIR site. However, FTIR measurements within a smoke plume, may sample the plume over several days, providing temporal converge. The emission ratios derived by FTIR measurements may therefore capture the temporal variability of the emissions, resulting in a time-averaged emission ratio since the emission ratio is derived from the slope of trace gas correlations during the course of the wildfire pollution event.

Using a long-term timeseries and network of FTIR instruments provides several advantages to quantifying the emission ratios of biomass burning species. The long-term timeseries enables the detection of greater number of wildfire pollution events as was illustrated in Section 3.3, all of which may have variable emissions due to vegetation type and the burning phase of combustion. The transport of emissions from a particular wildfire source to each FTIR site is dependent on the meteorological conditions, therefore each site is likely to sample different plumes of varying origins providing a means of capturing the variability of emissions between events. These aspects enable a network of FTIR instruments to capture a large number of wildfire events to quantify the emission ratios of HCN and C_2H_6 along with its variability. Emission ratios derived by a network of FTIR instruments therefore provide more robust estimates of the emission ratios and their respective variability.

Our reported mean emission ratios, and their comparison to literature values, should be interpreted in light of several limitations. The enhancement and emission ratios were obtained from measurements spanning several days, and therefore may not sufficiently capture shorter-term variability in wildfire emissions (e.g. Lutsch et al., 2019) and may be more susceptible to smoldering phase combustion. Smoldering phase combustion may be a persistent source of emissions that may last several weeks, leading to prolonged periods of fire-affected measurements. Chemical aging of the plume may also affect the calculated emission ratios. Here we have assumed lifetimes of CO, HCN and C_2H_6; however, the actual lifetimes of these species may vary within a smoke plume, which is dependent on the availability of OH. The assumed transport times of the plume may also influence emission ratio estimates. In this study, we calculated plume travel times based on the FLEXPART back-trajectories, which correspond to the sensitivity of column measurements to surface emissions. The injection of wildfire emissions into the free troposphere could enable more efficient transport, decreasing the plume travel time (Heilman et al., 2014). Thus, it is likely that the assumed travel times exceed the actual travel times. However, differences in travel times of several days will only have a minor influence on the calculated emission ratio as assumed lifetimes of each species is much longer the travel times. Plume diffusion and mixing with background air (McKeen and Liu, 1993; McKeen et al., 1996; Ehhalt et al., 1998; Xiao et al., 2007) may also decrease the emission ratios, which are not accounted for by the first-order loss assumed for each species; however, plume mixing may be partially captured by the loss of the linear correlation between the trace gas species in ambient or background conditions.

4.2 Wildfire Contribution to CO

The GEOS-Chem tagged CO simulation provides a means of evaluating the contribution of CO from anthropogenic, chemical and biomass burning sources to the measured CO columns at each FTIR site. Figures 7 to 10 show the daily-averaged GEOS-Chem and FTIR CO tropospheric columns (surface-12.71 km) for the simulation period from 2003-2018. The relative contribution of biomass burning tracers are also shown. Biomass burning tracers with a mean contribution of less than 3% are not shown. For all GEOS-Chem tagged CO tracers, the partial column profile was linearly interpolated onto the FTIR retrieval grid to account for the differences in surface elevation of the model and FTIR sites.

For all sites, the oxidation of CH_4 is the greatest contribution to the tropospheric CO column as illustrated in Figure 6. The magnitude of this source is similar amongst all sites, with the exception of Zugspitze and Jungfraujoch due to their high altitude. Anthropogenic Asian CO sources exhibit the greatest seasonal amplitude at all sites, due to the magnitude of the emissions and the influence of seasonally variable transport (Klonecki, 2003; Stohl et al., 2006; Fisher et al., 2010). European and North American anthropogenic sources show a similar seasonal cycle but smaller in amplitude in comparison to the Asian source. Of note, at Zugspitze and Jungfraujoch, comparable contributions from anthropogenic sources in Asia, North America, Europe and the rest of the world are observed. The oxidation of NMVOCs is a considerable source at all sites, with little seasonal dependence. A slight increase in the NMVOC contribution is observed in the summertime, particularly in July and August, as a result of emissions of NMVOC from biogenic sources and wildfires (Guenther et al., 2000; Wentworth et al., 2018).

Biomass burning sources of CO exhibit the greatest differences amongst sites as seen in Figure 6. For most sites, the onset of the biomass burning contribution begins in May with a maximum in August. Similar to the anthropogenic influence, Zugspitze and Jungfraujoch are generally isolated from the direct influence of biomass burning emissions and only show a minor enhancement in the summer. For Rikubetsu, the onset of the biomass burning contributions is observed earlier than for the other sites beginning in March as a result of the influence of Asian biomass burning sources (CEAS, SEAS and EQAS), with slight influence in the summer for boreal emissions from BOAS. The contributions of the biomass burning sources to each site ~~with respect to the results of Section ??~~ are discussed below.

4.2.1 High-Arctic Sites

The high-Arctic sites of Eureka, Ny-Ålesund and Thule illustrate strong summertime enhancements of CO and HCN as seen in Figures 2 and 3, with a moderate enhancement of C_2H_6 shown in Figure 4. These enhancements have a maximum in July and August and from Figure 7, it is observed that the enhancements are largely due to the influence of BONA and BOAS wildfires. Wildfires in temperate regions (TENA and CEAS) are a small contribution to the CO tropospheric column ($<5\%$) but do not contribute to the detected episodic enhancements. A moderate contribution to CO from CEAS and SEAS is observed, but these are not a source of anomalous enhancements.

Similar contributions are observed for BONA and BOAS among the high-Arctic sites, with a stronger influence from BONA to Eureka and Thule resulting in episodic enhancements of CO contributing greater than 40% to the CO tropospheric column. The strong influence of these sources is the result of the proximity of the high-Arctic sites to these source regions, as well as the efficient summertime isentropic transport (Stohl, 2006). As a result, the direct influence of wildfire plumes at the high-Arctic sites is observed in the FTIR time series, where the effects of plume dilution are minimal.

Furthermore, an early onset in April of the BOAS contribution is observed and is likely the result of the contribution from Siberian wildfires. Siberian wildfires are associated with low-level injected emissions, mainly within the planetary boundary layer and lower free troposphere (Val Martin et al., 2018). The low-level injection of these emissions and the high latitudes of the sources ~~favour~~ favor efficient transport to the Arctic (Stohl, 2006). In contrast, the Asian sources, CEAS and SEAS, show minor contributions to the CO tropospheric columns at the high-Arctic sites. Transport of these emissions to the Arctic are limited due to the higher potential temperature of these regions in the summertime, preventing isentropic transport to the Arctic (Klonecki, 2003; Stohl, 2006).

4.2.2 Arctic Sites

For the high-latitude European sites Kiruna and St. Petersburg, smaller contributions to CO from BONA and BOAS sources are observed, with peak contributions ranging from approximately 5 to 44% for BONA and 12 to 37% for BOAS, with slightly smaller contributions at Kiruna. The smaller contributions from these sites in comparison to the high-Arctic sites is partly due to the greater distances from the wildfire sources. The transport of emissions to these sites is a result of long-range westerly transport that ~~generally exceeds 10 days (Damoah et al., 2004)~~exceeds 11 days as shown in Table 4. Because of the long travel times, the plume is often diluted, and therefore, does not generally lead to the episodic enhancements observed at the high-Arctic sites. In contrast, Poker Flat is predominantly influenced by Alaskan wildfires, with contributions to the CO tropospheric column exceeding 50% in many cases. Similarly, the proximity of Poker Flat to BOAS sources makes BOAS a significant contributor to episodic CO enhancements, comparable to the local BONA source.

Similar to the high-Arctic sites, contributions from TENA, CEAS and SEAS to the Arctic sites are minimal and do not contribute to the episodic enhancements of CO, HCN and C_2H_6 detected in the FTIR time series. However, Poker Flat and St. Petersburg generally exhibit greater contributions from CEAS. For Poker Flat, this is the result of Asian outflow transporting emissions from ~~Asian~~ Asia over the Atlantic to Alaska. For St. Petersburg, the proximity to the CEAS sources makes it susceptible to this source. Particularly evident is the large enhancement in July and August of 2010 due to wildfires in the Moscow region (Konovalov et al., 2011; Witte et al., 2011; Yurganov et al., 2011) although not detected in the FTIR time series as there were no measurements during that period.

4.2.3 Alpine Sites

The alpine sites, Zugspitze and Jungfraujoch shown in Figure 9, differ the most from the other sites considered in this study as a result of their high altitude. It is seen that Zugspitze and Jungfraujoch are most strongly influenced by BOAS, with a mean seasonal maximum contribution of approximately 14% at both sites. The contribution of BOAS emissions to the enhanced columns at Zugspitze and Jungfraujoch are due to hemispheric-scale transport ~~(Damoah et al., 2004)~~with transport times exceeding 10 days, leading to a perturbation to background concentrations of each species. As a result, the enhancements detected in the FTIR time series or GEOS-Chem do not result in the large, episodic enhancements observed at the high-Arctic sites. The contributions from trans-Atlantic transport of BONA emissions, however, exhibit these anomalous enhancements on occasion. Particularly evident are the BONA wildfires of 2013-2015 and 2018. Emissions from boreal Canadian wildfires may be injected into the free troposphere (Val Martin et al., 2018) and in some cases the lower stratosphere (Fromm et al., 2000; Khaykin et al., 2018; Peterson et al., 2018) which may enable the efficient transport of the plume over inter-continental scales (Heilman et al., 2014).

SEAS emissions are a larger contributor to CO enhancements for Zugspitze and Jungfraujoch than for the Arctic or high-Arctic sites. However, such enhancements are not observed in the FTIR time series as the contribution from SEAS is small in comparison to Asian anthropogenic sources as illustrated in Figure 6. Transport of Asian biomass burning CO emissions to Europe had been identified in the springtime by Petetin et al. (2018) and attributed to uplifting of emissions into the free troposphere and efficient transport of the westerlies (Bey et al., 2001a). In all cases, Zugspitze and Jungfraujoch are most susceptible to emissions that reach the free troposphere where long-range transport is ~~favoured~~ favored (Petetin et al., 2018).

4.2.4 Mid-latitude Sites

Anomalous enhancements in the Rikubetsu time series are dominated by the outflow of BOAS emissions that begin in early springtime and persist throughout the summer and autumn. Episodic BOAS enhancements are observed annually, with contributions that generally exceed 20% and are larger than 50% in many years. The greatest enhancement from BOAS was observed in 2003 as result of the exceptional emissions from Siberia wildfires (Jaffe et al., 2004; Ikeda and Tanimoto, 2015). Although the contribution from BOAS at Rikubetsu is highly variable between years, anomalous enhancements are observed annually in the GEOS-Chem time series, while detection of events in the FTIR time series is limited by the temporal sampling of the FTIR instrument. CEAS and SEAS have moderate contributions (∼10%) to the CO tropospheric column at Rikubetsu in the spring and fall although the influence of these sources are often masked by the greater BOAS emissions during these periods. Other biomass burning sources have minimal contributions and Asian anthropogenic sources are dominant throughout the year as shown in Figure 6.

Toronto is most strongly influenced by wildfires of BONA, with detected events in the FTIR time series including 2014 from the Northwest Territories wildfires (Lutsch et al., 2016; Kochtubajda et al., 2019), 2015 from wildfires in Saskatchewan (Dreessen et al., 2016) and the 2017 British Columbia wildfires (Peterson et al., 2018). Although it is in close proximity to TENA sources, mainly from the Western and Southern United States, Toronto is minimally influenced by TENA as the magnitude of these emissions is much smaller than for BONA. Background contributions from CEAS and SEAS are also observed in the springtime although the contribution from Asian anthropogenic sources is dominant. BOAS is also a significant contribution to CO at Toronto in the summertime, but does not generally result in anomalous enhancements as a result of the longer transport times from this region. The 2018 enhancements were attributed to BOAS, while in June 2012, enhancements were present in the FTIR time series and appear to occur simultaneously with the large BOAS contribution (>30%). Minor contributions (<5%) from CEAS are observed in the springtime and autumn, while a moderate influence from SEAS of ∼10% is observed in the spring.

4.3 ~~GEOS-Chem to FTIR CO Comparison~~

~~The GEOS-Chem CO partial column profiles are smoothed by the normalized FTIR CO total column averaging kernel following Rodgers and Connor (2003):~~

$$\underline{\hat{x}_m = x_a + \mathbf{a}^T\left(\mathbf{x}_m - \mathbf{x}_a\right),}$$

~~where $\hat{x}_m$ is the smoothed model total column, x_a is the FTIR a priori total column, $\mathbf{x}_m$ is the model partial column profile, $\mathbf{a}$ is the FTIR total column averaging kernel, and $\mathbf{x}_a$ is the FTIR a priori partial column profile. Although the smoothing has a minor influence on the smoothed partial column (∼1%) it is performed here to mitigate any biases as a result of the a priori profile. The GEOS-Chem CO profiles, FTIR CO profiles and total column averaging kernels are daily averaged and the daily averaged GEOS-Chem profiles are subsequently smoothed. Correlations of the smoothed GEOS-Chem and FTIR CO tropospheric partial columns are shown in Figure **??**.~~

~~For all sites, moderate to strong linear correlations are observed with correlation coefficients (r) ranging from a minimum of 0.66 for Toronto to a maximum of 0.89 at Thule. The slope of the linear regression is indicative of the GEOS-Chem bias relative to the FTIR measurements, with a slope greater than 1.0 representing a high-bias and a slope less than 1.0 representative of a low-bias. For all sites, GEOS-Chem has a low bias as seen in Figures 7-10. The slopes range from a minimum of 0.49 at Jungfraujoch to a maximum of 0.84 at both St. Petersburg and Rikubetsu.~~

~~The underestimation of GEOS-Chem CO is common amongst global CTMs as a result of errors in emissions, transport, and biases in the OH concentrations (Shindell et al., 2006). It is likely that the consistent underestimation of GEOS-Chem CO at all sites is partly due to a high bias of OH (Muller et al., 2018). Seasonal variability of the GEOS-Chem bias is observed as shown in Figure **??**. The consistent underestimation of GEOS-Chem at Zugspitze and Jungfraujoch (as shown in Figure **??**) may be the result of excessive stratosphere-to-troposphere exchange (Fischer et al., 2000; Hoor et al., 2002; Pan et al., 2004) contributed by the coarse model resolution, resulting in a low bias of CO in the upper troposphere. A similar underestimation of GEOS-Chem CO in a full-chemistry simulation in comparison to Jungfraujoch FTIR measurements was observed by Té et al. (2016). The high altitude of Zugspitze and Jungfraujoch makes these sites more susceptible to this bias in comparison to the lower altitude sites (Ordóñez et al., 2007). The underestimation at Toronto, and the lower correlation (0.66) than all other sites is possibly the result of the temporal and spatial variability of CO being not well captured due to the coarse model resolution ($2^\circ\times2.5^\circ$).~~

~~Seasonal variability of the GEOS-Chem minus FTIR relative difference is also observed as shown in Figure **??** and tabulated in Table 3. The representation of the seasonal variability of transport at mid-latitudes and errors in the seasonality are likely to be contributing factors to the variability of the GEOS-Chem minus FTIR CO difference. However, biomass burning emissions are also seasonally dependent and underestimation of GEOS-Chem CO may be partially reflective of an underestimation of GFAS emissions. Particularly evident is the greater underestimation of GEOS-Chem at Rikubetsu in the summer months, during the boreal wildfire season. Eureka and Thule exhibit a greater underestimation of GEOS-Chem in July and August when the boreal wildfire influence is greatest as shown in Figure 7. A similar decrease in the GEOS-Chem minus FTIR relative difference is also observed at Kiruna, Poker Flat, St. Petersburg and Toronto. These differences could be indicative of the unresolved plume transport in the model as a result of its coarse vertical resolution (Rastigejev et al., 2010; Eastham and Jacob, 2017). Additionally, the summertime low CO bias in GEOS-Chem may also be contributed by an underestimation of the secondary production of CO from biogenic emissions of NMVOCs.~~

5 Conclusions

Boreal wildfires of North America (BONA) and Asia (BOAS) were found to be the greatest contributors to episodic CO enhancements at ten Northern hemisphere FTIR sites: Eureka, Ny-Ålesund, Thule, Kiruna, Poker Flat, St. Petersburg, Zugspitze, Jungfraujoch, Toronto and Rikubetsu. Wildfire pollution events were identified by detection of enhancements of CO in the FTIR time series. With the exception of Ny-Ålesund, Poker Flat and Rikubetsu, detected CO enhancements were correlated with coincident measurements of HCN and C_2H_6 to determine their enhancement ratios with respect to CO, providing evidence for ~~the detection of wildfire~~ wildfires as the source of these pollution events. ~~The GEOS-Chem tagged CO simulation allowed for source attribution of the detected events and for the source contribution to CO at each site to be evaluated.~~

~~The greatest numbers of FTIR enhancements were observed at Eureka (19) and Thule (17)due to their proximity to BONA~~ For the detected wildfire events, the calculated enhancement ratios of HCN and C_2H_6 were converted to emission ratios using a mean plume travel time calculated from FLEXPART back-trajectories. Plume travel times were found to vary between sites and source regions, with a minimum of 3 days for BONA events transported to Poker Flat, to maximum of 14 days for BOAS transported to Zugspitze. With the exception of Rikubetsu (8 days) and Zugspitze (14 days), travel times were comparable for BOAS sources at all sites, ranging from 10-12 days on average. For BONA, the travel times varied by site with a minimum of 3 days at Poker Flat to a maximum of 12 days at Kiruna and Ny-Ålesund.

A total of 23 emission ratios of HCN and C_2H_6 were found for BONA, and 38 for BOAS. The calculated emission ratios were found to agree well with previous published values, illustrating the FTIR observations of this kind are able to capture the long-range transport of wildfire emissions. Average emission ratios of HCN and C_2H_6 for BONA of 0.0047 and ~~BOAS~~0.0092, respectively, were found, with standard deviations of 0.0014 and 0.0046, respectively. Similarly, for BOAS, mean HCN and C_2H_6 emissions ratios of 0.0049 and 0.0100, respectively, with standard deviations of 0.0025 and 0.0042, respectively, were found. Due to the similarity of emission ratios found for BONA and BOAS, there is no clear distinction in emissions between the two sources. Furthermore, the emission ratios found here provide additional constraints on the variability of HCN and C_2H_6 emissions, adding to the sparsely populated literature dataset, particularly for BOAS. Moreover, the emission ratios quantified using the long-term time series obtained from a network of FTIR instruments enabled the detection of a larger number of wildfire pollution events, enabling more robust estimates of the HCN and C_2H_6 emission ratios whereas previous studies from aircraft-, ~~with both sourcescontributing~~ satellite- or ground-based measurement platforms have only focused on single and few number of events.

The results of this study confirm the ability of ground-based FTIR measurements to capture the transport of boreal wildfire emissions. Furthermore, we extend our findings by quantifying the contribution of wildfire sources to CO measurements at each site using the GEOS-Chem tagged CO simulations. For Eureka and Thule, BONA and BOAS sources were found to contribute to greater than 40% of the CO tropospheric partial column in many cases. A similar influence of BONA and BOAS wildfires was observed at Ny-Ålesund~~, but the sparsity of the CO measurements limited detection of events in the FTIR time series. Furthermore, the lack of coincident measurement of HCN and C_2H_6 did not allow for enhancement ratios to be calculated for Ny-Ålesund.~~

. Kiruna was also strongly influenced by the trans-Atlantic transport of BONA emissions and hemispheric transport of BOAS emissions, which may contribute ∼5-40% of the CO tropospheric partial column during the summer months from June though September of each year. A similar contribution was observed at St. ~~-~~Petersburg, albeit lower in magnitude. The ~~sparse measurements of CO, HCN and C_2H_6 at Poker Flat limited detection of events in the FTIR time series. However, the~~ GEOS-Chem tagged CO simulation illustrated the strong influence of both BONA and BOAS sources at Poker Flat, which in several years exceeded 60~~%~~ % of the CO tropospheric column.

The Alpine sites, Zugspitze and Jungfraujoch, are isolated from major biomass burning sources, but on occasion are subject to the transport of both BONA and BOAS emissions, which were detected in the FTIR time series at both sites. However, these emissions are generally a small contribution to the tropospheric CO partial column (∼10%). Toronto was mainly influenced by North American wildfires of BONA contributing ∼10-20% of the CO column. Asian anthropogenic sources strongly influence the CO background at Rikubetsu, which was also considerably influenced by BOAS wildfires.

~~The results of this study show the Northern Hemispheric influence of boreal~~ Given the substantial contribution of wildfire sources to CO at sites in this study, and the ability of FTIR to quantify wildfire emissions, ~~which were detected using FTIR measurements of CO and the coincident measurements of HCN and C_2H_6. The inter-annual variability of boreal wildfire emissions observed in the GEOS-Chem tagged CO simulation was also observed in the detected FTIR enhancements when measurements were available. The detected FTIR enhancements from 2013-2018 were in most cases attributed to BONA, consistent with the increase in the BONA contribution to CO during this period as observed in the GEOS-Chem time series.~~ future studies should examine the long-term effect of biomass burning emissions on reactive trace gas species. Reactive trace gas species of interest that are be readily measured by FTIR include acetylene (C_2H_2, e.g., Paton-Walsh et al., 2010; Vigouroux et al., 2012;), methanol (CH_3OH, e.g., Rinsland et al., 2009; Vigouroux et al., 2012; Viatte et al., 2014, 2015), formic acid (HCOOH, e.g. Zander et al., 2010; Viatte et al., 2014, 2015), formaldehyde (H_2CO,Paton-Walsh et al., 2004; Vigouroux et al., 2009; Viatte et al., 2014, 2) and ammonia (NH_3, e.g., Paton-Walsh et al., 2004; Dammers et al., 2015; Lutsch et al., 2016, 2019). FTIR measurements can inform future studies to characterize the long-range transport of these species to elucidate the chemical mechanisms within a smoke plume and potential impacts on air-quality.

Code and data availability. The FTIR data are available from the NDACC data repository at ftp://ftp.cpc.ncep.noaa.gov/ndacc/. The GEOS data used in this study have been provided by the Global Modeling and Assimilation Office (GMAO) at NASA Goddard Space Flight Center.The GEOS-Chem model code used is available here: http://dx.doi.org/10.5281/zenodo.2249246 (The International GEOS-Chem User Community, 2018). The AEORONET data used are available here: https://aeronet.gsfc.nasa.gov/cgi-bin/draw_map_display_aod_v3. The FLEXPART was downloaded from: https://www.flexpart.eu/downloads. Any additional data may be obtained from Erik Lutsch (elutsch@physics.utoronto.ca)

Appendix A: Averaging Kernels

The averaging kernel characterizes the vertical information content of the retrievals as described in Rodgers (2000). We consider the total column averaging kernel ($\mathbf{a}$), rather than the averaging kernel matrix ($\mathbf{A}$). We define the total column averaging kernel vector:

$$\mathbf{a} = \mathbf{C}^T\mathbf{A}, \tag{A1}$$

where $\mathbf{C}$ is the total column operator in units of molecules cm^{-2} and T denotes the transpose. The VMR averaging kernel matrix $\mathbf{A}$ is in VMR/VMR units. The total column averaging kernel may be normalized:

$$\hat{a}_i = a_i / C_i, \tag{A2}$$

where i is the index of the ith level of the FTIR vertical retrieval grid. The normalized total column averaging kernel ($\hat{\mathbf{a}}$) is unitless and represents the sensitivity to a change in partial column for the vertical level i. The normalized total column averaging kernel may then be applied to the partial column profile to obtain the smoothed column, as shown in Section 3.2.

For all species and sites, the total column averaging kernels are not highly variable in time. The variability of the total column averaging kernel is mainly due the changes in the vertical distribution of the species. In particular, total column averaging kernel values generally increase with greater concentration of the species. There is some dependence on the solar zenith angle (SZA) of the measurement which varies seasonally, as the SZA is related to the sampled slant path through the atmosphere. At high SZAs, the longer slant path results in greater degrees of freedom for signal (DOFS), and hence greater averaging kernel values. The a priori covariance matrix, which is site and species dependent, also influences the total column averaging kernel.

Author contributions. This study was designed by EL, KS and DBAJ. TB, SC, JWH, FH, YK, EM, MM, IM, TN, JN, IO, MO, AVP, RS and TW contributed to the FTIR measurements used. JAF contributed to the updated GEOS-Chem tagged CO simulation that was used. The analysis was performed by EL. The paper was prepared by EL with contributions from all authors.

Competing interests. The authors declare they have no competing interests.

Acknowledgements. Bruker FTIR measurements were made at PEARL by the Canadian Network for the Detection of Atmospheric Composition Change (CANDAC), which has been supported by the Atlantic Innovation Fund/Nova Scotia Research Innovation Trust, Canada Foundation for Innovation, Canadian Foundation for Climate and Atmospheric Sciences, Canadian Space Agency (CSA), Environment and Climate Change Canada (ECCC), Government of Canada International Polar Year funding, Natural Sciences and Engineering Research Council (NSERC), Northern Scientific Training Program, Ontario Innovation Trust, Polar Continental Shelf Program, and Ontario Research Fund. EL was partially supported by the NSERC CREATE Training Program in Arctic Atmospheric Science and the Probing Atmosphere in the High Arctic (PAHA) project. We thank CANDAC/PEARL/PAHA PI James Drummond, Canadian Arctic ACE/OSIRIS Validation Campaign PI Kaley Walker, PEARL Site Manager Pierre Fogal, CANDAC Data Manager Yan Tsehtik, the CANDAC operators, and the staff at ECCCs Eureka Weather Station for their contributions to data acquisition, and for logistical and on-site support.

The National Center for Atmospheric Research (NCAR) is sponsored by the U.S. National Science Foundation (NSF). The NCAR FTIR observation program at Thule, Greenland is supported under contract by the National Aeronautics and Space Administration (NASA). The Thule work is also supported by the NSF Office of Polar Programs (OPP). We wish to thank the Danish Meteorological Institute for support at the Thule site. KIT, IMK-ASF would like to thank Uwe Raffalski and Peter Voelger from the Swedish Institute of Space Physics (IRF) for their continuing support of the NDACC-FTIR site Kiruna. St. Petersburg State University was supported by the RFBR project #18-05-00011. MP gratefully acknowledges funding from the Deutsche Forschungsgemeinschaft (DFG, German Research Foundation; project number 268020496, TRR 172) within the Transregional Collaborative Research Center ArctiC Amplification: Climate Relevant Atmospheric and SurfaCe Processes, and Feedback Mechanisms (AC)3" in subproject E02. St. Petersburg FTIR measurements were carried out by the instrumentation of the Geomodel resource center of SPbU. The monitoring program of ULiège at Jungfraujoch was primarily supported by the Fonds de la Recherche Scientifique - FNRS under Grant no. J.0147.18, the Fédération Wallonie-Bruxelles and MeteoSwiss (GAW-CH program). E. Mahieu is a Research Associate with the F.R.S.–FNRS. We thank the International Foundation High Altitude Research Stations Jungfraujoch and Gornergrat (HFSJG, Bern). We are grateful to all colleagues who contributed to spectra acquisition for the Jungfraujoch site. JAF acknowledges funding from the University of Wollongong and the Australian Research Council (DP160101598) as well as computational resources provided at the NCI National Facility systems at the Australian National University through the National Computational Merit Allocation Scheme supported by the Australian Government. Operation at the Rikubetsu site is supported in part by the GOSAT series project.

The authors acknowledge the use of AERONET data and thank Norm O'Neill, Ihab Abboud Vitali Fioletov, Brent Holben, Piotr Sobolewski, Piotr Glowacki, Grzegorz Karasinski, Victoria E. Cachorro Revilla, Sandra Blindheim, John R. Vande Castle, Margit Aun, Natalia Kouremeti, Itaru Sano and their staff for establishing and maintaining the 9 sites used in this investigation. The authors acknowledge the use of the GFASv1.2 emissions inventory, which contains modified Copernicus Atmosphere Monitoring Service information (2019). We also acknowledge Mathew J. Evans, Eleanor Morris and Killian Murphy for providing the GFASv1.2 netCDF files. The authors also acknowledge the use of the FLEXPART Lagrangian dispersion model (https://www.flexpart.eu/wiki/FpDownloads). The GEOS data used in this study have been provided by the Global Modeling and Assimilation Office (GMAO) at NASA Goddard Space Flight Center.

References

Akagi, S. K., Yokelson, R. J., Wiedinmyer, C., Alvarado, M. J., Reid, J. S., Karl, T., Crounse, J. D., and Wennberg, P. O.: Emission factors for open and domestic biomass burning for use in atmospheric models, Atmospheric Chemistry and Physics, 11, 4039–4072, https://doi.org/10.5194/acp-11-4039-2011, 2011.

Amiro, B. D., Cantin, A., Flannigan, and de Groot, W. J.: Future emissions from Canadian boreal forest fires, Canadian Journal of Forest Research, 39, 383–395, https://doi.org/10.1139/X08-154, 2009.

Andreae, M. O.: Emission of trace gases and aerosols from biomass burning - An updated assessment, Atmospheric Chemistry and Physics, 19, 8523–8546, https://doi.org/10.5194/acp-19-8523-2019, 2019.

Andreae, M. O. and Merlet, P.: Emission of trace gases and aerosols from biomass burning, Global Biogeochemical Cycles, 15, 955–966, https://doi.org/10.1029/2000GB001382, 2001.

Arola, A., Lindfors, A., Natunen, A., and Lehtinen, K. E. J.: A case study on biomass burning aerosols: effects on aerosol optical properties and surface radiation levels, Atmospheric Chemistry and Physics, 7, 4257–4266, https://doi.org/10.5194/acp-7-4257-2007, 2007.

Barret, B., Mazière, M. D., and Mahieu, E.: Ground-based FTIR measurements of CO from the Jungfraujoch: characterisation and comparison with in situ surface and MOPITT data, Atmospheric Chemistry and Physics, 3, 2217–2223, https://doi.org/10.5194/acp-3-2217-2003, 2003.

Batchelor, R. L., Strong, K., Lindenmaier, R., Mittermeier, R. L., Fast, H., Drummond, J. R., and Fogal, P. F.: A new Bruker IFS 125HR FTIR spectrometer for the Polar Environment Atmospheric Research Laboratory at Eureka, Nunavut, Canada: measurements and comparison with the existing Bomem DA8 spectrometer, Journal of Atmospheric and Oceanic Technology, 26, 1328–1340, https://doi.org/10.1175/2009JTECHA1215.1, 2009.

Baum, M. M., Moss, J. A., Pastel, S. H., and Poskrebyshev, G. A.: Hydrogen cyanide exhaust emissions from in-use motor vehicles, Environmental Science & Technology, 41, 857–862, https://doi.org/10.1021/es061402v, 2007.

Bertschi, I., Yokelson, R. J., Ward, D. E., Babbitt, R. E., Susott, R. A., Goode, J. G., and Hao, W. M.: Trace gas and particle emissions from fires in large diameter and belowground biomass fuels, Journal of Geophysical Research: Atmospheres, 108, 8472, https://doi.org/10.1029/2002JD002100, 2003.

Bey, I., Jacob, D. J., Logan, J. A., and Yantosca, R. M.: Asian chemical outflow to the Pacific in spring: Origins, pathways, and budgets, Journal of Geophysical Research: Atmospheres, 106, 23 097–23 113, https://doi.org/10.1029/2001JD000806, 2001a.

Bey, I., Jacob, D. J., Yantosca, R. M., Logan, J. A., Field, B. D., Fiore, A. M., Li, Q., Liu, H. Y., Mickley, L. J., and Schultz, M. G.: Global modeling of tropospheric chemistry with assimilated meteorology: Model description and evaluation, Journal of Geophysical Research: Atmospheres, 106, 23 073–23 095, https://doi.org/10.1029/2001JD000807, 2001b.

Blumenstock, T., Hase, F., Kramer, I., Mikuteit, S., Fischer, H., Goutail, F., and Raffalski, U.: Winter to winter variability of chlorine activation and ozone loss as observed by ground-based FTIR measurements at Kiruna since winter 1993/94, International Journal of Remote Sensing, 30, 4055–4064, https://doi.org/10.1080/01431160902821916, 2009.

Blumenstock, T. H., Fisher, H., Friedle, A., Hase, F., and Thomas, P.: Column Amounts of $ClONO_2$, HCl, HNO_3, and HF from Ground-Based FTIR Measurements Made Near Kiruna, Sweden, in Late Winter 1994, Journal of Atmospheric Chemistry, 26, 311–321, https://doi.org/10.1023/A:1005728713762, 1997.

Bond, T. C. and Sun, H.: Can reducing black carbon emissions counteract global warming?, Environmental Science & Technology, 39, 5921–5926, 2005.

Boulanger, Y., Gauthier, S., and Burton, P. J.: A refinement of models projecting future Canadian fire regimes using homogeneous fire regime zones, Canadian Fournal of Forest Research, 44, 365–376, https://doi.org/10.1139/cjfr-2013-0372, 2014.

Cicerone, R. J. and Zellner, R.: The atmospheric chemistry of hydrogen cyanide (HCN), Journal of Geophysical Research: Atmospheres, 88, 10 689–10 696, https://doi.org/10.1029/JC088iC15p10689, 1983.

Conard, S. G. and Ivanova, G. A.: Wildfire in Russian Boreal Forests - Potential Impacts of Fire Regime Characteristics on Emissions and Global Carbon Balance Estimates, Environmental Pollution, 98, 305–313, https://doi.org/10.1016/S0269-7491(97)00140-1, 1997.

Crippa, M., Janssens-Maenhout, G., Dentener, F., Guizzardi, D., Sindelarova, K., Muntean, M., Van Dingenen, R., and Granier, C.: Forty years of improvements in European air quality: regional policy-industry interactions with global impacts, Atmospheric Chemistry and Physics, 16, 3825–3841, https://doi.org/10.5194/acp-16-3825-2016, 2016.

Dammers, E., Vigouroux, C., Palm, M., Mahieu, E., Warneke, T., Smale, D., Langerock, B., Franco, B., Van Damme, M., Schaap, M., Notholt, J., and Erisman, J. W.: Retrieval of ammonia from ground-based FTIR solar spectra, Atmospheric Chemistry and Physics, 15, 12 789–12 803, https://doi.org/10.5194/acp-15-12789-2015, 2015.

Damoah, R., Spichtinger, N., Forster, C., James, P., Mattis, I., Wandinger, U., Beirle, S., Wagner, T., and Stohl, A.: Around the world in 17 days - Hemispheric-scale transport of forest fire smoke from Russia in May 2003, Atmospheric Chemistry and Physics, 4, 1311–1321, https://doi.org/10.5194/acp-4-1311-2004, 2004.

De Mazière, M., Thompson, A. M., Kurylo, M. J., Wild, J. D., Bernhard, G., Blumenstock, T., Braathen, G. O., Hannigan, J. W., Lambert, J.-C., Leblanc, T., McGee, T. J., Nedoluha, G., Petropavlovskikh, I., Seckmeyer, G., Simon, P. C., Steinbrecht, W., and Strahan, S. E.: The Network for the Detection of Atmospheric Composition Change (NDACC): History, status and perspectives, Atmospheric Chemistry and Physics, 18, 4935–4964, https://doi.org/10.5194/acp-18-4935-2018, 2018.

Dreessen, J., Sullivan, J., and Delgado, R.: Observations and impacts of transported Canadian wildfire smoke on ozone and aerosol air quality in the Maryland region on June 9-12, 2015, Journal of the Air & Waste Management Association, 66, 842–862, https://doi.org/10.1080/10962247.2016.1161674, 2016.

Eastham, S. D. and Jacob, D. J.: Limits on the ability of global Eulerian models to resolve intercontinental transport of chemical plumes, Atmospheric Chemistry and Physics, 17, 2543–2553, https://doi.org/10.5194/acp-17-2543-2017, 2017.

Eck, T. F., Holben, B. N., Reid, J. S., Sinyuk, A., Hyer, E. J., O'Neill, N. T., Shaw, G. E., Vande Castle, J. R., Chapin, F. S., Dubovik, O., Smirnov, A., Vermote, E., Schafer, J. S., Giles, D., Slutsker, I., Sorokine, M., and Newcomb, W. W.: Optical properties of boreal region biomass burning aerosols in central Alaska and seasonal variation of aerosol optical depth at an Arctic coastal site, Journal of Geophysical Research: Atmospheres, 114, 722–4740, https://doi.org/10.1029/2008JD010870, 2009.

Ehhalt, D. H., Rohrer, F., Wahner, A., Prather, M. J., and Blake, D. R.: On the use of hydrocarbons for the determination of tropospheric OH concentrations, Journal of Geophysical Research: Atmospheres, 103, 18 981–18 997, https://doi.org/10.1029/98JD01106, 1998.

Evangeliou, N., Balkanski, Y., Hao, W. M., Petkov, A., Silverstein, R. P., Corley, R., Nordgren, B. L., Urbanski, S. P., Eckhardt, S., Stohl, A., and Others: Wildfires in northern Eurasia affect the budget of black carbon in the Arctic - A 12-year retrospective synopsis (2002-2013), Atmospheric Chemistry and Physics, 16, 7587–7604, 2016.

Eyring, V., Waugh, D. W., Bodeker, G. E., Cordero, E., Akiyoshi, H., Austin, J., Beagley, S. R., Boville, B. A., Braesicke, P., Brühl, C., Butchart, N., Chipperfield, M. P., Dameris, M., Deckert, R., Deushi, M., Frith, S. M., Garcia, R. R., Gettelman, A., Giorgetta, M. A., Kinnison, D. E., Mancini, E., Manzini, E., Marsh, D. R., Matthes, S., Nagashima, T., Newman, P. A., Nielsen, J. E., Pawson, S., Pitari, G., Plummer, D. A., Rozanov, E., Schraner, M., Scinocca, J. F., Semeniuk, K., Shepherd, T. G., Shibata, K., Steil, B., Stolarski, R. S., Tian, W., and Yoshiki, M.: Multimodel projections of stratospheric ozone in the 21st century, Journal of Geophysical Research: Atmospheres, 112, D03 304, https://doi.org/10.1029/2006JD008332, 2007.

Fischer, H., Wienhold, F. G., Hoor, P., Bujok, O., Schiller, C., Siegmund, P., Ambaum, M., Scheeren, H. A., and Lelieveld, J.: Tracer correlations in the northern high latitude lowermost stratosphere: Influence of cross-tropopause mass exchange, Geophysical Research Letters, 27, 97–100, https://doi.org/10.1029/1999GL010879, 2000.

Fisher, J. A., Jacob, D. J., Purdy, M. T., Kopacz, M., Sager, P. L., Carouge, C., Holmes, C. D., Yantosca, R. M., Batchelor, R. L., Strong, K., Diskin, G. S., Fuelberg, H. E., Holloway, J. S., Hyer, E. J., McMillan, W. W., Warner, J., Streets, D. G., Zhang, Q., Wang, Y., and Wu, S.: Source attribution and interannual variability of Arctic pollution in spring constrained by aircraft (ARCTAS, ARCPAC) and satellite (AIRS) observations of carbon monoxide, Atmospheric Chemistry and Physics, 10, 977–996, https://doi.org/10.5194/acp-10-977-2010, 2010.

Fisher, J. A., Murray, L., Jones, D. B. A., and Deutscher, N. M.: Improved method for linear carbon monoxide simulation and source attribution in atmospheric chemistry models illustrated using GEOS-Chem v9, Geophysical Model Development, 10, 4129–4144, https://doi.org/10.5194/gmd-10-4129-2017, 2017.

Flanner, M. G.: Arctic climate sensitivity to local black carbon, Journal of Geophysical Research: Atmospheres, 118, 1840–1851, 2013.

Flannigan, M. D., Krawchuk, M. A., de Groot, W. J., Mike Wotton, B., and Gowman, L. M.: Implications of changing climate for global wildland fire, International Journal of Wildland Fire, 18, 483–507, https://doi.org/10.1071/WF08187, 2009.

Franco, B., Bader, W., Toon, G. C., Bray, C., Perrin, A., Fischer, E. V., Sudo, K., Boone, C. D., Bovy, B., Lejeune, B., Servais, C., and Mahieu, E.: Retrieval of ethane from ground-based FTIR solar spectra using improved spectroscopy: Recent burden increase above Jungfraujoch, Journal of Quantitative Spectroscopy & Radiative Transfer, 160, 36–49, https://doi.org/10.1016/j.jqsrt.2015.03.017, 2015.

Franco, B., Mahieu, E., Emmons, L. K., Tzompa-Sosa, Z. A., Fischer, E. V., Sudo, K., Bovy, B., Conway, S., Griffin, D., Hannigan, J. W., Strong, K., and Walker, K. A.: Evaluating ethane and methane emissions associated with the development of oil and natural gas extraction in North America, Environmental Research Letters, 11, 044 010, https://doi.org/10.1088/1748-9326/11/4/044010, 2016.

Franklin, J. E., Drummond, J. R., Griffin, D., Pierce, J. R., Waugh, D. L., Palmer, P. I., Parrington, M., Lee, J. D., Lewis, A. C., Rickard, A. R., Taylor, J. W., Allan, J. D., Coe, H., Walker, K. A., Chisholm, L., Duck, T. J., Hopper, J. T., Blanchard, Y., Gibson, M. D., Curry, K. R., Sakamoto, K. M., Lesins, G., Dan, L., Kliever, J., and Saha, A.: A case study of aerosol scavenging in a biomass burning plume over eastern Canada during the 2011 BORTAS field experiment, Atmospheric Chemistry and Physics, 14, 8449–8460, https://doi.org/10.5194/acp-14-8449-2014, 2014.

Freitas, S. R., Longo, K. M., Chatfield, R., Latham, D., Silva Dias, M. A. F., Andreae, M. O., Prins, E., Santos, J. C., Gielow, R., and Carvalho, Jr, J. A.: Including the sub-grid scale plume rise of vegetation fires in low resolution atmospheric transport models, Atmospheric Chemistry and Physics, 7, 3385–3398, 2007.

Fromm, M., Alfred, J., Hoppel, K., Hornstein, J., Bevilacqua, R., Shettle, E., Servranckx, R., Li, Z., and Stocks, B.: Observations of boreal forest fire smoke in the stratosphere by POAM III, SAGE II, and lidar in 1998, Geophysical Research Letters, 27, 1407–1410, https://doi.org/10.1029/1999GL011200, 2000.

Gelaro, R., McCarty, W., Suárez, M. J., Todling, R., Molod, A., Takacs, L., Randles, C. A., Darmenov, A., Bosilovich, M. G., Reichle, R., Wargan, K., Coy, L., Cullather, R., Draper, C., Akella, S., Buchard, V., Conaty, A., da Silva, A. M., Gu, W., Kim, G.-K., Koster, R., Lucchesi, R., Merkova, D., Nielsen, J. E., Partyka, G., Pawson, S., Putman, W., Rienecker, M., Schubert, S. D., Sienkiewicz, M., and Zhao, B.: The Modern-Era Retrospective Analysis for Research and Applications, Version 2 (MERRA-2), Journal of Climate, 30, 5419–5454, https://doi.org/10.1175/JCLI-D-16-0758.1, 2017.

Giglio, L., Randerson, J. T., and van der Werf, G. R.: Analysis of daily, monthly, and annual burned area using the fourth-generation global fire emissions database (GFED4), Journal of Geophysical Research: Biogeosciences, 118, 317–328, https://doi.org/10.1002/jgrg.20042, 2013.

Giles, D. M., Sinyuk, A., Sorokin, M. G., Schafer, J. S., Smirnov, A., Slutsker, I., Eck, T. F., Holben, B. N., Lewis, J. R., Campbell, J. R., Welton, E. J., Korkin, S. V., and Lyapustin, A. I.: Advancements in the Aerosol Robotic Network (AERONET) Version 3 database - automated near-real-time quality control algorithm with improved cloud screening for Sun photometer aerosol optical depth (AOD) measurements, Atmospheric Measurement Techniques, 12, 169–209, https://doi.org/10.5194/amt-12-169-2019, 2019.

Giuseppe, F. D., Rémy, S., Pappenberger, F., and Wetterhall, F.: Using the Fire Weather Index (FWI) to improve the estimation of fire emissions from fire radiative power (FRP) observations, Atmospheric Chemistry and Physics, 18, 5359–5370, https://doi.org/10.5194/acp-18-5359-2018, 2018.

Goode, J. G., Yokelson, R. J., Susott, R. A., and Ward, D. E.: Trace gas emissions from laboratory biomass fires measured by open-path Fourier transform infrared spectroscopy: Fires in grass and surface fuels, Journal of Geophysical Research: Atmospheres, 104, 21 237–21 245, https://doi.org/10.1029/1999JD900360, 1999.

Goode, J. G., Yokelson, R. J., Ward, D. E., Susott, R. A., Babbitt, R. E., Davies, M. A., and Hao, W. M.: Measurements of excess O_3, CO_2, CO, CH_4, C_2H_4, C_2H_2, HCN, NO, NH_3, HCOOH, CH_3COOH, HCHO, and CH_3OH in 1997 Alaskan biomass burning plumes by airborne Fourier transform infrared spectroscopy (AFTIR), Journal of Geophysical Research: Atmospheres, 105, 22 147–22 166, https://doi.org/10.1029/2000JD900287, 2000.

Griffin, D., Walker, K. A., Franklin, J. E., Parrington, M., Whaley, C., Hopper, J., Drummond, J. R., Palmer, P. I., Strong, K., Duck, T. J., Abboud, I., Bernath, P. F., Clerbaux, C., Coheur, P.-F., Curry, K. R., Dan, L., Hyer, E., Kliever, J., Lesins, G., Maurice, M., Saha, A., Tereszchuk, K., and Weaver, D.: Investigation of CO, C_2H_6 and aerosols in a boreal fire plume over eastern Canada during BORTAS 2011 using ground- and satellite-based observations and model simulations, Atmospheric Chemistry and Physics, 13, 10 227–10 241, https://doi.org/10.5194/acp-13-10227-2013, 2013.

Gubler, S., Gruber, S., and Purves, R. S.: Uncertainties of parameterized surface downward clear-sky shortwave and all-sky longwave radiation, Atmospheric Chemistry and Physics, 12, 5077–5098, https://doi.org/10.5194/acp-12-5077-2012, 2012.

Guenther, A., Geron, C., Pierce, T., Lamb, B., Harley, P., and Fall, R.: Natural emissions of non-methane volatile organic compounds, carbon monoxide, and oxides of nitrogen from North America, Atmospheric Environment, 34, 2205–2230, https://doi.org/10.1016/S1352-2310(99)00465-3, 2000.

Guenther, A. B., Jiang, X., Heald, C. L., Sakulyanontvittaya, T., Duhl, T., Emmons, L. K., and Wang, X.: The Model of Emissions of Gases and Aerosols from Nature version 2.1 (MEGAN2.1): An extended and updated framework for modeling biogenic emissions, Geoscientific Model Development, 5, 1471–1492, https://doi.org/10.5194/gmd-5-1471-2012, 2012.

Hannigan, J. W., Coffey, M. T., and Goldman, A.: Semiautonomous FTS Observation System for Remote Sensing of Stratospheric and Tropospheric Gases, Journal of Atmospheric and Oceanic Technology, 26, 1814–1828, https://doi.org/10.1175/2009JTECHA1230.1, 2009.

Hase, F., Hannigan, J. W., Coffey, M. T., Goldman, A., Höpfner, M., Jones, N. B., Rinsland, C. P., and Wood, S. W.: Intercomparison of retrieval codes used for the analysis of high-resolution, ground-based FTIR measurements, Journal of Quantitative Spectroscopy & Radiative Transfer, 87, 25–52, https://doi.org/10.1016/j.jqsrt.2003.12.008, 2004.

Heilman, W. E., Liu, Y., Urbanski, S., Kovalev, V., and Mickler, R.: Wildland fire emissions, carbon, and climate: Plume rise, atmospheric transport, and chemistry processes, Forest Ecology and Management, 317, 70–79, https://doi.org/10.1016/j.foreco.2013.02.001, 2014.

Henne, S., Brunner, D., Folini, D., Solberg, S., Klausen, J., and Buchmann, B.: Assessment of parameters describing representativeness of air quality in-situ measurement sites, Atmospheric Chemistry and Physics, 10, 3561–3581, https://doi.org/10.5194/acp-10-3561-2010, 2010.

Holben, B. N., Eck, T. F., Slutsker, I., Tanré, D., Buis, J. P., Setzer, A., Vermote, E., Reagan, J. A., Kaufman, Y. J., Nakajima, T., Lavenu, F., Jankowiak, I., and Smirnov, A.: AERONET - A Federated Instrument Network and Data Archive for Aerosol Characterization, Remote Sensing of Environment, 66, 1–16, https://doi.org/10.1016/S0034-4257(98)00031-5, 1998.

Holloway, T., Levy, H., and Kasibhatla, P.: Global distribution of carbon monoxide, Journal of Geophysical Research: Atmospheres, 105, 12 123–12 147, https://doi.org/10.1029/1999JD901173, 2000.

Holtslag, A. A. M. and Boville, B. A.: Local Versus Nonlocal Boundary-Layer Diffusion in a Global Climate Model, Journal of Climate, 6, 1825–1842, https://doi.org/10.1175/1520-0442(1993)006<1825:LVNBLD>2.0.CO;2, 1993.

Honrath, R. E.: Regional and hemispheric impacts of anthropogenic and biomass burning emissions on summertime CO and O_3 in the North Atlantic lower free troposphere, Journal of Geophysical Research: Atmospheres, 109, https://doi.org/10.1029/2004JD005147, 2004.

Hoor, P., Fischer, H., Lange, L., Lelieveld, J., and Brunner, D.: Seasonal variations of a mixing layer in the lowermost stratosphere as identified by the CO-O_3 correlation from in situ measurements, Journal of Geophysical Research: Atmospheres, 107, ACL 1–1–ACL 1–11, https://doi.org/10.1029/2000JD000289, 2002.

Hornbrook, R. S., Blake, D. R., Diskin, G. S., Fried, A., Fuelberg, H. E., Meinardi, S., Mikoviny, T., Richter, D., Sachse, G. W., Vay, S. A., Walega, J., Weibring, P., Weinheimer, A. J., Wiedinmyer, C., Wisthaler, A., Hills, A., Riemer, D. D., and Apel, E. C.: Observations of nonmethane organic compounds during ARCTAS - Part 1: Biomass burning emissions and plume enhancements, Atmospheric Chemistry and Physics, 11, 11 103–11 130, https://doi.org/10.5194/acp-11-11103-2011, 2011.

Hu, Q., Goloub, P., Veselovskii, I., Bravo-Aranda, J.-A., Popovici, I. E., Podvin, T., Haeffelin, M., Lopatin, A., Dubovik, O., Pietras, C., Huang, X., Torres, B., and Chen, C.: Long-range-transported Canadian smoke plumes in the lower stratosphere over northern France, Atmospheric Chemistry and Physics, 19, 1173–1193, https://doi.org/10.5194/acp-19-1173-2019, 2019.

Ikeda, K. and Tanimoto, H.: Exceedances of air quality standard level of PM2.5 in Japan caused by Siberian wildfires, Environmental Research Letters, 10, 105 001, https://doi.org/10.1088/1748-9326/10/10/105001, 2015.

Jaffe, D., Anderson, T., Covert, D., Kotchenruther, R., Trost, B., Danielson, J., Simpson, W., Berntsen, T., Karlsdottir, S., Blake, D., Harris, J., Carmichael, G., and Uno, I.: Transport of Asian air pollution to North America, Geophysical Research Letters, 26, 711–714, https://doi.org/10.1029/1999GL900100, 1999.

Jaffe, D., Bertschi, I., Jaeglé, L., Novelli, P., Reid, J. S., Tanimoto, H., Vingarzan, R., and Westphal, D. L.: Long-range transport of Siberian biomass burning emissions and impact on surface ozone in western North America, Geophysical Research Letters, 31, https://doi.org/10.1029/2004GL020093, 2004.

Jeong, J. I., Park, R. J., and Youn, D.: Effects of Siberian forest fires on air quality in East Asia during May 2003 and its climate implication, Atmospheric Environment, 42, 8910–8922, https://doi.org/10.1016/j.atmosenv.2008.08.037, 2008.

Kaiser, J. W., Heil, A., Andreae, M. O., Benedetti, A., Chubarova, N., Jones, L., Morcrette, J.-J., Razinger, M., Schultz, M. G., Suttie, M., and van der Werf, G. R.: Biomass burning emissions estimated with a global fire assimilation system based on observed fire radiative power, Biogeosciences, 9, 527–554, https://doi.org/10.5194/bg-9-527-2012, 2012.

Kasai, Y. J., Kagawa, A., Jones, N., Fujiwara, A., Seki, K., Murayama, Y., and Murcray, F.: Seasonal variations of CO and HCN in the troposphere measured by solar absorption spectroscopy over Poker Flat, Alaska, Geophysical Research Letters, 32, 1–4, https://doi.org/10.1029/2005GL022826, 2005a.

Kasai, Y. J., Koshiro, T., Endo, M., Jones, N. B., and Murayama, Y.: Ground-based measurement of strato–mesospheric CO by a FTIR spectrometer over Poker Flat, Alaska, Advances in Space Research, 35, 2024–2030, https://doi.org/10.1016/j.asr.2005.04.099, 2005b.

Khaykin, S. M., Godin-Beekmann, S., Hauchecorne, A., Pelon, J., Ravetta, F., and Keckhut, P.: Stratospheric Smoke With Unprecedentedly High Backscatter Observed by Lidars Above Southern France, Geophysical Research Letters, 45, 1639–1646, https://doi.org/10.1002/2017GL076763, 2018.

Kirchmeier-Young, M. C., Gillett, N. P., Zwiers, F. W., Cannon, A. J., and Anslow, F. S.: Attribution of the Influence of Human-Induced Climate Change on an Extreme Fire Season, Earth's Future, 7, 2–10, https://doi.org/10.1029/2018EF001050, 2019.

Klonecki, A.: Seasonal changes in the transport of pollutants into the Arctic troposphere-model study, Journal of Geophysical Research: Atmospheres, 108, 8367, https://doi.org/10.1029/2002JD002199, 2003.

Kochtubajda, B., Stewart, R. E., Flannigan, M. D., Bonsal, B. R., Cuell, C., and Mooney, C. J.: An Assessment of Surface and Atmospheric Conditions Associated with the Extreme 2014 Wildfire Season in Canada's Northwest Territories, Atmosphere-Ocean, 57, 73–90, https://doi.org/10.1080/07055900.2019.1576023, 2019.

Konovalov, I. B., Beekmann, M., Kuznetsova, I. N., Yurova, A., and Zvyagintsev, A. M.: Atmospheric impacts of the 2010 Russian wildfires: Integrating modelling and measurements of an extreme air pollution episode in the Moscow region, Atmospheric Chemistry and Physics, 11, 10 031–10 056, https://doi.org/10.5194/acp-11-10031-2011, 2011.

Kozlov, V. S., Yausheva, E. P., Terpugova, S. A., Panchenko, M. V., Chernov, D. G., and Shmargunov, V. P.: Optical–microphysical properties of smoke haze from Siberian forest fires in summer 2012, International Journal of Remote Sensing, 35, 5722–5741, https://doi.org/10.1080/01431161.2014.945010, 2014.

Krause, A., Kloster, S., Wilkenskjeld, S., and Paeth, H.: The sensitivity of global wildfires to simulated past, present, and future lightning frequency, Journal of Geophysical Research: Biogeosciences, 119, 312–322, https://doi.org/10.1002/2013JG002502, 2014.

Kurylo, M. J.: Network for the Detection of Stratospheric Change, https://doi.org/10.1117/12.46658, 1991.

Law, K. S. and Stohl, A.: Arctic air pollution: origins and impacts, Science, 315, 1537–1540, https://doi.org/10.1126/science.1137695, 2007.

Le Breton, M., Bacak, A., Muller, J. B. A., O'Shea, S. J., Xiao, P., Ashfold, M. N. R., Cooke, M. C., Batt, R., Shallcross, D. E., Oram, D. E., Forster, G., Bauguitte, S. J.-B., Palmer, P. I., Parrington, M., Lewis, A. C., Lee, J. D., and Percival, C. J.: Airborne hydrogen cyanide measurements using a chemical ionisation mass spectrometer for the plume identification of biomass burning forest fires, Atmospheric Chemistry and Physics, 13, 9217–9232, https://doi.org/10.5194/acp-13-9217-2013, 2013.

Lefer, B. L., Talbot, R. W., Harriss, R. H., Bradshaw, J. D., Sandholm, S. T., Olson, J. O., Sachse, G. W., Collins, J., Shipham, M. A., Blake, D. R., Klemm, K. I., Klemm, O., Gorzelska, K., and Barrick, J.: Enhancement of acidic gases in biomass burning impacted air masses over Canada, Journal of Geophysical Research: Atmospheres, 99, 1721–1737, https://doi.org/10.1029/93JD02091, 1994.

Levine, J. S.: 4.05 - Biomass Burning: The Cycling of Gases and Particulates from the Biosphere to the Atmosphere, in: Treatise on Geochemistry, edited by Holland, H. D. and Turekian, K. K., pp. 143–158, Pergamon, Oxford, https://doi.org/10.1016/B0-08-043751-6/04143-8, 2003.

Lewis, A. C., Evans, M. J., Hopkins, J. R., Punjabi, S., Read, K. A., Purvis, R. M., Andrews, S. J., Moller, S. J., Carpenter, L. J., Lee, J. D., Rickard, A. R., Palmer, P. I., and Parrington, M.: The influence of biomass burning on the global distribution of selected non-methane organic compounds, Atmospheric Chemistry and Physics, 13, 851–867, https://doi.org/10.5194/acp-13-851-2013, 2013.

Li, Q., Jacob, D. J., Bey, I., Yantosca, R. M., Zhao, Y., Kondo, Y., and Notholt, J.: Atmospheric hydrogen cyanide (HCN): Biomass burning source, ocean sink?, Geophysical Research Letters, 27, 357–360, https://doi.org/10.1029/1999GL010935, 2000.

Li, Q., Jacob, D. J., Yantosca, R. M., Heald, C. L., Singh, H. B., Koike, M., Zhao, Y., Sachse, G. W., and Streets, D. G.: A global three-dimensional model analysis of the atmospheric budgets of HCN and CH_3CN: Constraints from aircraft and ground measurements, Journal of Geophysical Research: Atmospheres, 108, 8827, https://doi.org/10.1029/2002JD003075, 2003.

Li, Q., Palmer, P. I., Pumphrey, H. C., Bernath, P., and Mahieu, E.: What drives the observed variability of HCN in the troposphere and lower stratosphere?, Atmospheric Chemistry and Physics, 9, 8531–8543, https://doi.org/10.5194/acp-9-8531-2009, 2009.

Logan, J. A., Prather, M. J., Wofsy, S. C., and McElroy, M. B.: Tropospheric chemistry: A global perspective, Journal of Geophysical Research: Oceans, 86, 7210–7254, https://doi.org/10.1029/JC086iC08p07210, 1981.

Lutsch, E., Dammers, E., Conway, S., and Strong, K.: Long-range transport of NH_3, CO, HCN, and C_2H_6 from the 2014 Canadian Wildfires, Geophysical Research Letters, 43, 8286–8297, https://doi.org/10.1002/2016GL070114, 2016.

Lutsch, E., Strong, K., Jones, D. B. A., Ortega, I., Hannigan, J. W., Dammers, E., Shephard, M. W., Morris, E., Murphy, K., Evans, M. J., Parrington, M., Whitburn, S., Van Damme, M., Clarisse, L., Coheur, P., Clerbaux, C., Croft, B., Martin, R. V., Pierce, J. R., and Fisher, J. A.: Unprecedented Atmospheric Ammonia Concentrations Detected in the High Arctic From the 2017 Canadian Wildfires, Journal of Geophysical Research: Atmospheres, 124, 8178–8202, https://doi.org/10.1029/2019JD030419, 2019.

Macias Fauria, M. and Johnson, E. A.: Large-scale climatic patterns control large lightning fire occurrence in Canada and Alaska forest regions, Journal of Geophysical Research: Biogeosciences, 111, 2006.

Macias Fauria, M. and Johnson, E. A.: Climate and wildfires in the North American boreal forest, Philosophical transactions of the Royal Society of London. Series B, Biological Sciences, 363, 2315–2327, https://doi.org/10.1098/rstb.2007.2202, 2008.

Mack, M. C., Bret-Harte, M. S., Hollingsworth, T. N., Jandt, R. R., Schuur, E. A. G., Shaver, G. R., and Verbyla, D. L.: Carbon loss from an unprecedented Arctic tundra wildfire, Nature, 475, 489–492, https://doi.org/10.1038/nature10283, 2011.

Mahieu, E., Zander, R., Delbouille, L., Demoulin, P., Roland, G., and Servais, C.: Observed trends in total vertical column abundances of atmospheric gases from IR solar spectra recorded at the Jungfraujoch, Journal of Atmospheric Chemistry, 28, 227–243, https://doi.org/10.1023/A:1005854926740, 1997.

Makar, P. A., Akingunola, A., Aherne, J., Cole, A. S., Aklilu, Y.-A., Zhang, J., Wong, I., Hayden, K., Li, S.-M., Kirk, J., Scott, K., Moran, M. D., Robichaud, A., Cathcart, H., Baratzedah, P., Pabla, B., Cheung, P., Zheng, Q., and Jeffries, D. S.: Estimates of exceedances of critical loads for acidifying deposition in Alberta and Saskatchewan, Atmospheric Chemistry and Physics, 18, 9897–9927, https://doi.org/10.5194/acp-18-9897-2018, 2018.

Makarova, M. V., Poberovskii, A. V., and Osipov, S. I.: Time variations of the total CO content in the atmosphere near St. Petersburg, Izvestiya, Atmospheric and Oceanic Physics, 47, 739–746, https://doi.org/10.1134/S0001433811060090, 2011.

Marsh, D. R., Mills, M. J., Kinnison, D. E., Lamarque, J.-F., Calvo, N., and Polvani, L. M.: Climate Change from 1850 to 2005 Simulated in CESM1 (WACCM), Journal of Climate, 26, 7372–7391, https://doi.org/10.1175/JCLI-D-12-00558.1, 2013.

McConnell, J. R., Edwards, R., Kok, G. L., Flanner, M. G., Zender, C. S., Saltzman, E. S., Banta, J. R., Pasteris, D. R., Carter, M. M., and Kahl, J. D. W.: 20th-century industrial black carbon emissions altered Arctic climate forcing, Science, 317, 1381–1384, https://doi.org/10.1126/science.1144856, 2007.

McKeen, S. A. and Liu, S. C.: Hydrocarbon ratios and photochemical history of air masses, Geophysical Research Letters, 20, 2363–2366, https://doi.org/10.1029/93GL02527, 1993.

McKeen, S. A., Liu, S. C., Hsie, E.-Y., Lin, X., Bradshaw, J. D., Smyth, S., Gregory, G. L., and Blake, D. R.: Hydrocarbon ratios during PEM-WEST A: A model perspective, Journal of Geophysical Research: Atmospheres, 101, 2087–2109, https://doi.org/10.1029/95JD02733, 1996.

Moussa, S. G., Leithead, A., Li, S.-M., Chan, T. W., Wentzell, J. J. B., Stroud, C., Zhang, J., Lee, P., Lu, G., Brook, J. R., Hayden, K., Narayan, J., and Liggio, J.: Emissions of hydrogen cyanide from on-road gasoline and diesel vehicles, Atmospheric Environment, 131, 185–195, https://doi.org/10.1016/j.atmosenv.2016.01.050, 2016.

Muller, J.-F., Stavrakou, T., Bauwens, M., George, M., Hurtmans, D., Coheur, P.-F., Clerbaux, C., and Sweeney, C.: Top-Down CO Emissions Based On IASI Observations and Hemispheric Constraints on OH Levels, Geophysical Research Letters, 45, 1621–1629, https://doi.org/10.1002/2017GL076697, 2018.

Nance, J. D., Hobbs, P. V., Radke, L. F., and Ward, D. E.: Airborne measurements of gases and particles from an Alaskan wildfire, Journal of Geophysical Research, D: Atmospheres, 98, 14 873–14 882, https://doi.org/10.1029/93JD01196, 1993.

Notholt, J., Toon, G., Stordal, F., Solberg, S., Schmidbauer, N., Becker, E., Meier, A., and Sen, B.: Seasonal variations of atmospheric trace gases in the high Arctic at 79°N, Journal of Geophysical Research: Atmospheres, 102, 12 855–12 861, https://doi.org/10.1029/97JD00337, 1997a.

Notholt, J., Toon, G. C., Lehmann, R., Sen, B., and Blavier, J.-F.: Comparison of Arctic and Antarctic trace gas column abundances from ground-based Fourier transform infrared spectrometry, Journal of Geophysical Research: Atmospheres, 102, 12 863–12 869, https://doi.org/10.1029/97JD00358, 1997b.

Notholt, J., Toon, G. C., Rinsland, C. P., Pougatchev, N. S., Jones, N. B., Connor, B. J., Weller, R., Gautrois, M., and Schrems, O.: Latitudinal variations of trace gas concentrations in the free troposphere measured by solar absorption spectroscopy during a ship cruise, Journal of Geophysical Research: Atmospheres, 105, 1337–1349, https://doi.org/10.1029/1999JD900940, 2000.

O'Neill, N. T., Perro, C., Saha, A., Lesins, G., Duck, T. J., Eloranta, E. W., Nott, G. J., Hoffman, A., Karumudi, M. L., Ritter, C., Bourassa, A., Abboud, I., Carn, S. A., and Savastiouk, V.: Properties of Sarychev sulphate aerosols over the Arctic, Journal of Geophysical Research: Atmospheres, 117, https://doi.org/10.1029/2011JD016838, 2012.

Ordóñez, C., Brunner, D., Staehelin, J., Hadjinicolaou, P., Pyle, J. A., Jonas, M., Wernli, H., and Prévôt, A. S. H.: Strong influence of lowermost stratospheric ozone on lower tropospheric background ozone changes over Europe, Geophysical Research Letters, 34, https://doi.org/10.1029/2006GL029113, 2007.

Pan, L. L., Randel, W. J., Gary, B. L., Mahoney, M. J., and Hintsa, E. J.: Definitions and sharpness of the extratropical tropopause: A trace gas perspective, Journal of Geophysical Research: Atmospheres, 109, https://doi.org/10.1029/2004JD004982, 2004.

Parrington, M., Palmer, P. I., Lewis, A. C., Lee, J. D., Rickard, A. R., Carlo, P. D., Taylor, J. W., Hopkins, J. R., Punjabi, S., Oram, D. E., Forster, G., Aruffo, E., Moller, S. J., Bauguitte, S. J.-B., Allan, J. D., Coe, H., and Leigh, R. J.: Ozone photochemistry in boreal biomass burning plumes, Atmospheric Chemistry and Physics, 13, 7321–7341, https://doi.org/10.5194/acp-13-7321-2013, 2013.

Paton-Walsh, C., Jones, N., Wilson, S., Meier, A., Deutscher, N., Griffith, D., Mitchell, R., and Campbell, S.: Trace gas emissions from biomass burning inferred from aerosol optical depth, Geophysical Research Letters, 31, https://doi.org/10.1029/2003GL018973, 2004.

Paton-Walsh, C., Jones, N. B., Wilson, S. R., Haverd, V., Meier, A., Griffith, D. W. T., and Rinsland, C. P.: Measurements of trace gas emissions from Australian forest fires and correlations with coincident measurements of aerosol optical depth, Journal of Geophysical Research: Atmospheres, 110, https://doi.org/10.1029/2005JD006202, 2005.

Paton-Walsh, C., Deutscher, N. M., Griffith, D. W. T., Forgan, B. W., Wilson, S. R., Jones, N. B., and Edwards, D. P.: Trace gas emissions from savanna fires in northern Australia, Journal of Geophysical Research: Atmospheres, 115, https://doi.org/10.1029/2009JD013309, 2010.

Patra, P. K., Houweling, S., Krol, M., Bousquet, P., Belikov, D., Bergmann, D., Bian, H., Cameron-Smith, P., Chipperfield, M. P., Corbin, K., Fortems-Cheiney, A., Fraser, A., Gloor, E., Hess, P., Ito, A., Kawa, S. R., Law, R. M., Loh, Z., Maksyutov, S., Meng, L., Palmer,

P. I., Prinn, R. G., Rigby, M., Saito, R., and Wilson, C.: TransCom model simulations of CH_4 and related species: Linking transport, surface flux and chemical loss with CH_4 variability in the troposphere and lower stratosphere, Atmospheric Chemistry and Physics, 11, 12 813–12 837, https://doi.org/10.5194/acp-11-12813-2011, 2011.

Peterson, D. A., Campbell, J. R., Hyer, E. J., Fromm, M. D., Kablick, G. P., Cossuth, J. H., and DeLand, M. T.: Wildfire-driven thunderstorms cause a volcano-like stratospheric injection of smoke, Climate and Atmospheric Science, 1, 30, https://doi.org/10.1038/s41612-018-0039-3, 2018.

Petetin, H., Sauvage, B., Parrington, M., Clark, H., Fontaine, A., Athier, G., Blot, R., Boulanger, D., Cousin, J.-M., Nédélec, P., and Thouret, V.: The role of biomass burning as derived from the tropospheric CO vertical profiles measured by IAGOS aircraft in 2002-2017, Atmospheric Chemistry and Physics, 18, 17 277–17 306, https://doi.org/10.5194/acp-18-17277-2018, 2018.

Pougatchev, N. S., Connor, B. J., and Rinsland, C. P.: Infrared measurements of the ozone vertical distribution above Kitt Peak, Journal of Geophysical Research: Atmospheres, 100, 16 689–16 697, https://doi.org/10.1029/95JD01296, 1995.

Ramanathan, V. and Carmichael, G.: Global and regional climate changes due to black carbon, Nature Geoscience, 1, 221–227, https://doi.org/10.1038/ngeo156, 2008.

Rastigejev, Y., Park, R., Brenner, M. P., and Jacob, D. J.: Resolving intercontinental pollution plumes in global models of atmospheric transport, Journal of Geophysical Research: Atmospheres, 115, https://doi.org/10.1029/2009JD012568, 2010.

Rémy, S., Veira, A., Paugam, R., Sofiev, M., Kaiser, J. W., Marenco, F., Burton, S. P., Benedetti, A., Engelen, R. J., Ferrare, R., and Hair, J. W.: Two global data sets of daily fire emission injection heights since 2003, Atmospheric Chemistry and Physics, 17, 2921–2942, https://doi.org/10.5194/acp-17-2921-2017, 2017.

R'Honi, Y., Clarisse, L., Clerbaux, C., Hurtmans, D., Duflot, V., Turquety, S., Ngadi, Y., and Coheur, P.-F.: Exceptional emissions of NH_3 and HCOOH in the 2010 Russian wildfires, Atmospheric Chemistry and Physics, 13, 4171–4181, https://doi.org/10.5194/acp-13-4171-2013, 2013.

Rinsland, C. P., Jones, N. B., Connor, B. J., Logan, J. A., Pougatchev, N. S., Goldman, A., Murcray, F. J., Stephen, T. M., Pine, A. S., Zander, R., Mahieu, E., and Demoulin, P.: Northern and Southern hemisphere ground-based infrared spectroscopic measurements of tropospheric carbon monoxide and ethane, Journal of Geophysical Research: Atmospheres, 103, 28 197–28 217, https://doi.org/10.1029/98JD02515, 1998.

Rinsland, C. P., Dufour, G., Boone, C. D., Bernath, P. F., Chiou, L., Coheur, P.-F., e, and Clerbaux, C.: Satellite boreal measurements over Alaska and Canada during June-July 2004: Simultaneous measurements of upper tropospheric CO, C_2H_6 , HCN, CH_3Cl, CH_4 , C_2H_2 , CH_3OH, HCOOH, OCS, and SF_6 mixing ratios, Global Biogeochemical Cycles, 21, GB3008, https://doi.org/10.1029/2006GB002795, 2007.

Rinsland, C. P., Mahieu, E., Chiou, L., and Herbin, H.: First ground-based infrared solar absorption measurements of free tropospheric methanol (CH_3OH): Multidecade infrared time series from Kitt Peak (31.9° N 111.6° W), Journal of Geophysical Research, D: Atmospheres, 114, https://doi.org/10.1029/2008JD011003, 2009.

Rodgers, C. D.: Inverse Methods for Atmospheric Sounding: Theory and Practice, Series on Atmospheric, Oceanic and Planetary Physics, World Scientific, 2000.

Rodgers, C. D. and Connor, B. J.: Intercomparison of remote sounding instruments, Journal of Geophysical Research: Atmospheres, 108, 4116, https://doi.org/10.1029/2002JD002299, 2003.

Rodríguez, E., Toledano, C., Cachorro, V. E., Ortiz, P., Stebel, K., Berjón, A., Blindheim, S., Gausa, M., and de Frutos, A. M.: Aerosol characterization at the sub-Arctic site Andenes (69°N, 16°E), by the analysis of columnar optical properties, Quarterly Journal of the Royal Meteorological Society, 138, 471–482, https://doi.org/10.1002/qj.921, 2012.

Rozwadowska, A., Zieliński, T., Petelski, T., and Sobolewski, P.: Cluster analysis of the impact of air back-trajectories on aerosol optical properties at Hornsund, Spitsbergen, Atmospheric Chemistry and Physics, 10, 877–893, https://doi.org/10.5194/acp-10-877-2010, 2010.

Rudolph, J.: The tropospheric distribution and budget of ethane, Journal of Geophysical Research: Atmospheres, 100, 11 369–11 381, https://doi.org/10.1029/95JD00693, 1995.

Saha, A., O'Neill, N. T., Eloranta, E., Stone, R. S., Eck, T. F., Zidane, S., Daou, D., Lupu, A., Lesins, G., Shiobara, M., and Others: Pan-Arctic sunphotometry during the ARCTAS-A campaign of April 2008, Geophysical Research Letters, 37, 2010.

Saha, S., Moorthi, S., Wu, X., Wang, J., Nadiga, S., Tripp, P., Behringer, D., Hou, Y.-T., Chuang, H.-Y., Iredell, M., Ek, M., Meng, J., Yang, R., Mendez, M. P., van den Dool, H., Zhang, Q., Wang, W., Chen, M., and Becker, E.: NCEP Climate Forecast System Version 2 (CFSv2) 6-hourly Products, https://doi.org/10.5065/D61C1TXF, 2011.

Santín, C., Doerr, S. H., Preston, C. M., and González-Rodríguez, G.: Pyrogenic organic matter production from wildfires: A missing sink in the global carbon cycle, Global Change Biology, 21, 1621–1633, https://doi.org/10.1111/gcb.12800, 2015.

Schimel, D. and Baker, D.: Carbon cycle: the wildfire factor, Nature, 420, 29–30, https://doi.org/10.1038/420029a, 2002.

Sekimoto, K., Koss, A. R., Gilman, J. B., Selimovic, V., Coggon, M. M., Zarzana, K. J., Yuan, B., Lerner, B. M., Brown, S. S., Warneke, C., Yokelson, R. J., Roberts, J. M., and de Gouw, J.: High- and low-temperature pyrolysis profiles describe volatile organic compound emissions from western US wildfire fuels, Atmospheric Chemistry and Physics, 18, 9263–9281, https://doi.org/10.5194/acp-18-9263-2018, 2018.

Sharma, S., Lavoué, D., Cachier, H., Barrie, L. A., and Gong, S. L.: Long-term trends of the black carbon concentrations in the Canadian Arctic, Journal of Geophysical Research: Atmospheres, 109, 2004.

Sharma, S., Andrews, E., Barrie, L. A., Ogren, J. A., and Lavoué, D.: Variations and sources of the equivalent black carbon in the high Arctic revealed by long-term observations at Alert and Barrow: 1989–2003, Journal of Geophysical Research: Atmospheres, 111, 2006.

Sharma, S., Ishizawa, M., Chan, D., Lavoué, D., Andrews, E., Eleftheriadis, K., and Maksyutov, S.: 16-year simulation of Arctic black carbon: Transport, source contribution, and sensitivity analysis on deposition, Journal of Geophysical Research: Atmospheres, 118, 943–964, 2013.

Shindell, D. T., Faluvegi, G., Stevenson, D. S., Krol, M. C., Emmons, L. K., Lamarque, J.-F., Pétron, G., Dentener, F. J., Ellingsen, K., Schultz, M. G., Wild, O., Amann, M., Atherton, C. S., Bergmann, D. J., Bey, I., Butler, T., Cofala, J., Collins, W. J., Derwent, R. G., Doherty, R. M., Drevet, J., Eskes, H. J., Fiore, A. M., Gauss, M., Hauglustaine, D. A., Horowitz, L. W., Isaksen, I. S. A., Lawrence, M. G., Montanaro, V., Müller, J.-F., Pitari, G., Prather, M. J., Pyle, J. A., Rast, S., Rodriguez, J. M., Sanderson, M. G., Savage, N. H., Strahan, S. E., Sudo, K., Szopa, S., Unger, N., van Noije, T. P. C., and Zeng, G.: Multimodel simulations of carbon monoxide: Comparison with observations and projected near-future changes, Journal of Geophysical Research: Atmospheres, 111, L01 104, https://doi.org/10.1029/2006JD007100, 2006.

Shindell, D. T., Chin, M., Dentener, F., Doherty, R. M., Faluvegi, G., Fiore, A. M., Hess, P., Koch, D. M., MacKenzie, I. A., Sanderson, M. G., and Others: A multi-model assessment of pollution transport to the Arctic, Atmospheric Chemistry and Physics, 8, 5353–5372, https://doi.org/10.5194/acp-8-5353-2008, 2008.

Simpson, I. J., Akagi, S. K., Barletta, B., Blake, N. J., Choi, Y., Diskin, G. S., Fried, A., Fuelberg, H. E., Meinardi, S., Rowland, F. S., Vay, S. A., Weinheimer, A. J., Wennberg, P. O., Wiebring, P., Wisthaler, A., Yang, M., Yokelson, R. J., and Blake, D. R.: Boreal forest fire emissions in fresh Canadian smoke plumes: C_1-C_{10} volatile organic compounds (VOCs), CO_2, CO, NO_2, NO, HCN and CH_3CN, Atmospheric Chemistry and Physics, 11, 6445–6463, https://doi.org/10.5194/acp-11-6445-2011, 2011.

Singh, H. B.: In situ measurements of HCN and CH_3CN over the Pacific Ocean: Sources, sinks, and budgets, Journal of Geophysical Research: Atmospheres, 108, 8795, https://doi.org/10.1029/2002JD003006, 2003.

Sioris, C. E., Abboud, I., Fioletov, V. E., and McLinden, C. A.: AEROCAN, the Canadian sub-network of AERONET: Aerosol monitoring and air quality applications, Atmospheric Environment, 167, 444–457, https://doi.org/10.1016/j.atmosenv.2017.08.044, 2017.

Sofiev, M., Ermakova, T., and Vankevich, R.: Evaluation of the smoke-injection height from wild-land fires using remote-sensing data, Atmospheric Chemistry and Physics, 12, 1995–2006, https://doi.org/10.5194/acp-12-1995-2012, 2012.

Spivakovsky, C. M., Logan, J. A., Montzka, S. A., Balkanski, Y. J., Foreman-Fowler, M., Jones, D. B. A., Horowitz, L. W., Fusco, A. C., Brenninkmeijer, C. A. M., Prather, M. J., Wofsy, S. C., and McElroy, M. B.: Three-dimensional climatological distribution of tropospheric OH: Update and evaluation, Journal of Geophysical Research: Atmospheres, 105, 8931–8980, https://doi.org/10.1029/1999JD901006, 2000.

Stohl, A.: Characteristics of atmospheric transport into the Arctic troposphere, Journal of Geophysical Research: Atmospheres, 111, https://doi.org/10.1029/2005JD006888, 2006.

Stohl, A., Forster, C., Frank, A., Seibert, P., and Wotawa, G.: Technical note: The Lagrangian particle dispersion model FLEXPART version 6.2, Atmospheric Chemistry and Physics, 5, 2461–2474, https://doi.org/10.5194/acp-5-2461-2005, 2005.

Stohl, A., Andrews, E., Burkhart, J. F., Forster, C., Herber, A., Hoch, S. W., Kowal, D., Lunder, C., Mefford, T., Ogren, J. A., Sharma, S., Spichtinger, N., Stebel, K., Stone, R., Ström, J., Tørseth, K., Wehrli, C., and Yttri, K. E.: Pan-Arctic enhancements of light absorbing aerosol concentrations due to North American boreal forest fires during summer 2004, Journal of Geophysical Research: Atmospheres, 111, https://doi.org/10.1029/2006JD007216, 2006.

Streets, D. G., Yarber, K. F., Woo, J.-H., and Carmichael, G. R.: Biomass burning in Asia: Annual and seasonal estimates and atmospheric emissions, Global Biogeochemical Cycles, 17, 1099, https://doi.org/10.1029/2003GB002040, 2003.

Sussmann, R. and Buchwitz, M.: Initial validation of ENVISAT/SCIAMACHY columnar CO by FTIR profile retrievals at the Ground-Truthing Station Zugspitze, Atmospheric Chemistry and Physics, 5, 1497–1503, https://doi.org/10.5194/acp-5-1497-2005, 2005.

Sussmann, R. and Schäfer, K.: Infrared spectroscopy of tropospheric trace gases: combined analysis of horizontal and vertical column abundances, Applied Optics, 36, 735–741, https://doi.org/10.1364/AO.36.000735, 1997.

Tanimoto, H., Kajii, Y., Hirokawa, J., Akimoto, H., and Minko, N. P.: The atmospheric impact of boreal forest fires in far eastern Siberia on the seasonal variation of carbon monoxide: Observations at Rishiri, A northern remote island in Japan, Geophysical Research Letters, 27, 4073–4076, https://doi.org/10.1029/2000GL011914, 2000.

Té, Y., Jeseck, P., Franco, B., Mahieu, E., Jones, N., Paton-Walsh, C., Griffith, D. W. T., Buchholz, R. R., Hadji-Lazaro, J., Hurtmans, D., and Janssen, C.: Seasonal variability of surface and column carbon monoxide over the megacity Paris, high-altitude Jungfraujoch and Southern Hemispheric Wollongong stations, Atmospheric Chemistry and Physics, 16, 10 911–10 925, https://doi.org/10.5194/acp-16-10911-2016, 2016.

Teakles, A. D., So, R., Ainslie, B., Nissen, R., Schiller, C., Vingarzan, R., McKendry, I., Macdonald, A. M., Jaffe, D. A., Bertram, A. K., Strawbridge, K. B., Leaitch, W. R., Hanna, S., Toom, D., Baik, J., and Huang, L.: Impacts of the July 2012 Siberian fire plume on air quality in the Pacific Northwest, Atmospheric Chemistry and Physics, 17, 2593–2611, https://doi.org/10.5194/acp-17-2593-2017, 2017.

Tereszchuk, K. A., González Abad, G., Clerbaux, C., Hurtmans, D., Coheur, P.-F., and Bernath, P. F.: ACE-FTS measurements of trace species in the characterization of biomass burning plumes, Atmospheric Chemistry and Physics, 11, 12 169–12 179, https://doi.org/10.5194/acp-11-12169-2011, 2011.

Tereszchuk, K. A., González Abad, G., Clerbaux, C., Hadji-Lazaro, J., Hurtmans, D., Coheur, P.-F., and Bernath, P. F.: ACE-FTS observations of pyrogenic trace species in boreal biomass burning plumes during BORTAS, Atmospheric Chemistry and Physics, 13, 4529–4541, https://doi.org/10.5194/acp-13-4529-2013, 2013.

The International GEOS-Chem User Community: geoschem/geos-chem: GEOS-Chem 12.1.1, https://doi.org/10.5281/zenodo.2249246, 2018.

Thoning, K. W., Tans, P. P., and Komhyr, W. D.: Atmospheric carbon dioxide at Mauna Loa Observatory: 2. Analysis of the NOAA GMCC data, 1974-1985, Journal of Geophysical Research: Atmospheres, 94, 8549–8565, https://doi.org/10.1029/JD094iD06p08549, 1989.

Timofeyev, Y., Virolainen, Y., Makarova, M., Poberovsky, A., Polyakov, A., Ionov, D., Osipov, S., and Imhasin, H.: Ground-based spectroscopic measurements of atmospheric gas composition near Saint Petersburg (Russia), Journal of Molecular Spectroscopy, 323, 2–14, https://doi.org/10.1016/j.jms.2015.12.007, 2016.

Tomasi, C., Kokhanovsky, A. A., Lupi, A., Ritter, C., Smirnov, A., O'Neill, N. T., Stone, R. S., Holben, B. N., Nyeki, S., Wehrli, C., Stohl, A., Mazzola, M., Lanconelli, C., Vitale, V., Stebel, K., Aaltonen, V., de Leeuw, G., Rodriguez, E., Herber, A. B., Radionov, V. F., Zielinski, T., Petelski, T., Sakerin, S. M., Kabanov, D. M., Xue, Y., Mei, L., Istomina, L., Wagener, R., McArthur, B., Sobolewski, P. S., Kivi, R., Courcoux, Y., Larouche, P., Broccardo, S., and Piketh, S. J.: Aerosol remote sensing in polar regions, Earth-Science Reviews, 140, 108–157, https://doi.org/10.1016/j.earscirev.2014.11.001, 2015.

Tzompa-Sosa, Z. A., Mahieu, E., Franco, B., Keller, C. A., Turner, A. J., Helmig, D., Fried, A., Richter, D., Weibring, P., Walega, J., Yacovitch, T. I., Herndon, S. C., Blake, D. R., Hase, F., Hannigan, J. W., Conway, S., Strong, K., Schneider, M., and Fischer, E. V.: Revisiting global fossil fuel and biofuel emissions of ethane, Journal of Geophysical Research: Atmospheres, 122, 2493–2512, https://doi.org/10.1002/2016JD025767, 2017.

Urbanski, S.: Wildland fire emissions, carbon, and climate: Emission factors, Forest Ecology and Management, 317, 51–60, https://doi.org/10.1016/j.foreco.2013.05.045, 2014.

Urbanski, S. P.: Combustion efficiency and emission factors for wildfire-season fires in mixed conifer forests of the northern Rocky Mountains, US, Atmospheric Chemistry and Physics, 13, 7241–7262, https://doi.org/10.5194/acp-13-7241-2013, 2013.

Val Martin, M., Honrath, R. E., Owen, R. C., Pfister, G., Fialho, P., and Barata, F.: Significant enhancements of nitrogen oxides, black carbon, and ozone in the North Atlantic lower free troposphere resulting from North American boreal wildfires, Journal of Geophysical Research: Atmospheres, 111, https://doi.org/10.1029/2006JD007530, 2006.

Val Martin, M., Kahn, R. A., and Tosca, M. G.: A Global Analysis of Wildfire Smoke Injection Heights Derived from Space-Based Multi-Angle Imaging, Remote Sensing, 10, 1609, https://doi.org/10.3390/rs10101609, 2018.

van der Werf, G. R., Randerson, J. T., Giglio, L., van Leeuwen, T. T., Chen, Y., Rogers, B. M., Mu, M., van Marle, M. J. E., Morton, D. C., Collatz, G. J., Yokelson, R. J., and Kasibhatla, P. S.: Global fire emissions estimates during 1997–2016, Earth System Science Data, 9, 697–720, https://doi.org/10.5194/essd-9-697-2017, 2017.

Veraverbeke, S., Rogers, B. M., Goulden, M. L., Jandt, R. R., Miller, C. E., Wiggins, E. B., and Randerson, J. T.: Lightning as a major driver of recent large fire years in North American boreal forests, Nature Climate Change, 7, 529–534, https://doi.org/10.1038/nclimate3329, 2017.

Viatte, C., Strong, K., Paton-Walsh, C., Mendonca, J., O'Neill, N. T., and Drummond, J. R.: Measurements of CO, HCN, and C_2H_6 total columns in smoke plumes transported from the 2010 Russian boreal forest fires to the Canadian high Arctic, Atmosphere-Ocean, 51, 522–531, https://doi.org/10.1080/07055900.2013.823373, 2013.

Viatte, C., Strong, K., Walker, K. A., and Drummond, J. R.: Five years of CO, HCN, C_2H_6, C_2H_2, CH_3OH, HCOOH and H_2CO total columns measured in the Canadian high Arctic, Atmospheric Measurement Techniques, 7, 1547–1570, https://doi.org/10.5194/amt-7-1547-2014, 2014.

Viatte, C., Strong, K., Hannigan, J., Nussbaumer, E., Emmons, L. K., Conway, S., Paton-Walsh, C., Hartley, J., Benmergui, J., and Lin, J.: Identifying fire plumes in the Arctic with tropospheric FTIR measurements and transport models, Atmospheric Chemistry and Physics, 15, 2227–2246, https://doi.org/10.5194/acp-15-2227-2015, 2015.

Vigouroux, C., Hendrick, F., Stavrakou, T., Dils, B., Smedt, I. D., Hermans, C., Merlaud, A., Scolas, F., Senten, C., Vanhaelewyn, G., and Others: Ground-based FTIR and MAX-DOAS observations of formaldehyde at Reunion Island and comparisons with satellite and model data, Atmospheric Chemistry and Physics, 9, 9523–9544, https://doi.org/10.5194/acp-9-9523-2009, 2009.

Vigouroux, C., Stavrakou, T., Whaley, C., Dils, B., Duflot, V., Hermans, C., Kumps, N., Metzger, J.-M., Scolas, F., Vanhaelewyn, G., Müller, J.-F., Jones, D. B. A., Li, Q., and De Mazière, M.: FTIR time-series of biomass burning products (HCN, C_2H_6, C_2H_2, CH_3OH, and HCOOH) at Reunion Island (21°S, 55°E) and comparisons with model data, Atmospheric Chemistry and Physics, 12, 10 367–10 385, https://doi.org/10.5194/acp-12-10367-2012, 2012.

Vigouroux, C., Bauer Aquino, C. A., Bauwens, M., Becker, C., Blumenstock, T., Mazière, M. D., García, O., Grutter, M., Guarin, C., Hannigan, J., Hase, F., Jones, N., Kivi, R., Koshelev, D., Langerock, B., Lutsch, E., Makarova, M., Metzger, J.-M., Müller, J.-F., Notholt, J., Ortega, I., Palm, M., Paton-Walsh, C., Poberovskii, A., Rettinger, M., Robinson, J., Smale, D., Stavrakou, T., Stremme, W., Strong, K., Sussmann, R., Té, Y., and Toon, G.: NDACC harmonized formaldehyde time series from 21 FTIR stations covering a wide range of column abundances, Atmospheric Measurement Techniques, 11, 5049–5073, https://doi.org/10.5194/amt-11-5049-2018, 2018.

Wang, Q., Jacob, D. J., Fisher, J. A., Mao, J., Leibensperger, E. M., Carouge, C. C., Sager, P. L., Kondo, Y., Jimenez, J. L., Cubison, M. J., and Others: Sources of carbonaceous aerosols and deposited black carbon in the Arctic in winter-spring: Implications for radiative forcing, Atmospheric Chemistry and Physics, 11, 12 453–12 473, https://doi.org/10.5194/acp-11-12453-2011, 2011.

Ward, D. E. and Hardy, C. C.: Smoke emissions from wildland fires, Environment International, 17, 117–134, https://doi.org/10.1016/0160-4120(91)90095-8, 1991.

Warneke, C., Bahreini, R., Brioude, J., Brock, C. A., de Gouw, J. A., Fahey, D. W., Froyd, K. D., Holloway, J. S., Middlebrook, A., Miller, L., Montzka, S., Murphy, D. M., Peischl, J., Ryerson, T. B., Schwarz, J. P., Spackman, J. R., and Veres, P.: Biomass burning in Siberia and Kazakhstan as an important source for haze over the Alaskan Arctic in April 2008, Geophysical Research Letters, 36, https://doi.org/10.1029/2008GL036194, 2009.

Wentworth, G. R., Aklilu, Y.-A., Landis, M. S., and Hsu, Y.-M.: Impacts of a large boreal wildfire on ground level atmospheric concentrations of PAHs, VOCs and ozone, Atmospheric Environment, 178, 19–30, https://doi.org/10.1016/j.atmosenv.2018.01.013, 2018.

Westerling, A. L., Hidalgo, H. G., Cayan, D. R., and Swetnam, T. W.: Warming and earlier spring increase western US forest wildfire activity, Science, 313, 940–943, https://doi.org/10.1126/science.1128834, 2006.

Whaley, C. H., Strong, K., Jones, D. B. A., Walker, T. W., Jiang, Z., Henze, D. K., Cooke, M. A., McLinden, C. A., Mittermeier, R. L., Pommier, M., and Fogal, P. F.: Toronto area ozone: Long-term measurements and modeled sources of poor air quality events, Journal of Geophysical Research: Atmospheres, 120, 11,368–11,390, https://doi.org/10.1002/2014JD022984, 2015.

Wiacek, A., Taylor, J. R., Strong, K., Saari, R., Kerzenmacher, T. E., Jones, N. B., and Griffith, D. W. T.: Ground-Based Solar Absorption FTIR Spectroscopy: Characterization of Retrievals and First Results from a Novel Optical Design Instrument at a New NDACC Complementary Station, Journal of Atmospheric and Oceanic Technology, 24, 432–448, https://doi.org/10.1175/JTECH1962.1, 2007.

Winiger, P., Barrett, T. E., Sheesley, R. J., Huang, L., Sharma, S., Barrie, L. A., Yttri, K. E., Evangeliou, N., Eckhardt, S., Stohl, A., Klimont, Z., Heyes, C., Semiletov, I. P., Dudarev, O. V., Charkin, A., Shakhova, N., Holmstrand, H., Andersson, A., and Gustafsson, Ö.: Source apportionment of circum-Arctic atmospheric black carbon from isotopes and modeling, Science Advances, 5, 8052, https://doi.org/10.1126/sciadv.aau8052, 2019.

Witte, J. C., Douglass, A. R., Silva, A. d., Torres, O., Levy, R., and Duncan, B. N.: NASA A-Train and Terra observations of the 2010 Russian wildfires, Atmospheric Chemistry and Physics, 11, 9287–9301, 2011.

Wofsy, S. C., Sachse, G. W., Gregory, G. L., Blake, D. R., Bradshaw, J. D., Sandholm, S. T., Singh, H. B., Barrick, J. A., Harriss, R. C., Talbot, R. W., Shipham, M. A., Browell, E. V., Jacob, D. J., and Logan, J. A.: Atmospheric chemistry in the Arctic and subarctic: Influence of natural fires, industrial emissions, and stratospheric inputs, Journal of Geophysical Research: Atmospheres, 97, 16 731–16 746, https://doi.org/10.1029/92JD00622, 1992.

Wotton, B. M., Nock, C. A., and Flannigan, M. D.: Forest fire occurrence and climate change in Canada, International Journal of Wildland Fire, 19, 253–271, https://doi.org/10.1071/WF09002, 2010.

Xiao, Y., Jacob, D. J., and Turquety, S.: Atmospheric acetylene and its relationship with CO as an indicator of air mass age, Journal of Geophysical Research, 112, 955, https://doi.org/10.1029/2006JD008268, 2007.

Xiao, Y., Logan, J. A., Jacob, D. J., Hudman, R. C., Yantosca, R., and Blake, D. R.: Global budget of ethane and regional constraints on U.S. sources, Journal of Geophysical Research: Atmospheres, 113, https://doi.org/10.1029/2007JD009415, 2008.

Yasunari, T. J., Kim, K.-M., da Silva, A. M., Hayasaki, M., Akiyama, M., and Murao, N.: Extreme air pollution events in Hokkaido, Japan, traced back to early snowmelt and large-scale wildfires over East Eurasia: Case studies, Scientific Reports, 8, 6413, https://doi.org/10.1038/s41598-018-24335-w, 2018.

Yevich, R. and Logan, J. A.: An assessment of biofuel use and burning of agricultural waste in the developing world, Global Biogeochemical Cycles, 17, 1095, https://doi.org/10.1029/2002GB001952, 2003.

Yokelson, R. J., Griffith, D. W. T., and Ward, D. E.: Open-path Fourier transform infrared studies of large-scale laboratory biomass fires, Journal of Geophysical Research: Atmospheres, 101, 21 067–21 080, 1996.

Yokelson, R. J., Goode, J. G., Ward, D. E., Susott, R. A., Babbitt, R. E., Wade, D. D., Bertschi, I., Griffith, D. W. T., and Hao, W. M.: Emissions of formaldehyde, acetic acid, methanol, and other trace gases from biomass fires in North Carolina measured by airborne Fourier transform infrared spectroscopy, Journal of Geophysical Research: Atmospheres, 104, 30 109–30 125, https://doi.org/10.1029/1999JD900817, 1999.

Yokelson, R. J., Bertschi, I. T., Christian, T. J., Hobbs, P. V., Ward, D. E., and Hao, W. M.: Trace gas measurements in nascent, aged, and cloud-processed smoke from African savanna fires by airborne Fourier transform infrared spectroscopy (AFTIR), Journal of Geophysical Research: Atmospheres, 108, 8478, https://doi.org/10.1029/2002JD002322, 2003.

Yokelson, R. J., Crounse, J. D., DeCarlo, P. F., Karl, T., Urbanski, S., Atlas, E, Campos, T., Shinozuka, Y., Kapustin, V., Clarke, A. D., Weinheimer, A., Knapp, D. J., Montzka, D. D., Holloway, J., Weibring, P., Flocke, F., Zheng, W., Toohey, D., Wennberg, P. O., Wiedinmyer, C., Mauldin, L., Fried, A., Richter, D., Walega, J., Jimenez, J. L., Adachi, K., Buseck, P. R., Hall, S. R., and Shetter, R.: Emissions from biomass burning in the Yucatan, Atmospheric Chemistry and Physics, 9, 5785–5812, https://doi.org/10.5194/acp-9-5785-2009, 2009.

Yokelson, R. J., Andreae, M. O., and Akagi, S. K.: Pitfalls with the use of enhancement ratios or normalized excess mixing ratios measured in plumes to characterize pollution sources and aging, Atmospheric Measurement Techniques, 6, 2155–2158, https://doi.org/10.5194/amt-6-2155-2013, 2013.

York, D., Evensen, N. M., Martińez, M. L., and De Basabe Delgado, J.: Unified equations for the slope, intercept, and standard errors of the best straight line, American Journal of Physics, 72, 367–375, https://doi.org/10.1119/1.1632486, 2004.

Yurganov, L. N.: A quantitative assessment of the 1998 carbon monoxide emission anomaly in the Northern Hemisphere based on total column and surface concentration measurements, Journal of Geophysical Research: Atmospheres, 109, https://doi.org/10.1029/2004JD004559, 2004.

Yurganov, L. N., Duchatelet, P., Dzhola, A. V., Edwards, D. P., Hase, F., Kramer, I., Mahieu, E., Mellqvist, J., Notholt, J., Novelli, P. C., Rockmann, A., Scheel, H. E., Schneider, M., Schulz, A., Strandberg, A., Sussmann, R., Tanimoto, H., Velazco, V., Drummond, J. R., and Gille, J. C.: Increased Northern Hemispheric carbon monoxide burden in the troposphere in 2002 and 2003 detected from the ground and from space, Atmospheric Chemistry and Physics, 5, 563–573, https://doi.org/10.5194/acp-5-563-2005, 2005.

Yurganov, L. N., Rakitin, V., Dzhola, A., August, T., Fokeeva, E., George, M., Gorchakov, G., Grechko, E., Hannon, S., Karpov, A., Ott, L., Semutnikova, E., Shumsky, R., and Strow, L.: Satellite and ground-based CO total column observations over 2010 Russian fires: accuracy of top-down estimates based on thermal IR satellite data, Atmospheric Chemistry and Physics, 11, 7925–7942, https://doi.org/10.5194/acp-11-7925-2011, 2011.

Zander, R., Mahieu, E., Demoulin, P., Duchatelet, P., Roland, G., Servais, C., De Mazière, M., Reimann, S., and Rinsland, C. P.: Our changing atmosphere: evidence based on long-term infrared solar observations at the Jungfraujoch since 1950, The Science of the Total Environment, 391, 184–195, https://doi.org/10.1016/j.scitotenv.2007.10.018, 2008.

Zander, R., Duchatelet, P., Mahieu, E., Demoulin, P., Roland, G., Servais, C., Auwera, J. V., Perrin, A., Rinsland, C. P., and Crutzen, P. J.: Formic acid above the Jungfraujoch during 1985–2007: Observed variability, seasonality, but no long-term background evolution, Atmospheric Chemistry and Physics, 10, 10 047–10 065, https://doi.org/10.5194/acp-10-10047-2010, 2010.

Zellweger, C., Hüglin, C., Klausen, J., Steinbacher, M., Vollmer, M., and Buchmann, B.: Inter-comparison of four different carbon monoxide measurement techniques and evaluation of the long-term carbon monoxide time series of Jungfraujoch, Atmospheric Chemistry and Physics, 9, 3491–3503, https://doi.org/10.5194/acp-9-3491-2009, 2009.

Zhao, Y., Kondo, Y., Murcray, F. J., Liu, X., Koike, M., Kita, K., Nakajima, H., Murata, I., and Suzuki, K.: Carbon monoxide column abundances and tropospheric concentrations retrieved from high resolution ground-based infrared solar spectra at 43.5°N over Japan, Journal of Geophysical Research: Atmospheres, 102, 23 403–23 411, https://doi.org/10.1029/97JD01970, 1997.

Zhao, Y., Kondo, Y., Murcray, F. J., Liu, X., Koike, M., Irie, H., Strong, K., Suzuki, K., Sera, M., and Ikegami, Y.: Seasonal variations of HCN over Northern Japan measured by ground-based infrared solar spectroscopy, Geophysical Research Letters, 27, 2085–2088, https://doi.org/10.1029/1999GL011218, 2000.

Zhao, Y., Strong, K., Kondo, Y., Koike, M., Matsumi, Y., Irie, H., Rinsland, C. P., Jones, N. B., Suzuki, K., Nakajima, H., Nakane, H., and Murata, I.: Spectroscopic measurements of tropospheric CO, C_2H_6, C_2H_2, and HCN in Northern Japan, Journal of Geophysical Research: Atmospheres, 107, 4343–4359, https://doi.org/10.1029/2001JD000748, 2002.

Table 1. Summary of NDACC and AERONET sites used in this study.

	Site	Latitude, Longitude	Elevation [m a.s.l.]	Measurement Years	Key References
NDACC	**Eureka**	80.05°N, 86.42°W	610	2006-2018	Batchelor et al., 2009; Lutsch et al., 2016, 2019, Viatte et al., 2013, 2014, 2015
AERONET	PEARL	80.05°N, 86.42°W	610	2007-2018	Saha et al., 2010; O'Neill et al., 2012
	Ny-Ålesund	78.92°N, 11.93°E	15	1992-2018	Notholt et al., 1997a, b, 2000
	Horsund	77.00°N, 86.42°W	12	2004-2018	Rozwadowska et al., 2010
	Thule	76.53°N, 68.74°W	225	1999-2018	Hannigan et al., 2009; Viatte et al., 2015 Lutsch et al., 2019
	Thule	76.52°N, 68.77°W	225	2007-2018	Tomasi et al., 2015
	Kiruna	67.84°N, 20.41°E	419	1996-2018	Blumenstock et al., 1997, 2009
	Andenes	69.28°N, 16.01°E	379	2002-2018	Rodríguez et al., 2012
	Poker Flat	65°N, 142°W	610	1999-2011	Kasai et al., 2005a, b
	Bonanza Creek	65.74°N, 148/32°W	353	1994-2018	Eck et al., 2009
	St. Petersburg	59.88°N, 29.83°E	20	2009-2018	Makarova et al., 2011; Timofeyev et al., 2016
	Toravere	58.27°N, 26.47°E	85	2002-2018	Arola et al., 2007
	Zugspitze	47.42°N, 10.98°E	2964	1995-2018	Sussmann and Schäfer, 1997, Sussmann and Buchwitz, 2005
	Davos	46.81°N, 9.84°E	1589	2001-2018	Gubler et al., 2012
	Jungfraujoch	46.55°N, 7.98°E	3580	1984-2018	Mahieu et al., 1997; Zander et al., 2008,
	Davos	46.81°N, 9.84°E	1589	2001-2018	Gubler et al., 2012
	Toronto	43.66°N, 79.40°W	174	2002-2018	Wiacek et al., 2007; Whaley et al., 2015, Lutsch et al., 2016
	Toronto	43.79°N, 79.47°E	186	1996-2018	Sioris et al., 2017
	Rikubetsu	43.46°N, 143.77°E	380	2002-2018	Zhao et al., 1997, 2000, 2002
	Noto	37.34°N, 137.14°E	200	2001-2018	Makar et al., 2018

Table 2. Summary of the source regions used in the GEOS-Chem tagged CO simulation.

Type	Name	Description
Anthropogenic	NA	North America
	EU	Europe
	AS	Asia
	ROW	Rest of World
Biomass Burning	BONA	Boreal North America
	TENA	Temperate North America
	CEAM	Central America
	NHSA	Northern Hemisphere South America
	SHSA	Southern Hemisphere South America
	EURO	Europe
	MIDE	Middle East
	NHAF	Northern Hemisphere Africa
	SHAF	Southern Hemisphere Africa
	BOAS	Boreal Asia
	CEAS	Central East Asia
	SEAS	Southeast Asia
	EQAS	Equatorial Asia
	AUST	Australia and New Zealand
Other	CH_4	Methane oxidation
	NMVOC	Non-methane volatile organic compound oxidation

Table 3. Correlation coefficient (r) and slope of GEOS-Chem versus FTIR CO tropospheric partial columns and the monthly-mean relative difference of GEOS-Chem minus FTIR [(model-FTIR)/FTIR] CO tropospheric partial columns over all years for measurements from 2003-2018.

			Relative Difference [%]												
Site	r	Slope	Jan.	Feb.	Mar.	Apr.	May	Jun.	Jul.	Aug.	Sep.	Oct.	Nov.	Dec.	**Yearly**
Eureka	0.81	0.82	–	-3.5	-2.6	-1.3	5.0	1.7	2.2	-6.5	-8.0	-7.5	–	–	-1.5
Ny-Ålesund	0.86	0.74	–	–	-4.2	-2.4	0.1	4.3	2.1	-2.5	-3.8	–	–	–	-0.8
Thule	0.86	0.79	–	3.2	-4.0	-4.6	0.5	-0.2	1.5	-6.1	-10.0	-6.8	–	–	-3.0
Kiruna	0.86	0.78	-5.6	-4.5	-6.2	-7.3	-7.6	-6.0	-9.7	-14.6	-12.3	-6.4	1.7	–	-7.6
Poker Flat	0.81	0.67	–	-23.9	-22.2	-22.0	-16.2	-15.5	-15.2	-21.3	-24.3	-19.3	-9.2	–	-19.4
St. Petersburg	0.84	0.82	-0.6	-0.9	-1.8	-4.9	-4.7	-4.3	-7.7	-12.2	-10.1	-2.0	2.5	4.7	-5.2
Zugspitze	0.82	0.57	-14.4	-15.7	-18.2	-20.2	-19.9	-19.0	-21.3	-21.8	-17.3	-13.2	-12.3	-11.9	-16.9
Jungfraujoch	0.83	0.49	-21.6	-21.5	-24.0	-25.0	-24.8	-22.3	-24.9	-23.6	-21.4	-18.6	-18.5	-18.7	-22.3
Toronto	0.66	0.51	-1.0	-2.2	-6.6	-7.8	-8.4	-8.5	-11.3	-11.4	-9.3	-5.0	-0.4	-0.0	-7.2
Rikubetsu	0.72	0.84	-5.4	-6.9	-2.8	-1.8	-0.9	-14.3	-14.0	-17.4	-15.0	-8.1	1.9	-1.9	-7.2

Table 4. Mean emission ratios of HCN and C_2H_6 for BONA and BOAS for all detected wildfire events. The value in parenthesis is the 1σ standard deviation of the mean, or the uncertainty for single events. The number of detected events for each site and mean travel times (days) are also given. The summarized studies were selected based on the availability of HCN and C_2H_6 emission ratios for boreal North American and boreal Asian sources. The studies included consists of emission ratios derived from multiple platforms including aircraft, ground-based FTIR and satellite observations. For each of these studies emissions ratios are reported for a single event or for the mean of several events. The value in parentheses is the reported error or standard deviation.

	BONA				BOAS			
Site	Num. Events	Travel Time	ER HCN	ER C_2H_6	Num. Events	Travel Time	ER HCN	ER C_2H_6
Eureka	6	8 (1)	0.0046 (0.0011)	0.0082 (0.0019)	15	10 (2)	0.0048 (0.0018)	0.0105 (0.0036)
Ny Ålesund	5	12 (1)	–	–	10	10 (2)	–	–
Thule	7	9 (2)	0.0052 (0.0009)	0.0081 (0.0021)	8	11 (1)	0.0072 (0.0035)	0.0094 (0.0024)
Kiruna	3	12 (2)	0.0042 (0.0010)	0.0136 (0.0091)	5	12 (1)	0.0040 (0.0017)	0.0076 (0.0023)
Poker Flat	3	3 (2)	–	–	7	10 (2)	–	–
St. Petersburg	0	–	–	–	1	11 (2)	0.0034 (0.0009)	0.0071 (0.0014)
Zugspitze	1	10 (3)	0.0026 (0.0005)	0.0108 (0.0005)	1	14 (1)	0.0021 (0.0010)	0.0069 (0.0006)
Jungfraujoch	5	10 (1)	0.0050 (0.0020)	0.0092 (0.0049)	7	12 (2)	0.0033 (0.0012)	0.0092 (0.0023)
Toronto	2	7 (0)	0.0044 (0.0013)	0.0086 (0.0000)	2	11 (2)	0.0065 (0.0018)	0.0208 (0.0065)
Rikubetsu	1	11 (3)	–	–	7	8 (2)	–	–
Average	23		0.0047 (0.0014)	0.0092 (0.0046)	39		0.0049 (0.0025)	0.0100 (0.0042)
Reference		Source (Platform)	ER HCN	ER C_2H_6		Source (Platform)	ER HCN	ER C_2H_6
Bertschi et al. 2003		Canada, USA (Aircraft)	0.0084	0.0157				
Goode et al. 2000		Alaska (Aircraft)	0.0069	0.0073				
Griffin et al. 2013		Canada (Ground-based)	0.0100 (0.0060)					
Hornbrook et al. 2011		Canada (Aircraft)	0.0077 (0.0032)	0.0055 (0.0002)		Asia, Siberia	0.0088 (0.0038)	0.0070 (0.0030)
Le Breton et al. 2013		Canada (Aircraft)	0.0037 (0.0015)					
Lewis et al. 2013		Canada (Aircraft)		0.0051 (0.0004)				
Lutsch et al. 2016		Canada (Ground-based)	0.0033 (0.0022)	0.0110 (0.0016)				
Nance et al. 1993		Alaska (Aircraft)		0.0076				
Rinsland et al. 2007		Canada, Alaska (Satellite)	0.0024 (0.0003)	0.0098 (0.0007)				
Simpson et al. 2011		Canada (Aircraft)	0.0082 (0.0020)	0.0046 (0.0009)				
Tereszchuk et al. 2011		N. America (Satellite)	0.0010 (0.0005)	0.0041 (0.0010)				
Tereszchuk et al. 2013		Canada (Satellite)	0.0020 (0.0009)	0.0061 (0.0001)		Siberia (Satellite)	0.0029 (0.0004)	0.0069 (0.0010)
Viatte et al. 2013						Russia (Ground-based)	0.0054 (0.0022)	0.0108 (0.0036)
Viatte et al. 2015		N. America (Ground-based)	0.0034 (0.0028)	0.0069 (0.0027)		Siberia (Ground-based)	0.0034 (0.0013)	0.0095 (0.0035)
Wofsy et al. 1992		Alaska (Aircraft)		0.0055 (0.0002)				

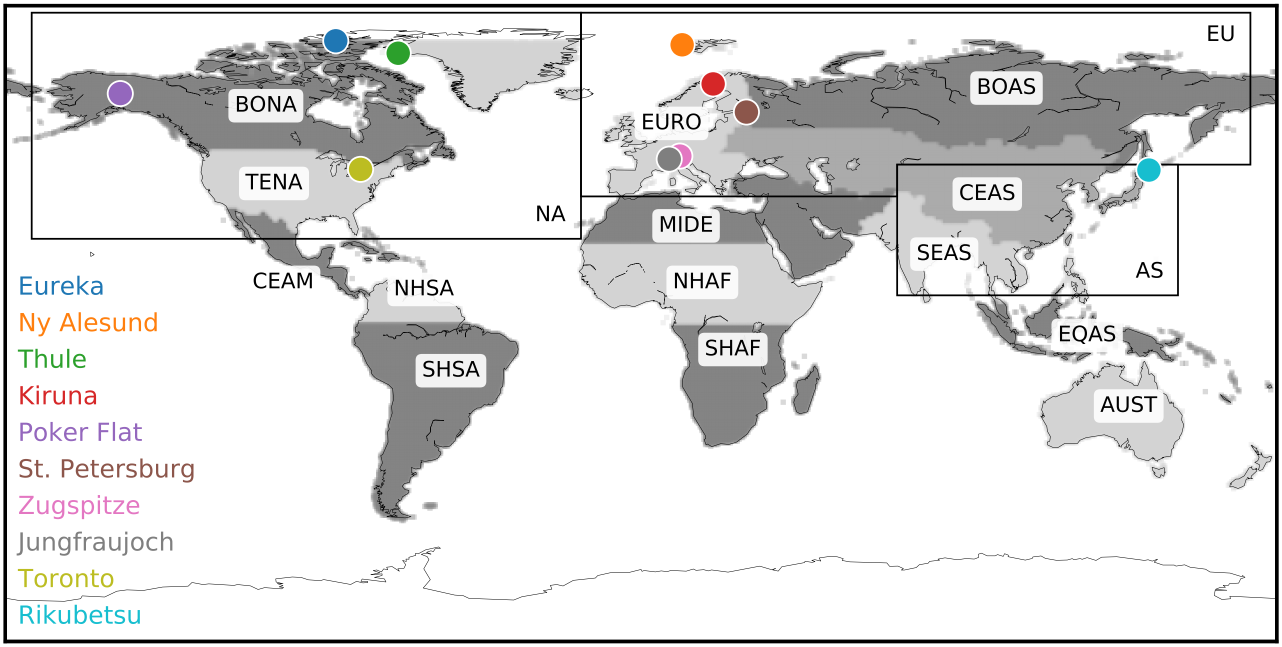

Figure 1. Locations of ground-based FTIR sites used in this study. The biomass burning regions (shaded), and anthropogenic source regions (black rectangles) used for the GEOS-Chem tagged CO simulation are also shown and summarized in Table 2.

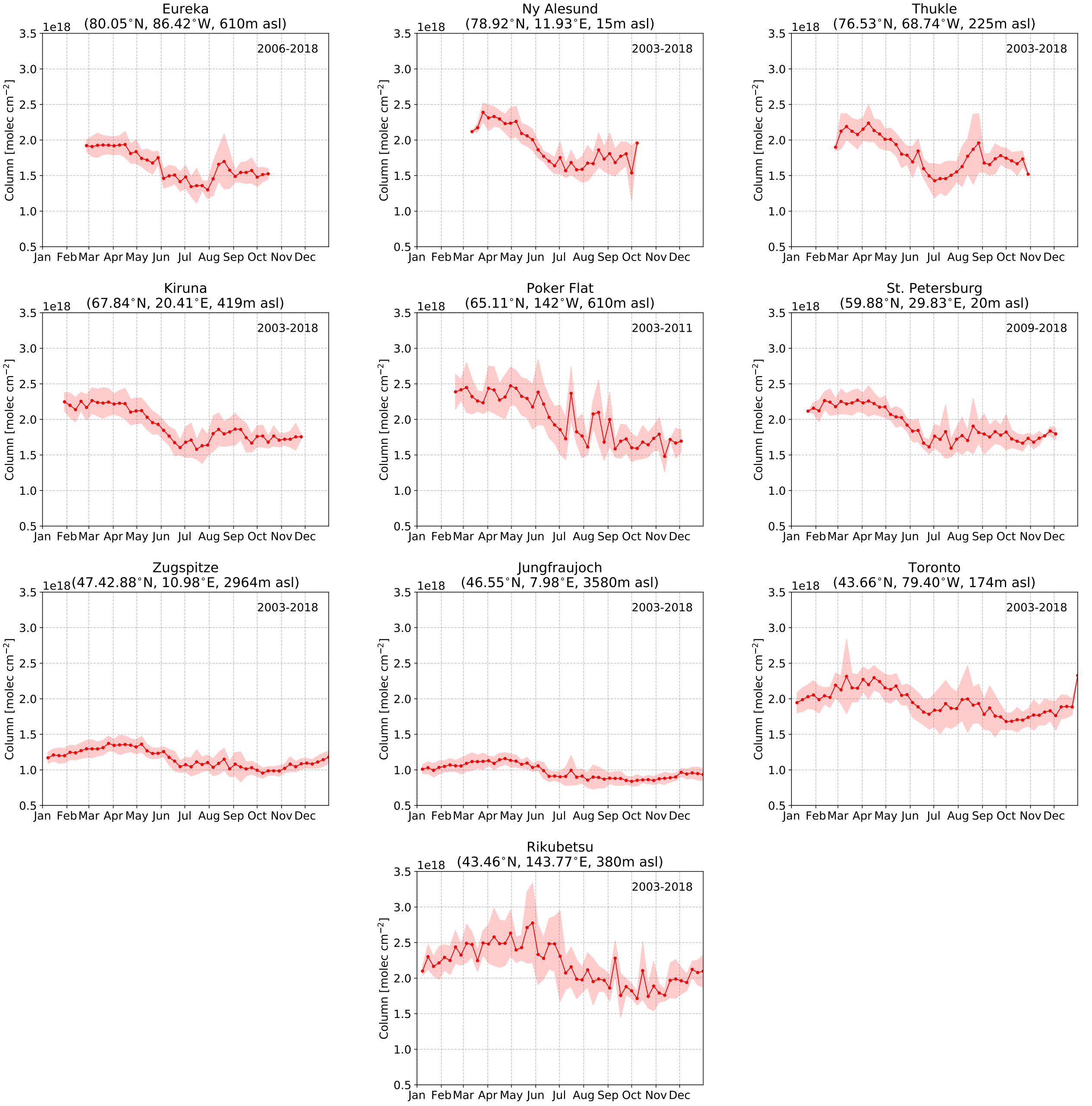

Figure 2. Mean CO tropospheric partial columns weekly-averaged over all years of measurements at each site. The years included in the mean are listed in the top right corner of each panel. The shaded region represents a 1σ standard deviation from the mean.

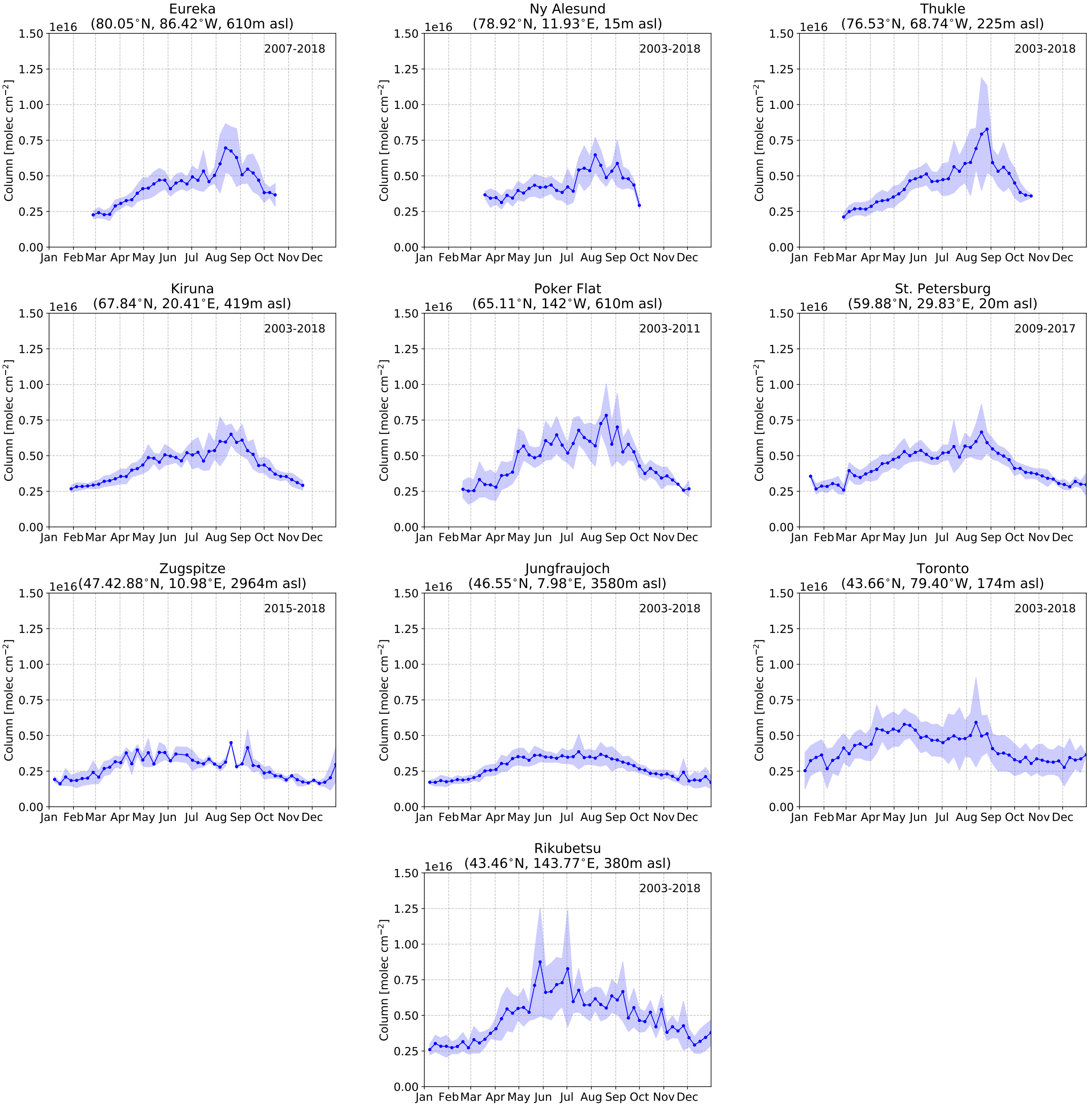

Figure 3. Same as Fig. 2 but for HCN.

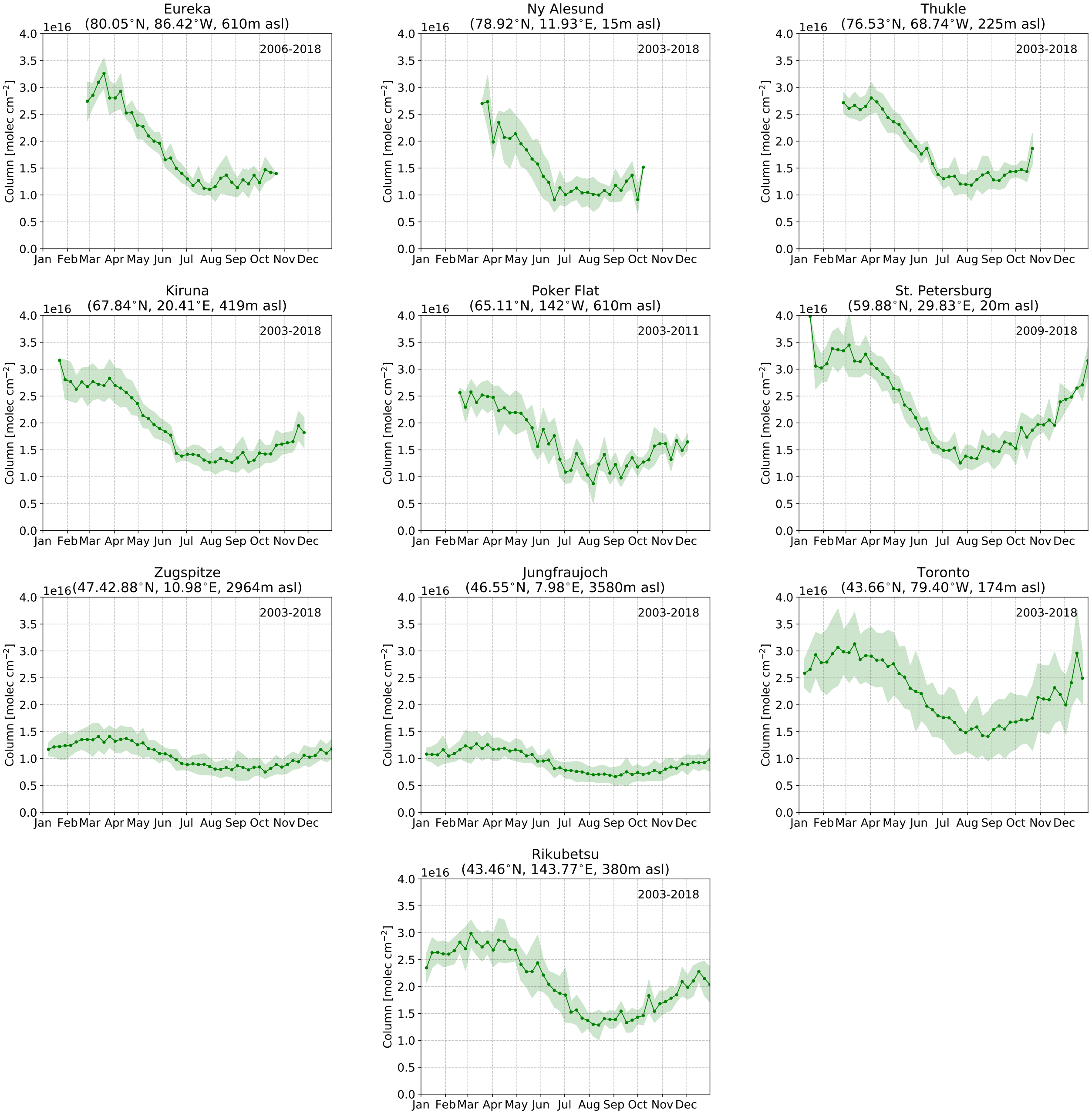

Figure 4. Same as Fig. 2 but for C_2H_6.

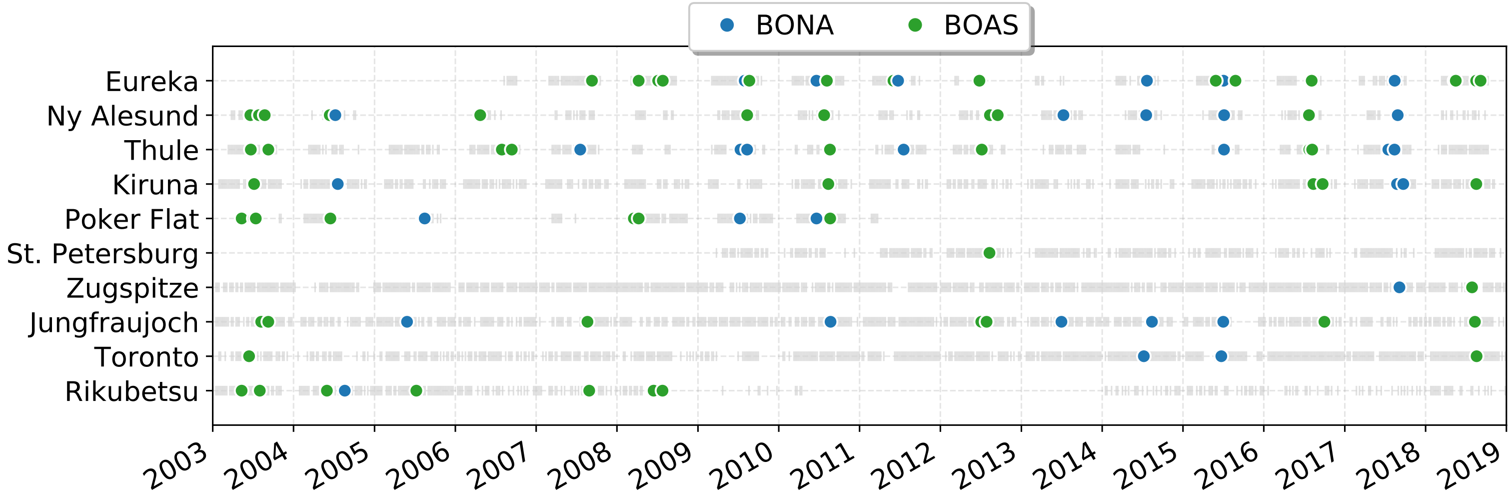

Figure 5. Summary of detected wildfire pollution events. The grey bars indicate periods of CO measurements and the coloured points represent the identified wildfire pollution events and their respective source attributed by the GEOS-Chem tagged CO simulation.

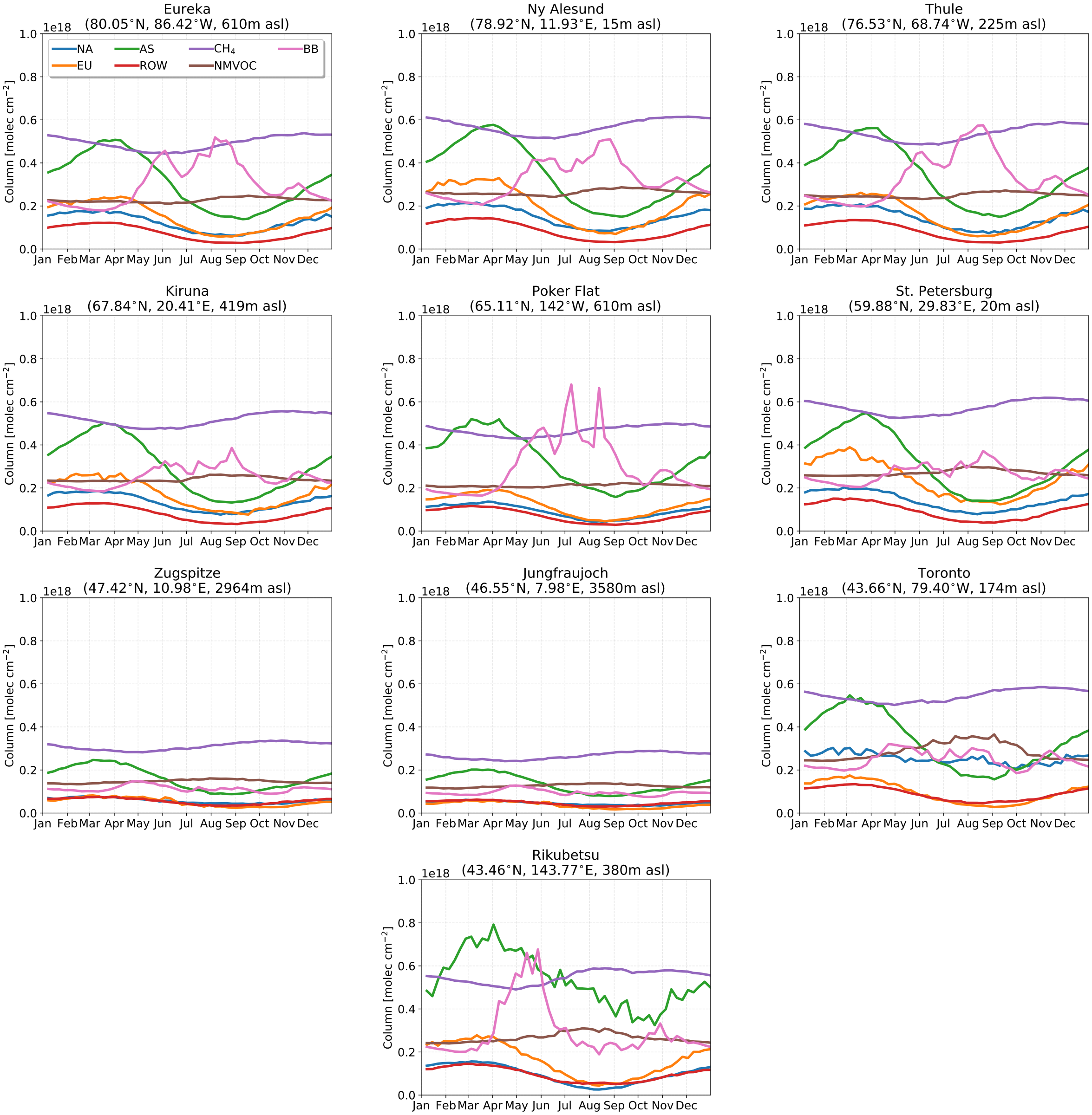

Figure 6. Weekly-mean GEOS-Chem tagged CO tracer tropospheric columns. The tagged CO tracer correspond to those listed in Table 2. The total biomass burning (BB) contribution is shown and is the sum of all biomass burning tracers from Table 2.

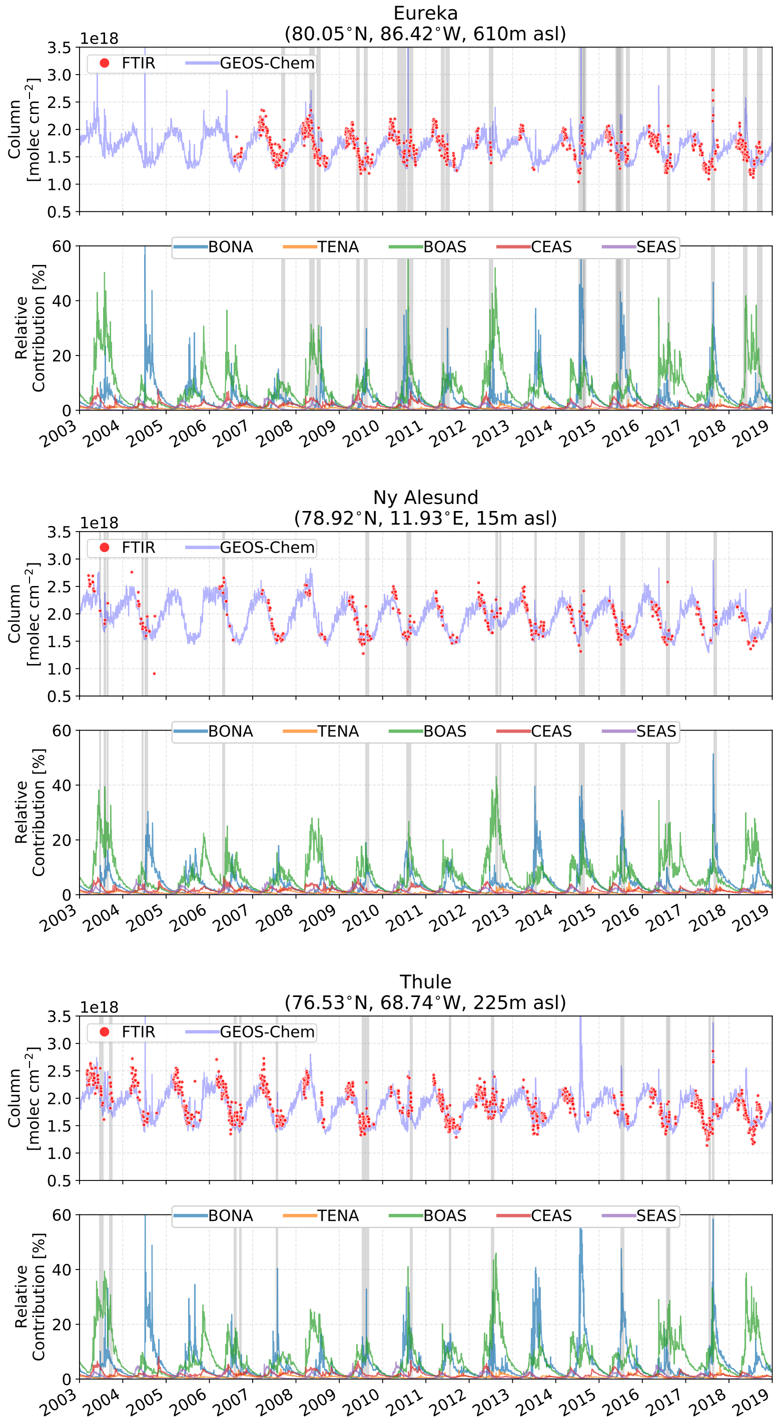

Figure 7. Daily-mean CO tropospheric column time series for FTIR and GEOS-Chem (top panel) from 2003-2018 for the high-Arctic sites: Eureka, Ny-Ålesund and Thule. The bottom panel shows the relative contribution (%) of the BONA, TENA, BOAS, CEAS and SEAS CO tracers in the GEOS-Chem simulation to the total CO tropospheric column. The grey shaded regions indicate periods of fire-affected measurements identified in the FTIR time series and summarized in Figure 5

.

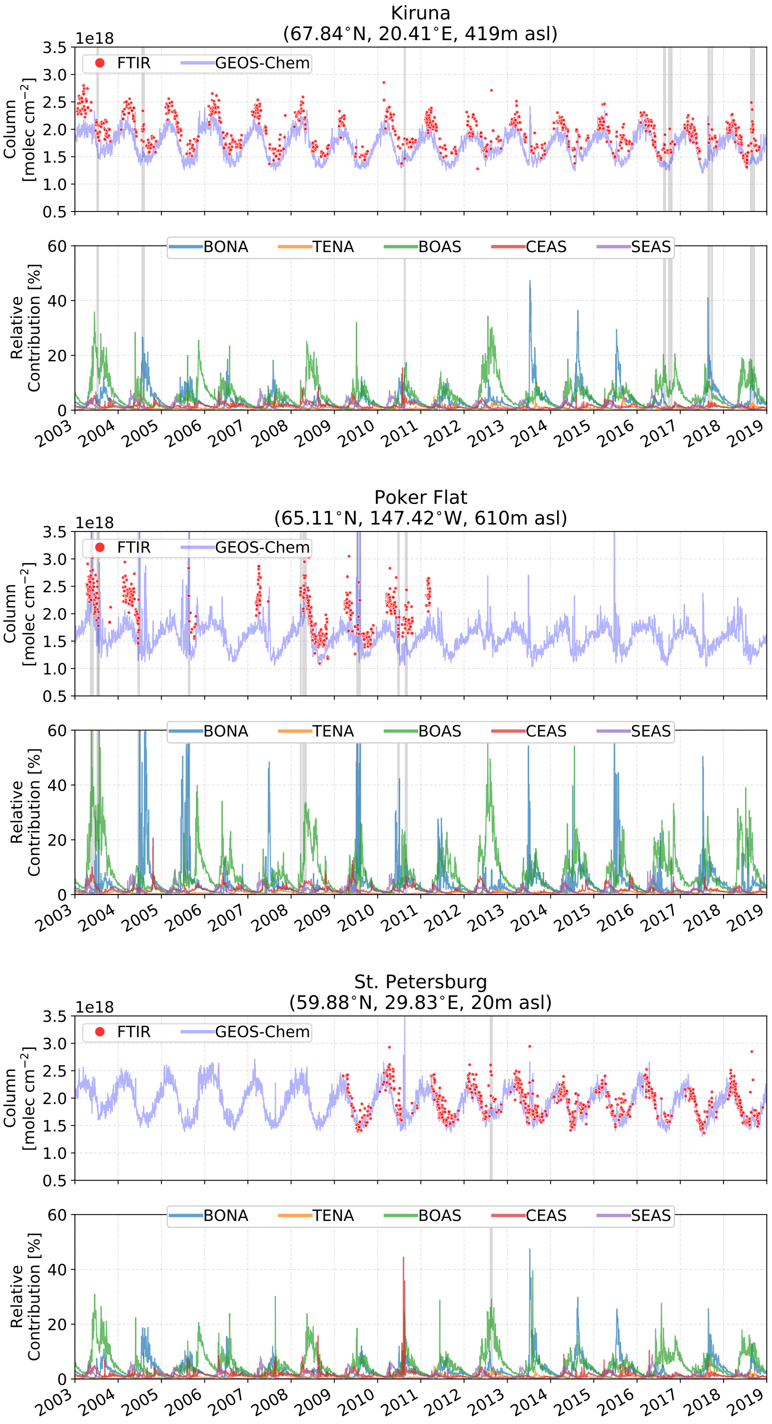

Figure 8. Same as Figure 7 but for the Arctic sites: Kiruna, Poker Flat and St. Petersburg .

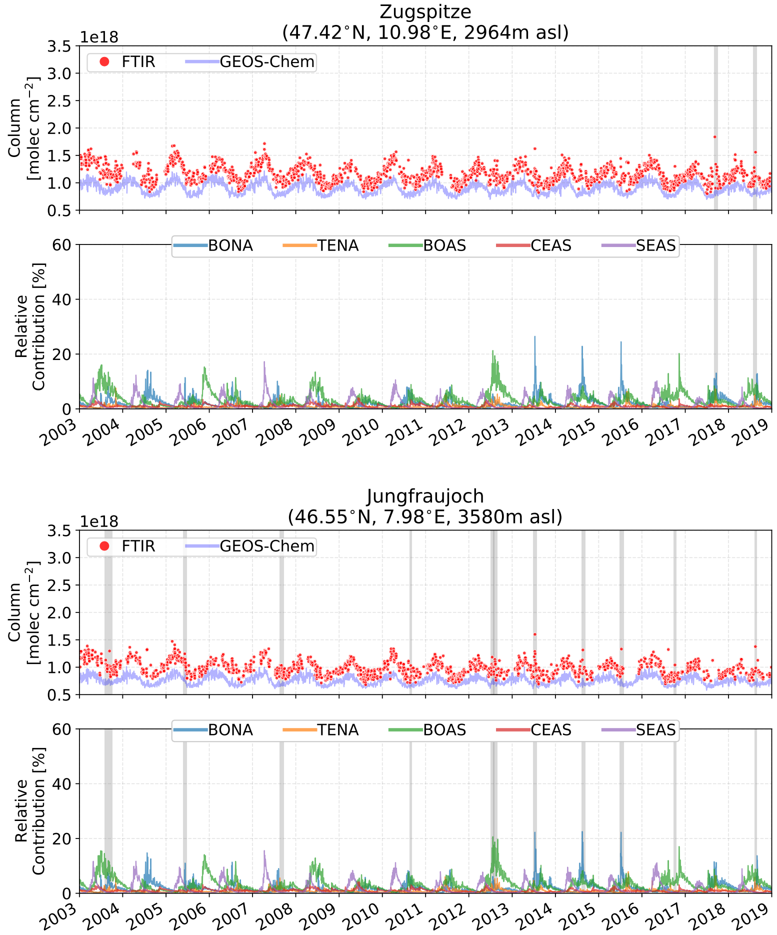

Figure 9. Same as Figure 7 but for the alpine sites: Zugspitze and Jungfraujoch.

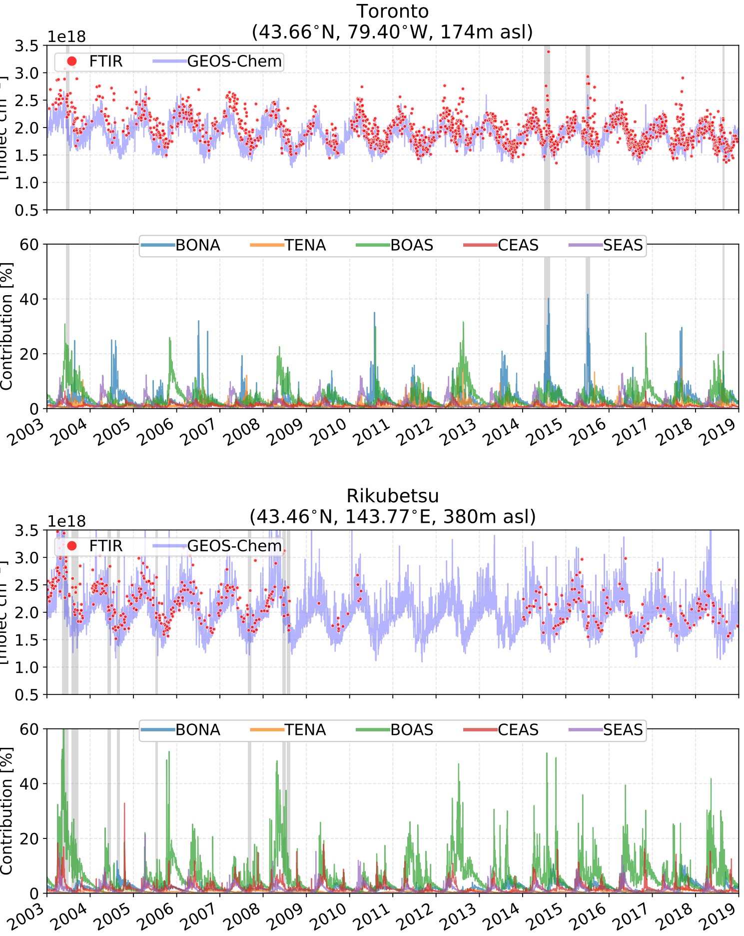

Figure 10. Same as Figure 7 but for the mid-latitude sites: Rikubetsu and Toronto.

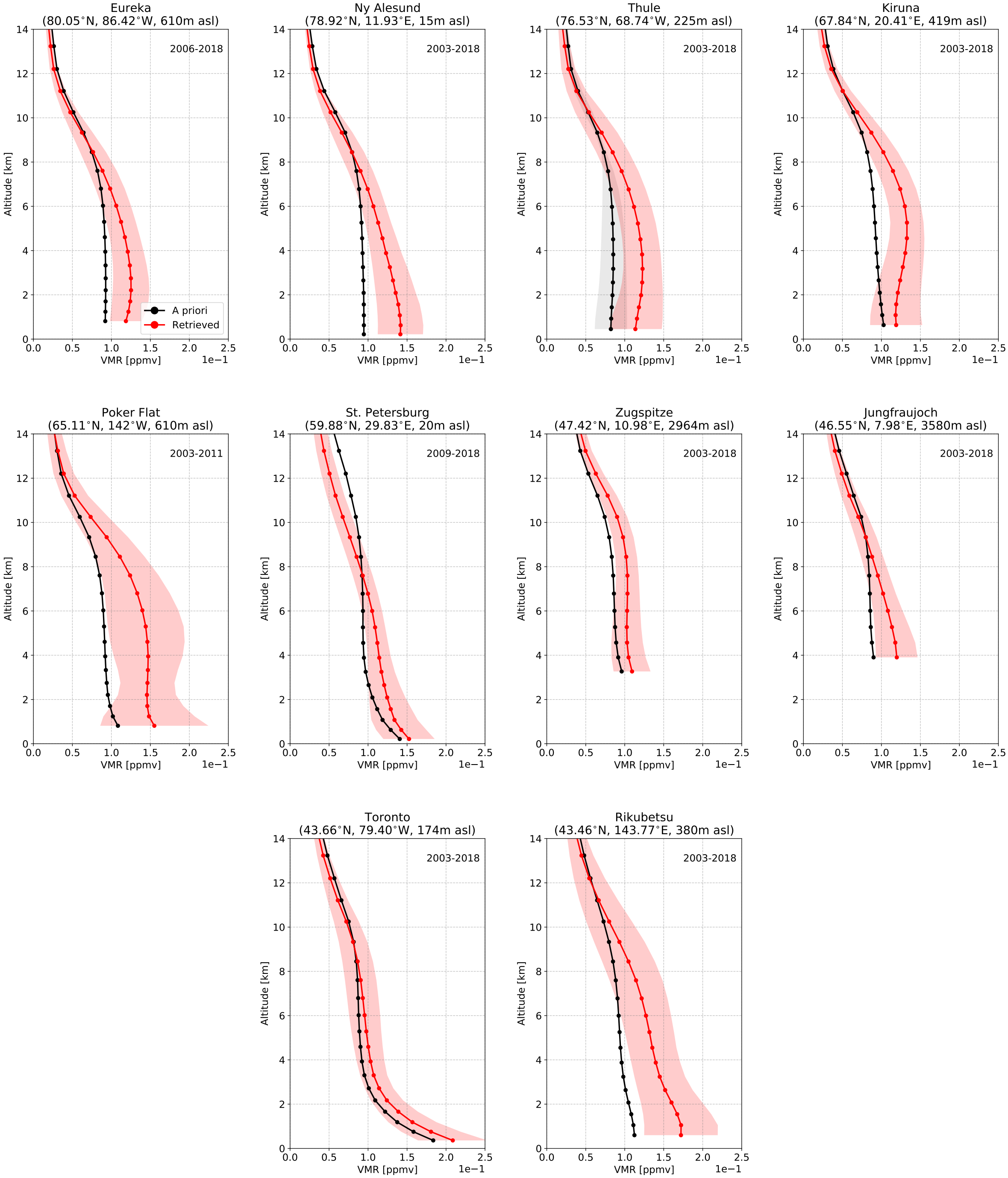

Figure A1. Mean retrieved (red) and a priori (black) VMR profiles of CO taken over all years of measurements at each site. The shaded region indicates the 1σ standard deviation from the mean. The circle markers indicate the layer centers of the FTIR vertical retrieval grid.

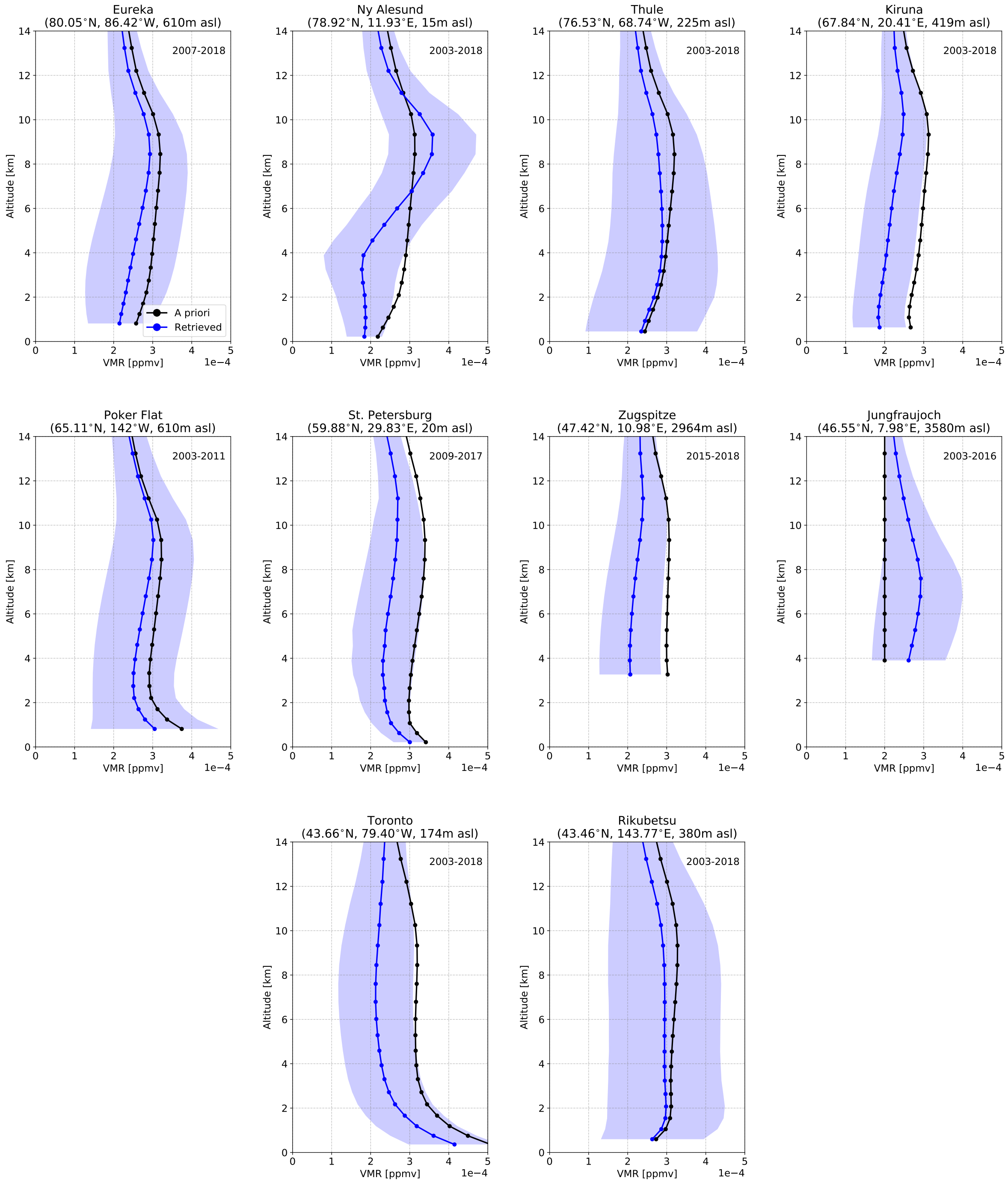

Eureka (80.05°N, 86.42°W, 610m asl)

Ny Alesund (78.92°N, 11.93°E, 15m asl)

Thule (76.53°N, 68.74°W, 225m asl)

Kiruna (67.84°N, 20.41°E, 419m asl)

Poker Flat (65.11°N, 142°W, 610m asl)

St. Petersburg (59.88°N, 29.83°E, 20m asl)

Zugspitze (47.42°N, 10.98°E, 2964m asl)

Jungfraujoch (46.55°N, 7.98°E, 3580m asl)

Toronto (43.66°N, 79.40°W, 174m asl)

Rikubetsu (43.46°N, 143.77°E, 380m asl)

Figure A2. Same as Fig. A1 but for HCN.

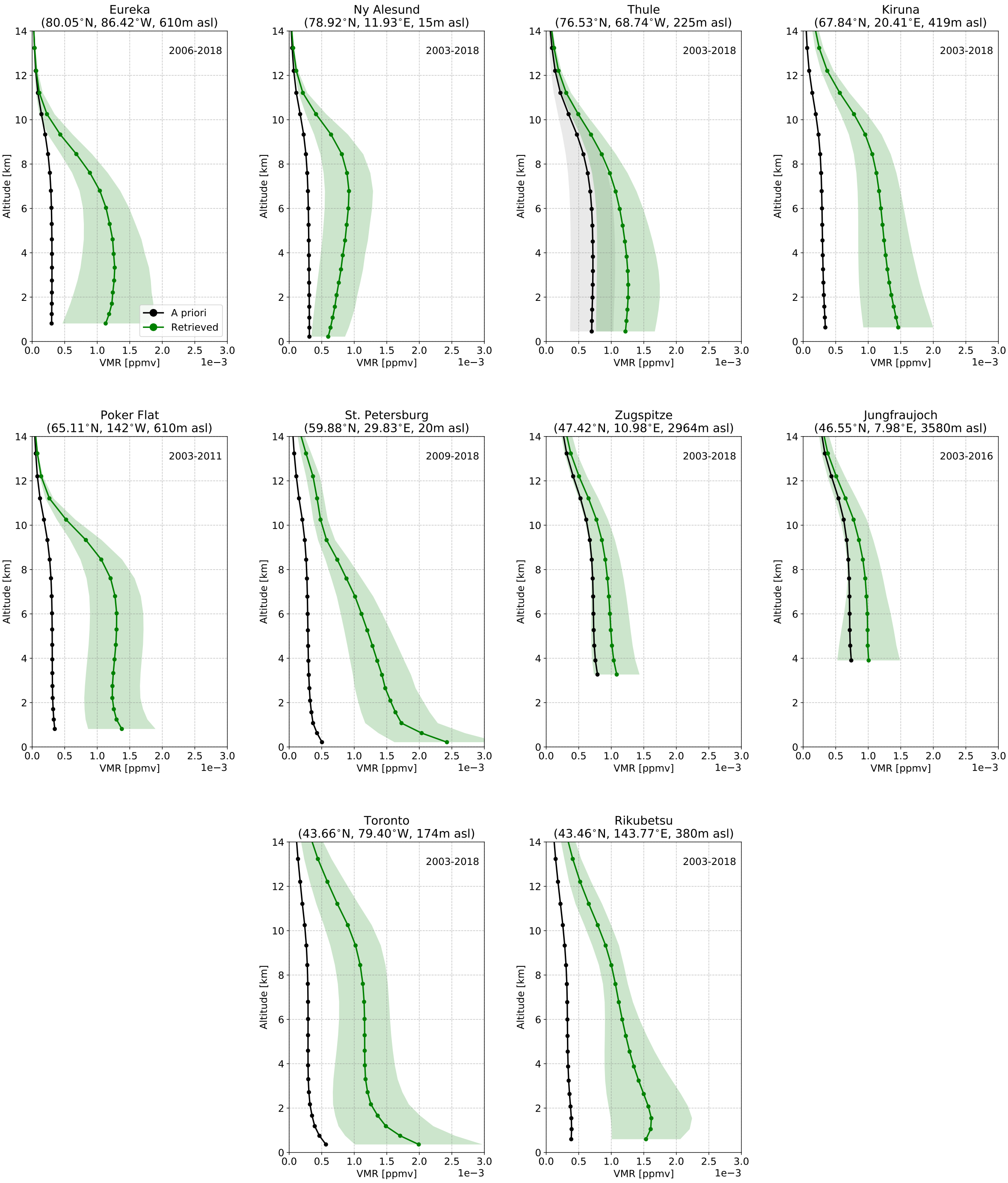

Figure A3. Same as Fig. A1 but for C_2H_6

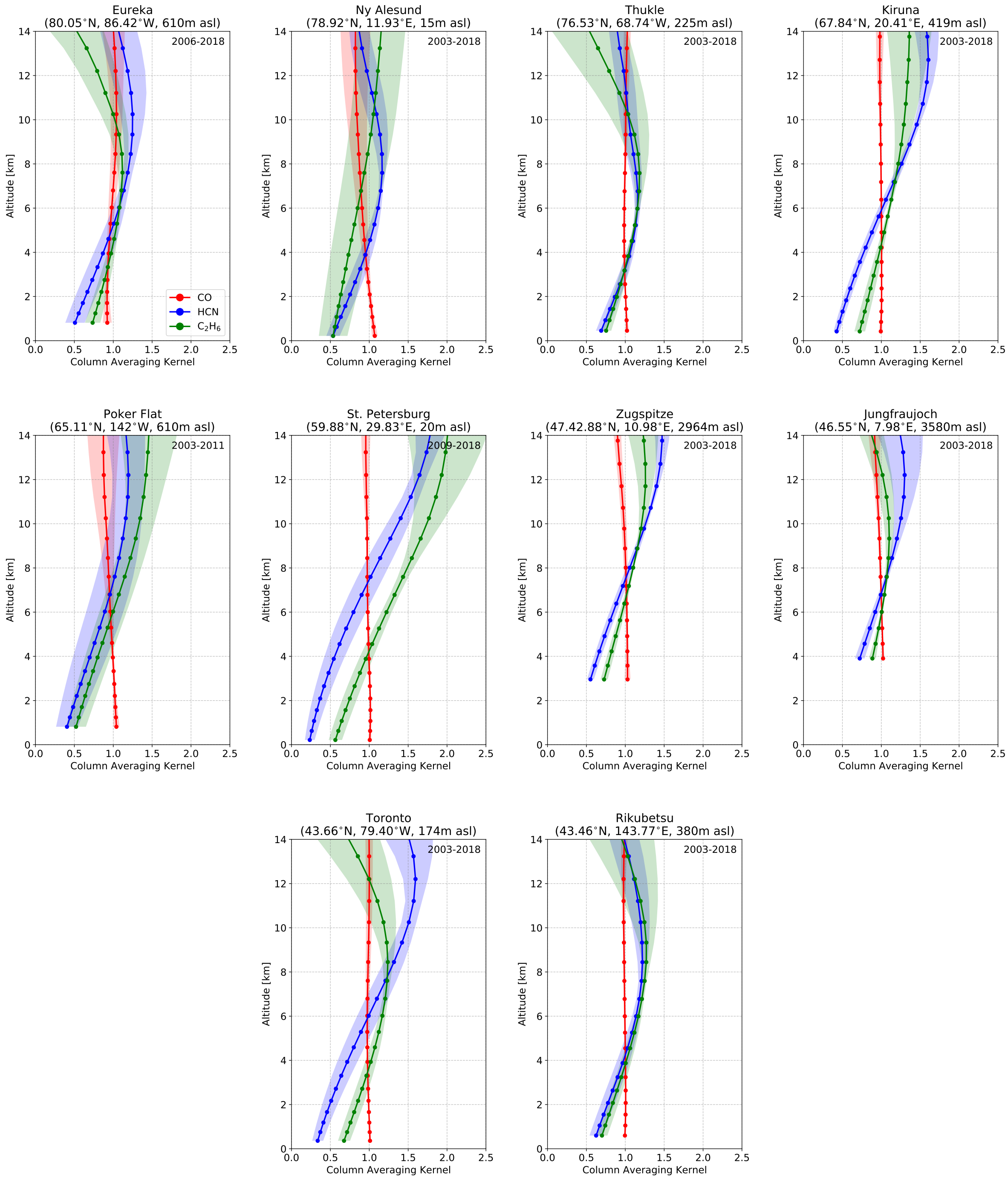

Figure A4. Mean CO, HCN and C_2H_6 normalized total column averaging kernels in units of molec cm^{-2}/ molec cm^{-2}, taken over all years of measurements at each site. The shaded region indicates a 1σ standard deviation from the mean. The circle markers indicate the layer centers of the FTIR vertical retrieval grid.